THE UNIVERSITY OF CALGARY

DEVELOPMENT OF A
RLG STRAPDOWN INERTIAL SURVEY SYSTEM

by

RICHARD V. C. WONG

A THESIS

SUBMITTED TO THE FACULTY OF GRADUATE STUDIES

IN PARTIAL FULFILMENT OF THE REQUIREMENTS FOR THE

DEGREE OF DOCTOR OF PHILOSOPHY IN ENGINEERING

DEPARTMENT OF SURVEYING ENGINEEERING

CALGARY, ALBERTA

1988

ISBN 0-315-50425-0

THE UNIVERSITY OF CALGARY

FACULTY OF GRADUATE STUDIES

The undersigned certify that they have read, and recommend to the Faculty of Graduate Studies for acceptance, a thesis entitle "A RLG Strapdown Inertial Survey System", submitted by Richard V. C. Wong in partial fulfillment of the requirements for the degree of Doctor of Philosophy in Engineering.

K.P. Schwarz

Prof. K-P Schwarz (Supervisor)
Dept. of Surveying Engineering

Prof. E. J. Krakiwsky
Dept. of Surveying Engineering

J.A.R. Blais

Prof. J. A. R. Blais
Dept. of Surveying Engineering

Gérard Lachapelle

Prof. G. Lachapelle
Dept. of Surveying Engineering

Robert B Streets

Prof. R. B. Streets
Dept. of Electrical Engineering

Dr. D. Liang
DREO, Dept. of National Defence

1988

ABSTRACT

The thesis describes the successful modification of a ring-laser-gyro (RLG) strapdown inertial reference unit into a strapdown inertial survey system (SISS) for geodetic positioning. The RLG system, a Litton LTN-90-100, has been modified into a land-vehicle mode inertial survey system, by developing specialized software and error control techniques. The software package integrates the raw body rate and acceleration data from the LTN-90-100 into velocities and coordinates of the system. The error states of the SISS are estimated by a Kalman filter-smoother using regular zero velocity measurements and occasional control coordinates as updates. The system was tested on two L-shaped baselines near Calgary and results show that a positioning accuracy of better than 1 m (1σ) is achievable. The thesis describes the developed SISS, the data integration, alignment and error estimation software as well as the results of the baseline tests.

ACKNOWLEDGEMENTS

The author would like to thank Prof. K-P Schwarz for providing the advice and support needed to complete his graduate studies and thesis. Mr. H. Martell, Mr. M. Szarmes, Mrs. E. Knickmeyer, Ms. A. Rauhut and Mr. A. Tam of the Department of Surveying Engineering are acknowledged for helping the author to gather the data neccesary for this research. Thanks are due to Mr. J. Smith of Pulsearch Canada Ltd., Calgary and Mr. J. Hogan of Litton Systems Canada, Toronto for their advice on the data acquisition system and LTN-90-100 used in this research. Nortech Survey (Canada) Ltd. is acknowledged for providing the baseline needed in the field tests

Profs. E. J. Krakiwsky, J. A. R. Blais and G. Lachapelle of the Department of Surveying Engineering, Prof. R. B. Streets of the Department of Electrical Engineering and Dr. D. Liang of Defence Research Establishment, Ottawa, are acknowledged for their critiques of this thesis. The author also wishes to thank Prof. L. Turner of the Department of Electrical Engineering for his assistance in the development of the noise filter.

Funding for this research project was provided by Natural Science and Engineering Research Council of Canada and Litton Systems Canada of Toronto.

TABLE OF CONTENTS

LIST OF TABLES

LIST OF FIGURES

NOTATION

1. CONVENTIONS

1.1 Vectors and matrices are typed in boldface.

1.2 Vectors are represented by lower case letters.

1.3 Matrices are represented by upper case letters.

1.4 "Vector" means coordinates of a vector. A superscript will be used to indicate the particular coordinate frame in which the vector is defined, e.g.

$$\mathbf{r}^b = [\, r_x^b, r_y^b, r_z^b,]^T$$

1.5 Rotation matrices, R are specified by two indices so that the transformation from frame b to frame n is given by,

$$\mathbf{r}^n = \mathbf{R}_b^n \mathbf{r}^b$$

1.6 Angular velocity of frame e with respect to frame i, coordinatized in frame b is described as, ω_{ie}^b

1.7 The following symbols specify an arbitrary quantity x :

x	true value
$\bar{x}$	approximate value
$\hat{x}$	estimated value
$\tilde{x}$	measured value
$E\{x\}$	expected value
δx	perturbation in x
Δx	difference in x
$\dot{x}$	time differential of x
x_k	value at epoch k

2. COORDINATE FRAMES

2.1 Inertial, i

origin - at the mass centre of the earth

x-axis - pointing towards vernal equinox at t_o

y-axis - completes right-handed system

z-axis - towards north celestial pole at epoch t_o

2.2 Earth-fixed, e

origin - at the mass centre of the earth

x-axis - towards the Mean Greenwich meridian, in the equatorial plane

y-axis - 90° east of Greenwich meridian, in the equatorial plane

z-axis - mean spin axis of the earth, coinciding with minor axis of the reference ellipsoid

2.3 Local-level, n

origin - at topocentre

x-axis - ellipsoidal east (also denoted as E axis)

y-axis - ellipsoidal north (also denoted as N axis)

z-axis - upward direction along the ellipsoidal normal (also denoted as U axis)

2.4 Wander, w

origin - at topocentre

x-axis - rotated from the east towards the north on the level plane by an angle α. The angle α is called the wander angle and it is selected to be equal to the meridian convergence from the point of alignment

y-axis - orthogonal to the x-axis on the level plane

z-axis - upwards along the ellipsoidal normal

2.5 Body, b

origin - at centre of inertial survey system

x-axis - towards the left side of the inertial survey system (ISS) y-axis - towards the back of the ISS, i.e. through the output pins

z-axis - upwards and perpendicular to the x-y plane

.2.6 Platform, p

origin - at the centre of the inertial survey system

x-axis - slightly misaligned from the x axis of the n or w frame

y-axis - slightly misaligned from the y axis of the n or w frame

and orthogonal to the x axis mentioned above

z-axis - completes the orthogonal right-handed system

3. LIST OF SYMBOLS

SYMBOL	DESCRIPTION
a	Semi-major axis of the reference ellipsoid
b	Semi-minor axis of the reference ellipsoid
$\mathbf{b}$	Accelerometer biases
C_x	Covariance matrix of the state vector
C_w	Covariance matrix derived from the spectral densities
$\mathbf{d}$	Gyro drift rates
$\dot{\mathbf{D}}$	Variance matrix of the misclosure vector
e^2	Second eccentricity of the reference ellipsoid
$\mathbf{e}$	Measurement noise
$\mathbf{f}$	Specific force
$\mathbf{F}$	Dynamics matrix
$\mathbf{g}'$	Gravitational acceleration
$\mathbf{g}$	Gravity acceleration
Δg	Gravity anomaly
$\mathbf{H}$	Design matrix
h	Ellipsoidal height
$\mathbf{I}$	Identity matrix
$\mathbf{K}$	Kalman gain matrix
$\mathbf{n}$	White noise
$\mathbf{Q}$	Spectral density matrix
$\mathbf{q}$	Quaternion vector
R_M	Radius of the meridian
R_P	Radius of the prime vertical

$\mathbf{r}$	Position vector from the mass centre of the earth to the point of interest
t	Time
$\mathbf{v}$	Velocity vector
$\mathbf{V}$	Skew-symmetric matrix of $\mathbf{v}$
$\mathbf{u}$	Forcing function
$\mathbf{w}$	System noise
$\mathbf{x}$	State vector
$\mathbf{x}_0$	Initial state vector
$\hat{x}(-)$	State vector before measurement update
$\hat{x}(+)$	State vector after measurement update
γ	Normal gravity
$\Delta\theta$	Vector of incremental gyro output
ϕ	Geodetic latitude
Φ	Transition matrix
ω_e	Magnitude of the earth rate of rotation
ω_s	Schuler frequency
Ω_{ij}^{b}	Skew-symmetric form of ω_{ij}^{b}
λ	Geodetic longitude
υ	Angular rotation experienced by an inertial survey system due to its movement on the earth's surface

CHAPTER 1

INTRODUCTION

In the vast and sparsely populated regions of Canada where the terrain is undulating and covered by dense vegetation, establishment of geodetic control points is a difficult and expensive task. The cost of second-order network densification in the past decade has been reduced by extensive use of gimballed inertial survey systems (Babbage, 1981 and Pfeifer et al, 1985). The level of accuracy achievable is about 10 ppm. Research and field experiment have shown that, with improved hardware and software, these gimballed systems can also be used to determine the earth's anomalous gravity field. Results reported indicate that accuracies of < 1 arcsec (1σ) for the components of the deflection of the vertical and 5 mgal (1σ) for the gravity anomaly can be obtained with a gimballed inertial survey system (Todd, 1981, Hadfield, 1985, and Forsberg and Wong, 1987). However, the gimballed systems are very expensive. The initial capital cost of these systems is at least half a million dollars and they also require frequent maintenance. Today, efforts are being made to develop less costly strapdown inertial survey systems (SISS) to replace the existing gimballed systems as their useful life expires.

At present, there are three types of inertial survey systems available on the market : space-stabilized systems, local level systems and strapdown systems. These systems contain a set of gyros and three accelerometers that are orthogonally mounted in a sensor block. The first two types of systems are gimballed systems which rotate their sensor block such that their axes are pointing in the direction of the axes of a well defined coordinate frame. The chosen coordinate frame is usually the frame in which the raw data is processed into velocities, e.g.. the inertial or local-level coordinate frame. The strapdown systems allow their sensor block to rotate with the body of the carrier such that the axes of the sensors are aligned with the along-track, cross-track and normal axes of the trajectory of the systems. The output of the sensors are analytically transformed to a well defined coordinate frame for processing.

The gimballed inertial survey systems have been well accepted in the surveying community mainly because they are accurate and well developed for positioning and gravity survey. They are designed to utilize the power sources in various kinds of land vehicles and aircraft used in geodetic surveying. However, the advance in ring-laser-gyro (RLG) technology in recent years, has made it possible to produce a new generation of less expensive strapdown inertial survey systems that are comparable to the gimballed systems. The RLG strapdown inertial survey systems are in general more reliable, and require less power than the gimballed systems. The ring-laser-gyros are noisier than the conventional gyros used in most of the gimballed systems but, with improved software and accurate surveying measurements, ring-laser-gyro SISS have the potential to achieve the same positioning accuracy as the inertial survey systems being used today.

The objective of the research described in this thesis is to convert a RLG strapdown inertial reference unit into a land-vehicle mode inertial survey system. The basic theory for strapdown inertial navigation and error estimation is well known. The main task of the research is the implementation of the theory. It is usually published in general form in the context of navigation and has to be adapted to the practical land surveying environment using a particular inertial reference unit. The task can be subdivided into three parts : development of hardware needed to support the inertial reference unit and the data acquisition, development of estimation software that utilizes surveying measurements, and field testing of the SISS.

The inertial reference unit used is a Litton LTN-90-100 RLG strapdown system which is designed for aircraft navigation purposes. Its software was modified by the manufacturer to allow the use for land surveying. An IBM PC-compatible data acquisition system was built by a company in Calgary for recording the data from the LTN-90-100 for post-mission data processing. Two types of data are available from the LTN-90-100. They are the 16 Hz velocity data and the 64 Hz rate data. A simple routine was developed to process the velocity data into coordinates which can be fed into a Kalman filter developed at The University of of Calgary. The Kalman filter is designed to estimate the errors of the velocities and coordinates using zero velocity measurements obtained while the vehicle stops at the survey points and the control coordinates of known stations on the traverse. The LTN-90-100 is designed to output vertical velocity and height only when external height information is available to the system. At present, the interface device in the data acquisition system cannot send such information back to the LTN-90-100, therefore it is not possible to determine the height of the system using the velocity data only. However, the horizontal coordinates as well as the height can be estimated from the rate data of the LTN-90-100 which consist of three body rotation rates and three body accelerations. A computer package containing an integration and an alignment module was developed to integrate the rate data into velocities and coordinates and to align the SISS, i.e. to determine the initial roll, pitch and azimuth of the system. Like the data integrated from the 16 Hz velocity data, the output of the integration module is fed into the Kalman filter for error estimation. The same filter used for error estimation process is also used during the alignment to fine-tune the estimated initial attitude of the system. An optimal smoother was developed to refine the estimates from the Kalman filter. The smoother basically uses all the information gathered after a specific epoch to improve the Kalman filter estimates at that epoch. Here, the combination of the Kalman filter and the optimal smoother is called Kalman filter-smoother.

The integration and alignment module, and Kalman filter-smoother were tested with data from two different L-shaped baselines in Calgary and Cochrane. The 10-km Calgary baseline was surveyed once with the LTN-90-100 to get the velocity data needed to test the Kalman filter-smoother. The rate data obtained from four surveys on the 25-km Cochrane baseline were used to test the integration module and the alignment module.

This thesis is divided into nine chapters. The first chapter explains the objective of the research. The various coordinate frames used in the description of the SISS are defined in the Chapter 2. A general description of the characteristics of the two types of gimballed systems and a more detailed explanation of the LTN-90-100 are given in Chapter 3. The formulae used in the integration and alignment modules are derived in Chapter 4 and 5. Chapter 6 outlines the error estimation process and the Kalman filter-smoother. The detailed description of the baseline tests are given in Chapter 7 and the results of the analysis of the tests are presented in Chapter 8. The final chapter of the thesis contains the conclusions derived from the results obtained and the recommendations for the use of the SISS in the future.

CHAPTER 2

COORDINATE FRAMES

In land surveying and geodetic positioning, the final output required by the client are usually the coordinates of a point in terms of latitude, longitude and height, and thier accuracies. The measurements sensed by an inertial survey system are three orthogonal components of the body rotation rates and three accelerations in a coordinate frame which is not directly related to any geodetic curvilinear coordinate frame. These measurements have to be analytically integrated and transformed, through several coordinate frames, to yield changes in the ellipsoidal coordinates. It is, therefore, important that all coordinate frames involved in the transformation of the measurements and the results of the integrations are well defined before any discussion of the inertial survey system is presented. The definition of various coordinate frames associated with the SISS are given in this chapter.

2.1 Inertial Frame

According to the Newtonian definition, the inertial frame is a frame which does not rotate or accelerate. Such a frame is easy to define in theory but it is almost impossible to realize in practice. The best approximation to a truly inertial frame would be one that is inertial with respect to the distant stars. One approximation to such a frame known to surveyors is the right ascension system. The right ascension system as given in a cataloque precesses and nutates at the rate of less than $3.6 \cdot 10^{-7}$ arcsec/s (see Mueller, 1977) which is well below the noise level of the sensors in present inertial survey systems. Thus, for all practical inertial surveying purposes, the right ascension system can be treated as an inertial coordinate frame.

The definition of the inertial frame for this thesis is the following:

origin - at the mass centre of the earth.

x-axis - towards mean vernal equinox at t_o;

y-axis - completes a right-handed system; and

z-axis - towards the north celestial pole at epoch t_o.

A graphical representation of the inertial frame is shown in Figure 2-1. Note that this is an abstract definition of an inertial frame for computational purposes. Measurements are done with respect to an inertial frame defined by gyros which has a much poorer accuracy.

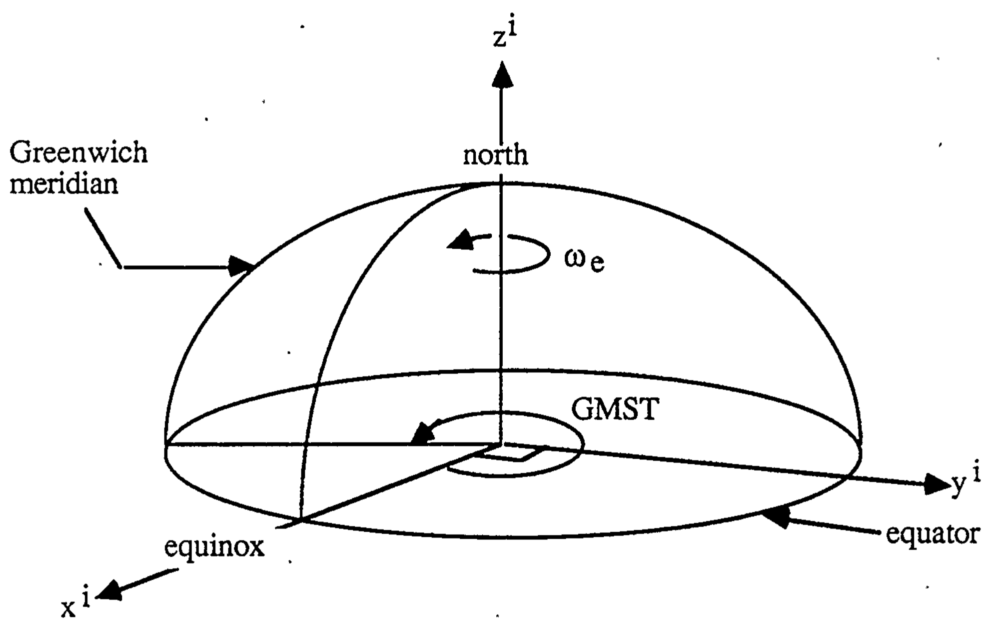

Figure 2-1 : Inertial Frame

2.2 Earth-fixed Frame

The Earth-fixed frame is the frame in which the output coordinates of the inertial survey system are given. This frame is not inertial. It is revolving around the sun and rotating at a rate of $7.292115 \cdot 10^{-5}$ rad/s. The definition of the earth fixed frame is the following:

origin - at the mass centre of the earth;

x-axis - pointing towards the Greenwich meridian, in the equatorial plane;

y-axis - 90° east of Greenwich meridian, in the equatorial plane; and

z-axis - axis of rotation of the reference ellipsoid.

The coordinates in the earth-fixed frame can be transformed to the inertial frame by a negative rotation about the z-axis of the frame by the amount of the Greenwich Mean Sidereal Time (GMST). The reference ellipsoid used in this research is the WGS 80 system. The semi-major and semi-minor axes are

$$a = 6378137.0 \text{ m} \tag{2-1}$$

and

$$b = 6356752.3 \text{ m}, \tag{2-2}$$

respectively.

The relationship between the ellipsoidal coordinates that a surveyor wants and the orthogonal Cartesian coordinates of the earth-fixed frame is given by the expressions

$$X^e = (R_P + h) \cos\phi \cos\lambda, \tag{2-3}$$

$$Y^e = (R_P + h) \cos\phi \sin\lambda \tag{2-4}$$

and

$$Z^e = (R_P b^2/a^2 + h) \sin\phi, \tag{2-5}$$

where

ϕ, λ and h are the ellipsoidal latitude, longitude and height, and

R_P is the radius of curvature along the prime vertical at the point of interest.

The value of R_P can be computed with the equation

$$R_P = \frac{a}{(1-e^2\sin^2\phi)^{1/2}}, \tag{2-6}$$

where

$$e^2 = \frac{a^2 - b^2}{a^2}. \tag{2-7}$$

The derivation of equations (2-3) to (2-7) can be found in Krakiwsky and Wells (1971). The direction of the axes of the earth-fixed frame are illustrated in Figure 2-2.

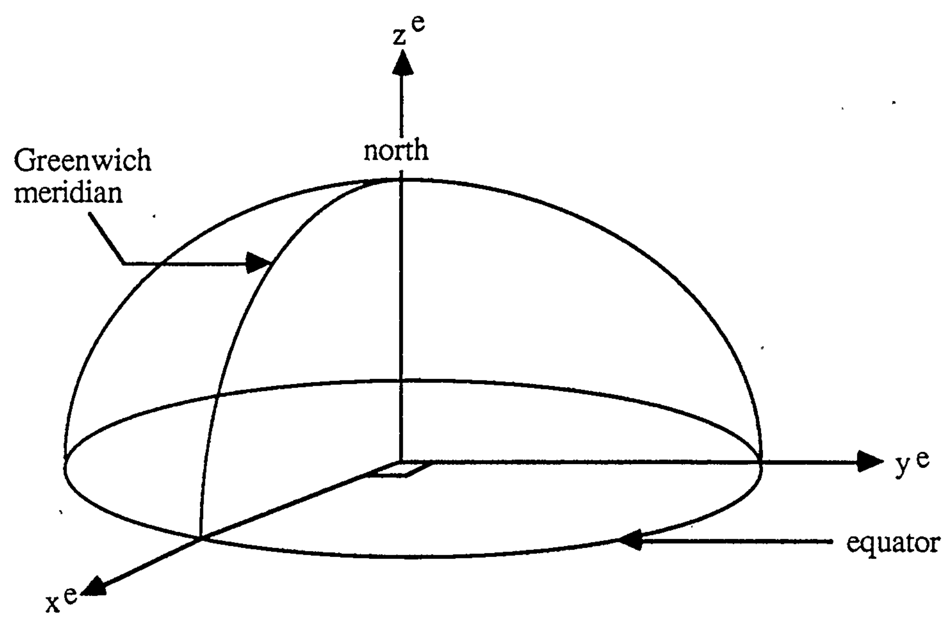

Figure 2-2 : Earth-fixed Frame

2.3 Local-level Frame

The local-level frame is a coordinate frame which is known to surveyors as local geodetic frame if a change in the direction of the x and y axes is made. The velocity of an inertial survey system is usually outputed as components along the axes of the local-level frame. The definition of the local-level frame is the following:

origin - at topocentre;

x axis - ellipsoidal east (also denoted as E axis);

y axis - ellipsoidal north (also denoted as N axis); and

z axis - upward direction along the ellipsoidal normal (also denoted as U axis).

A vector **x** in the local-level frame can be transformed to the earth-fixed frame via the equation

$$x^e = R_n^e \, x^n ,\tag{2-8}$$

where

$$R_n^e = R_3(-\lambda-90°)\, R_1(\phi-90°).\tag{2-9}$$

Here, $\mathbf{R}_1$ and $\mathbf{R}_3$ are the rotation matrices about the x and z axes of the coordinate frame. The direction of the axes of the local-level frame and the components of the earth's rate of rotation along them are shown in Figure 2-3.

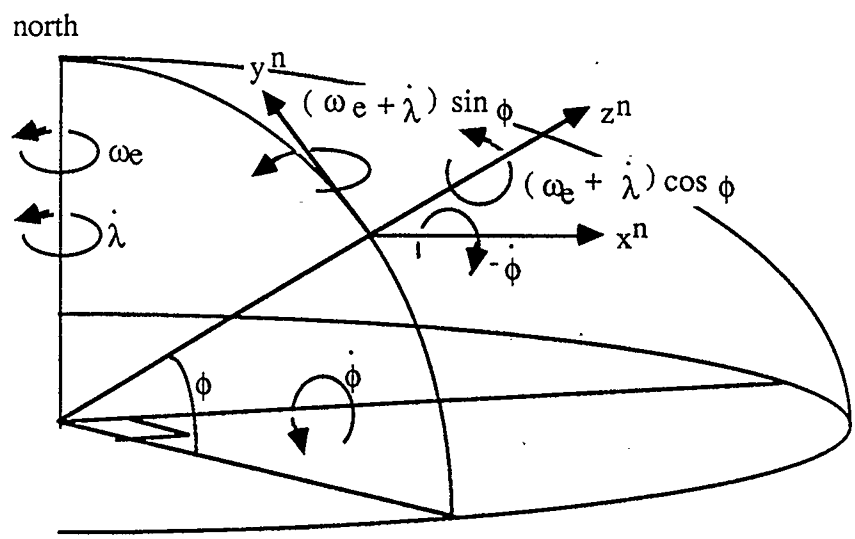

Figure 2-3 : Local-level frame

2.4 Wander Frame

The local-level frame is convenient for expressing a direction but it is not the best coordinate frame in which to perform the integration of the data from an inertial survey system. The y axis of the local-level frame is always pointing towards the north. At very high latitudes, a large rotation about the z axis is necessary to maintain the orientation of the local-level frame whenever it is moved towards the east, even by a small movement. This problem may be avoided by performing all the computations in a coordinate frame that does not point north. Such a coordinate frame is called a wander frame. The wander frame is the same as the local-level frame in all aspects except that its y axis is not slaved to the north direction. It is, therefore, allowed to wander off the north axis at a rate chosen by the user. The angle between the y and north axes is called the wander angle. In this research, the rate of change of the wander angle is chosen to be

$$\dot{\alpha} = -\dot{\lambda}\sin\phi \tag{2-10}$$

The definition of the wander frame is the following :

origin - at topocentre;

x-axis - rotated in the level plane by an angle α from the east towards the north. The angle α is called the wander angle and it is chosen to be equal to the meridian convergence from the point of alignment;

y-axis - orthogonal to the x-axis in the level plane; and

z-axis - upwards along the ellipsoidal normal.

The transformation matrix between the wander frame and the local-level frame is

$$\mathbf{R}_w^n = \begin{pmatrix} \cos\alpha & -\sin\alpha & 0 \\ \sin\alpha & \cos\alpha & 0 \\ 0 & 0 & 1 \end{pmatrix} \tag{2-11}$$

and the one between the wander frame and earth-fixed frame is

$$\mathbf{R}_w^e = \begin{pmatrix} -\sin\lambda\cos\alpha-\cos\lambda\sin\phi\sin\alpha & \sin\lambda\sin\alpha-\cos\lambda\sin\phi\cos\alpha & \cos\lambda\cos\phi \\ \cos\lambda\cos\alpha-\sin\lambda\sin\phi\sin\alpha & -\cos\lambda\sin\alpha-\sin\lambda\sin\phi\cos\alpha & \sin\lambda\cos\phi \\ \cos\phi\sin\alpha & \cos\phi\cos\alpha & \sin\phi \end{pmatrix}. \tag{2-12}$$

Figure 2-4 shows that orientation of the wander frame used in this research.

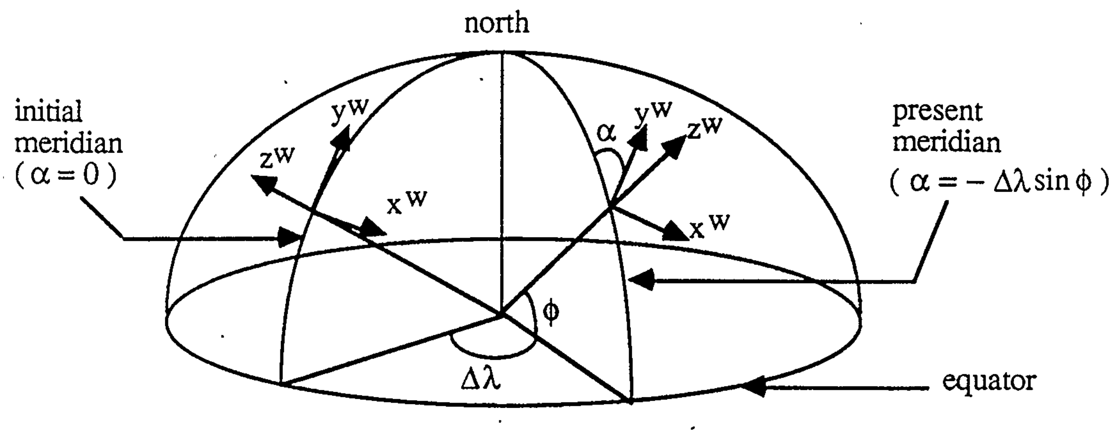

Figure 2-4 : Wander Frame

2.5 Body Frame

The body frame is the orthogonal frame in which the measurements of a strapdown inertial survey system are made. Its axes coincide with the output axes of the sensor block. Thus, the raw data output of a SISS are the components of the rotation rate and the acceleration experienced by the sensor block along the body axes. The local-level frame can be rotated to the body frame by three consecutive right-handed rotations about its three axes. The first rotation is made about its z-axis and the angular change is called the yaw of the SISS. The second rotation takes place about the rotated x-axis and the amount rotated is the pitch of the SISS. The third rotation about the rotated y-axis completes the total rotation between the two frames. The amount of rotation about the y-axis is called the roll of the SISS. The three angles: roll, pitch and yaw, are commonly referred to as the Euler angles , e.g. Giardina et al. (1981). The definition of the body frame of the strapdown inertial survey system used in this research is the following:

origin - at the centre of the strapdown inertial survey system;

x-axis - towards the left side of the SISS;

y-axis - towards the back of the SISS, i.e. through the output pins; and

z-axis - upwards and perpendicular to the x-y plane.

Quantities in the body frame can be analytically transformed to the local-level frame using the transformation matrix

$$R_b^n = R_3(y)\, R_1(p)\, R_2(r)\,, \qquad (2\text{-}13)$$

where y, p and r are the yaw, pitch and roll of the system. The elements in the matrix R_b^n are given below:

$$R(1,1) = \cos(y)\cos(r) - \sin(y)\sin(p)\sin(r) \qquad (2\text{-}14a)$$

$$R(1,2) = -\sin(y)\cos(p) \qquad (2\text{-}14b)$$

$$R(1,3) = \cos(y)\sin(r) + \sin(y)\sin(p)\cos(r) \qquad (2\text{-}14c)$$

$$R(2,1) = \sin(y)\cos(r) + \cos(y)\sin(p)\sin(r) \qquad (2\text{-}14d)$$

$$R(2,2) = \cos(y)\cos(p) \qquad (2\text{-}14e)$$

$$R(2,3) = \sin(y)\sin(r) - \cos(y)\sin(p)\cos(r) \qquad (2\text{-}14f)$$

$$R(3,1) = -\cos(y)\sin(r) \qquad (2\text{-}14g)$$

$$R(3,2) = \sin(p) \qquad (2\text{-}14h)$$

$$R(3,3) = \cos(p)\cos(r)\,. \qquad (2\text{-}14i)$$

For simplicity, the superscript n and subscript b have been eliminated from equations (2-14a) to (2-14i).

The transformation matrix between the body frame and the wander frame similar to the one given in equation (2-11) can be derived by substituting the yaw in the equation by the wander yaw, i.e.

$$y^w = y - \alpha\,. \qquad (2\text{-}15)$$

The orientation of the body axes with respect to the strapdown inertial survey system is shown in Figure 2-5. and the relationships between the three topocentric frames are plotted in Figure 2-6.

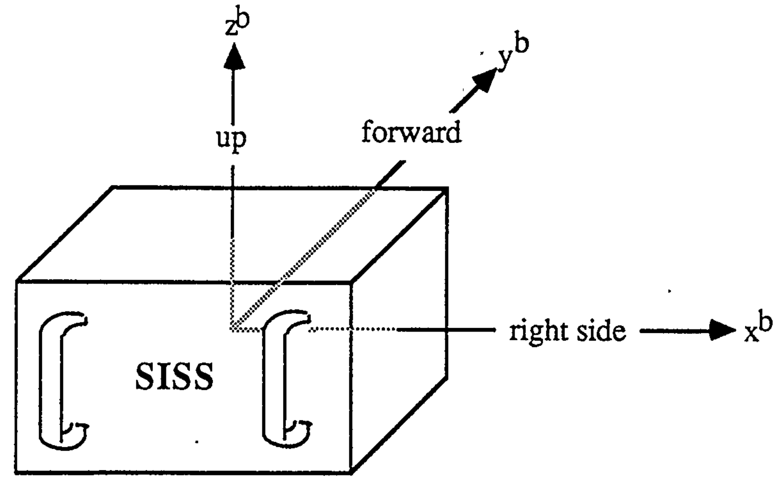

Figure 2-5 : Body Frame

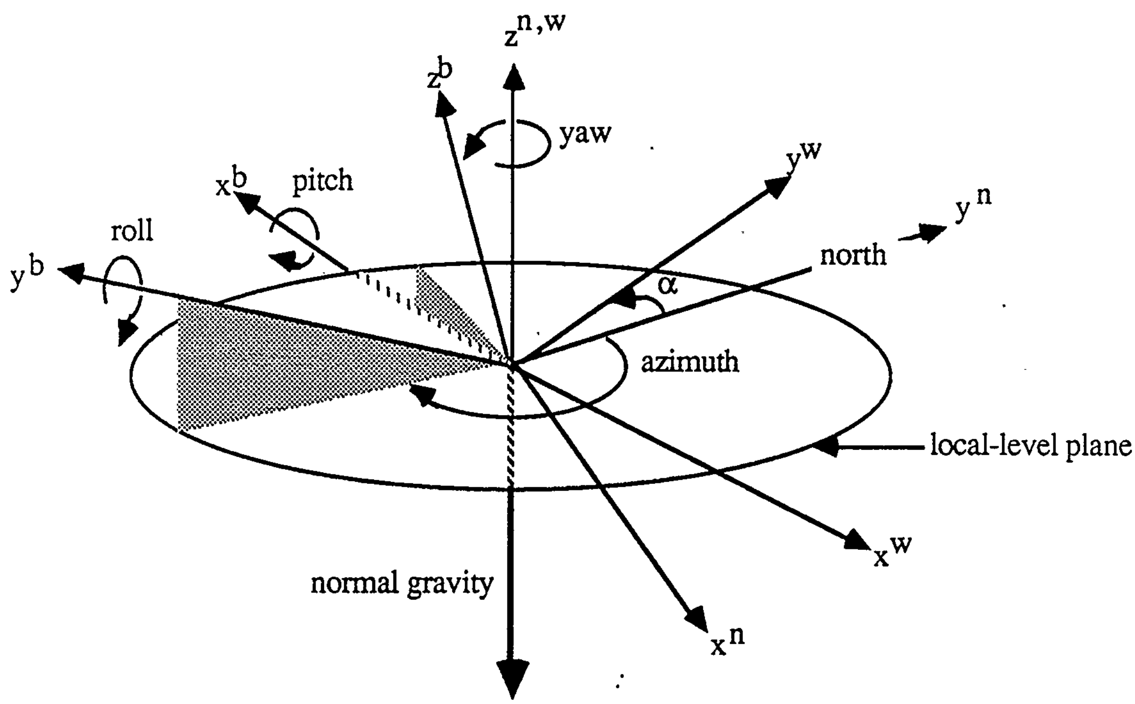

Figure 2-6 : Relationship Between the Three Topocentric Systems

2.6 Platform Frame

The platform frame was created mainly for the derivation of the error equations. The frame is very close to the local-level frame. It is an approximation to the local-level frame established with the data, i.e. Euler angles, velocities and coordinates integrated from the raw data, from the SISS. The angular deviation of the frame from the local-level frame is called platform misalignment. The definition of the platform frame is listed below:

origin - at the centre of the inertial survey system;

x-axis - slightly misaligned from the x axis of the local-level frame;

y-axis - slightly misaligned from the y axis of the local-level frame and orthogonal to the x axis mentioned above; and

z-axis - completes the orthogonal right-handed system.

CHAPTER 3

INERTIAL SURVEY SYSTEMS

It has been thirteen years since inertial survey systems were introduced to the surveyors. The most commonly known ones are the gimballed local-level systems. Today, there are three major inertial survey systems available. Honeywell's GEO-SPIN, Litton's LASS II and Ferranti's FILS Mark II. The Honeywell system is a space-stabilized system that utilizes electrically suspended gyros for maintaining the orientation of its sensor platform. The Litton and Ferranti systems are local-level systems that contain 2 to 3 conventional gyros in their sensor blocks. Detailed descriptions of these three systems can be found in Harris (1981), Pfeifer (1985) and Hagglund (1987).

A new generation of RLG strapdown inertial navigation/reference systems are being developed by various manufacturers for the commercial aviation market. These systems are designed to meet the requirements of aircraft navigation and to use only the measurements from the instruments available in an aircraft to estimate the errors of the systems. Since the requirements of aircraft navigation are very different from geodetic surveying, these systems cannot be used for surveying as they are built. However, the sensors inside these systems are usually accurate enough for surveying purposes. Thus, with accurate surveying measurements and proper estimation techniques, it is possible to convert these strapdown systems into inertial survey systems. In this research, the Litton LTN-90-100 inertial reference unit was selected for such a conversion.

In this chapter, the general characteristics of the three types of inertial survey systems are briefly discussed. This is followed by the a more detailed description of the LTN-90-100 and its output. Readers who are interested in learning more about other aspects of inertial survey systems and the basic theory associated with inertial navigation are referred to Britting (1971) and Farrell (1976).

3.1 Gimballed Systems

In a gimballed system, the sensors, i.e. the gyros and accelerometers, are mounted orthogonally on a platform. The platform is constantly torqued such that the output axes of the sensors are always aligned with the axes of a well-defined frame. This requires real-time computation of the velocity and rate of rotation of the platform from the raw data measured by the sensors. Based on the rate of rotation of the platform with respect to a chosen coordinate frame computed from the data, the sensors are torqued back to alignment with the axes of the frame. Since the raw data contain random and systematic errors, the sensor axes are not perfectly aligned to the chosen coordinate frame. The misalignments in turn introduce errors in the computed velocities and rates of rotation of the system. This results in a characteristic error behaviour of inertial survey systems which, in real time, is dependent on the errors in the velocities and rotation rates of the system. Any systematic errors in hardware and alignment software, and the resulting system errors are very difficult if not impossible to remove or reduce in post-mission processing. Fortunately, the hardware and software in the gimballed inertial survey systems available on the market are well developed. The only problem is the accumulating system errors which must be removed periodically to keep the error behaviour linear.

3.1.1 Space-stabilized Systems

The space-stabilized system is a system that keeps its sensor axes aligned with the inertial frame or a set of fixed orientations with respect to the frame. This requires the system to establish its orientation with respect to the inertial frame and torque the platform back by the amount of rotation it senses. The integration of the raw data can then be performed in the inertial frame and the output of the system are the velocities and coordinates of the system in that frame. All natural rotation and acceleration such as the earth's rotation and gravity must be modelled in the inertial frame so that they can be removed from the sensor output. The space-stabilized system performs more computations than the local-level system in real-time but it requires less mechanical torquing.

3.1.2 Local-level Systems

The local-level system differs form the space-stabilized system in the sense that it aligns its sensor axes with the local-level frame. This is accomplished by removing the earth's rate of rotation from the rate of rotation sensed by the system and by torquing the platform back at the reduced rate. Modelling of the gravity field is simple because the z axis of the local-level frame coincides with the normal gravity vector. In the absence of any knowledge of the anomalous gravity field, the gravity vector can be approximated by the normal gravity vector. The computations in the system are performed in the local-level frame and no transformation of the normal gravity and velocity data before output is necessary. The major limitation of the local-level system is that it cannot be used at very high latitude. Near the poles, a small movement to the east would force the system to perform a relatively large rotation of its platform about its z axis in order to maintain its alignment with the local-level frame.

3.2 Strapdown Systems

Although strapdown systems are relatively new in inertial surveying, the basic differential equations that describe a moving triad have been around for more than a century. A strapdown inertial survey system consists of a triad of sensors which is fixed to the body of the system. The sensors measure the components of the rotation rates and the specific force as experienced by the unit as it is moved along its trajectory. If the initial Euler angles and velocity of the system are known, the rate of rotation of the system due to earth rate and system velocity can be removed from the measured rates to obtain the attitude rates. By integrating the attitude rates, one can determine increments in the Euler angles of the system. Once the Euler angles are known, the sensed components of specific force and the normal gravity vector can be transformed to the wander or the local-level frames where they can be converted into components of acceleration in those frames. The velocities and coordinates of the system can be obtained by integrating the accelerations and adding the results to the initial velocity and coordinates. The process repeats itself as the system moves along its trajectory.

Obviously, no real-time computation or torquing is necessary to operate a strapdown system if real-time results are not needed. Users can just record the raw output from the gyros and accelerometers and apply, in post mission, any mathematical models they choose for data integration, alignment and error estimation. The disadvantage of using the strapdown system is that more computation is required to process the data into velocities and coordinates.

Today, there are several strapdown reference/navigation units available on the market. Some use conventional gyros for rate measurement while others utilize RLG technology. The ring-laser-gyros are in general noisier than the well developed conventional gyros but, due to the absence of moving parts, they do not require as much power and frequent maintenance as the conventional ones. The new generation of ring-laser-gyros available to civilian user today are becoming comparable to conventional gyros in terms of accuracy and have the advantage of lower cost and higher reliability. Detailed descriptions of various kinds of strapdown gyros and accelerometers used in inertial navigation can be found in Savage (1978). The flexibility, reliability and lower initial cost are the main reasons for this effort to convert an RLG strapdown inertial reference unit into a SISS.

3.2.1 LTN-90-100

The Litton LTN-90-100 is a ring-laser-gyro inertial reference unit developed for civilian airlines. The system together with its control units weights about 29 kg. The system was designed to utilize the 400 Hz 115 VAC or 28 VDC current available in an aircraft. The total power requirement of the LTN-90-100 is about 150 watts. The system comes in four separate components : the inertial reference unit (IRU), mode selector unit (MSU), inertial sensor display unit (ISDU), and a DC or AC support tray. The inertial measurement unit contains the sensor block, microprocessors and the internal power supply. There is a panel of pins at the back of the IRU which allows the system to communicate with the other units or flight instruments and to receive power from the aircraft. The mode selection unit is a small instrument which is used to activate the system. It also displays the type of electric current used and indicates whether the system is still in alignment state. The inertial sensor display unit is the control unit which accepts the initial horizontal coordinates and displays horizontal coordinates, ground speed, track angle, azimuth and status of the system. The ISDU is designed to control three separate IRU simultaneously. The IRU can be supported by a tray which has a AC fans mounted on its bottom for cooling of the system. The tray is wired to take DC current from the IRU to power the fan. An AC version of the tray is also available to users who have access to continuous 400 Hz AC supply.

In its standard navigation mode, the LTN-90-100 requires 10 minutes for system alignment. At the beginning of the alignment, the user is expected to enter the initial latitude and longitude of the system. The LTN-90-100 also tries to obtain height information from the baro-altimeter in the aircraft, and will not output any vertical velocity and height data during alignment or navigation until the information is available. The initial latitude and temperature of the system must be between $\pm$ 70° and 0 to 80°C, respectively, for the system to initiate the alignment process. The LTN-90-100 outputs the roll and pitch of the sensor block almost immediately after it goes into alignment but it needs 4.5 minutes to determine a valid initial azimuth. The system also checks the validity of the input latitude by comparing it with the latitude it derives from the measurements. If the difference is greater than 30 arc minutes, the system remains in the alignment mode until it receives a set of valid initial coordinates. The system issues a flashing warning on the MSU during alignment when it experiences difficulties in getting the power or air for the AC fan to operate. The LTN-90-100 displays its ground speed immediately after it finishes the alignment and goes into navigation. During navigation, the LTN-90-100 checks the magnitude of its velocity and body rotation rates continuously and resets its velocity to zero if they are below a set of limits for more than three minutes. The system also performs a coordinate reset after the aircraft has remained stationary for more than 12 minutes. These features are built into the LTN-90-100 to improve the positioning accuracy of the system when the aircraft makes any intermediate stops along its route.

Several hardware and software modifications were made to the LTN-90-100 at The University of Calgary before it could be used for inertial surveying. A metallic case was built to hold all three units and the DC tray together. Wiring work was done to the DC tray to connect the power and I/O pins on the LTN-90-100 to an external DC power supply and the two control/display units. These modifications were done with information supplied by the staff of Litton Systems Canada in Toronto. After the wiring, the LTN-90-100 can be started with 24 VDC power from two deep-cycle batteries arranged in series. Special pins on the LTN-90-100 normally not used were connected to a switch so that the system can be changed from the standard navigation mode to the lab testing mode. In the lab testing mode, the LTN-90-100 disables the velocity and coordinates reset functions.

The output of the LTN-90-100 was designed to meet the requirements of aircraft navigation, and it is not precise enough for land surveying. Software modification were made by the manufacturer to output the data relevant to surveyors in higher precisions. This is accomplished by storing the data in larger numbers of bits in the data words. For example, the number of bits of the data word that carries the body acceleration was changed from 15 to 18. The data frequency was doubled to minimize the errors incurred during integration due to system noise and discretization error. In case of the body rates, the frequency was changed from 32 to 64 Hz. The precision of the modified output of the LTN-90-100 is shown in Table 3-1. The LTN-90-100 filters the data with a first-order lag filter or a second-order Butterworth filter before they are sent to the user. The second-order Butterworth filter for the body rates and accelerations was removed from the software to reduce the time delay of the output, and to avoid any systematic smoothing effect that the filter may have on the data. A very detailed description of the LTN-90-100 is given in Litton (1984).

3.2.2 Data Acquisition System

The raw output of the LTN-90-100 is sent to the flight computer and radar onboard an aircraft in ARINC 429 format through several output pins on the system. A survey user can record the data with an ARINC 429 compatible interface device. One such device was built by Pulsearch Technology Consolidated Ltd. of Calgary for The University of Calgary to receive data from the LTN-90-100. The device was designed to be fitted into an IBM PC-compatible computer such that a simple program can be run on the computer to record the incoming data rapidly. At present, the interface device is not yet capable of sending height information back to the LTN-90-100. Therefore no vertical velocity or height is output by the system to the user. A custom made 6/10 MHz IBM PC-compatible data acquisition system was built by the same company for recording the data and other surveying information in real time using DC power from an aircraft or two deep-cycle batteries. There are two 20-Mbyte hard disks in the data acquisition system. About 12 Mbytes of disk space is permanently used to store system software and processing programs and a maximum of 19 Mbytes of data can be stored in the system at a time. The data acquisition system can operate at either 6 or 10 MHz clock frequency but it can only record the data properly at 10 MHz. The combined power requirement of the LTN-90-100 and the data acquisition system is about 240 watt. A mass storage device capable of storing up to 2 Gbytes of data was acquired to store the large amount of data directly from the data acquisition system. A picture of the LTN-90-100 and the data acquisition system is shown in Figure 3-1.

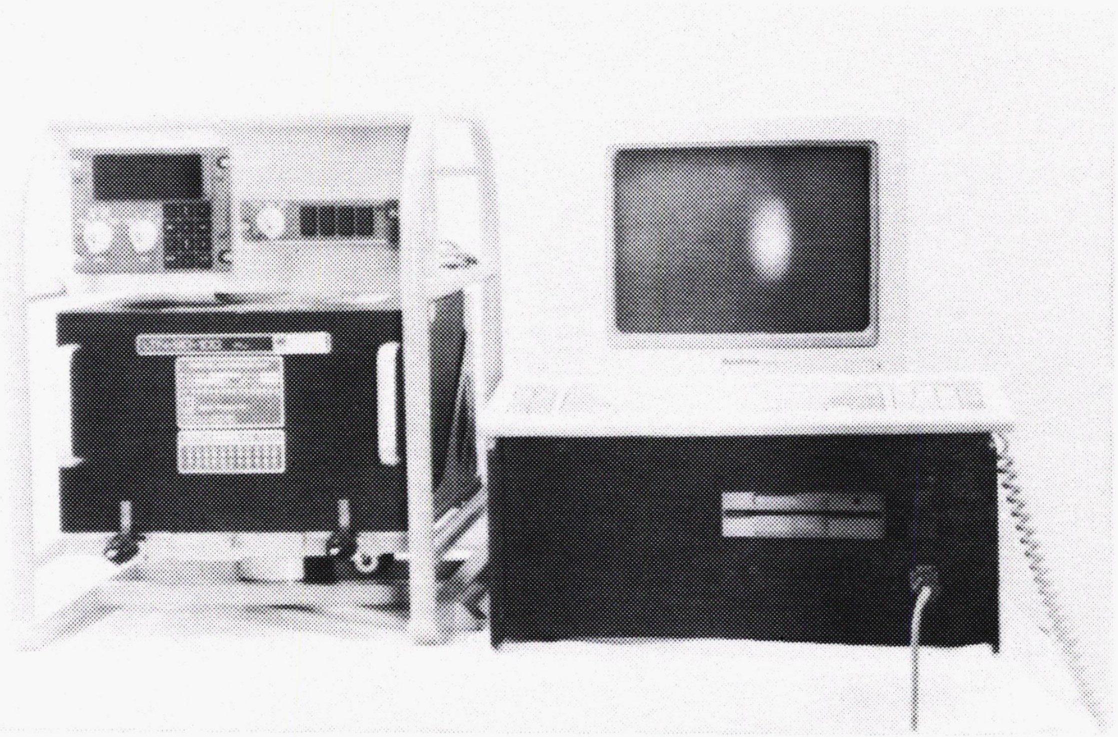

Figure 3-1 : The LTN-90-100 Based Strapdown Inertial Survey System

Two simple programs written in C language were developed with subroutines from Pulsearch to record the raw data as well as surveying station information supplied by the operator at the start of the survey. The first program records, at 16 Hz, the time, horizontal velocities and the Euler angles of the system. When the vehicle stops at a station, the program permits the operator to interact with the data acquisition system in real time so that he can mark the stop with the station number he entered into the system at the start of the survey. The operator can interrupt the data recording process by pressing a key on the keyboard of the data acquisition system. The keys to be pressed for various functions are :

(a) "c" for stop on a survey station and the beginning of velocity observation period;

(b) "z" for stop on an arbitrary point and the beginning of the velocity observation period;

(c) "f" for closing a data file and opening a second file; and

(d) "s" for terminating the execution of the program.

The number of every station is entered by the operator at the beginning of the survey. For a two-way survey, i.e. one forward run over the entire traverse and then a backward run, the number of each station is entered twice : once for the forward run and once for the backward run. The program is usually run right after the system finishes the alignment process. The data are stored in binary form and the program records about 1 Mbytes of data for every hour of navigation.

The second program has the same features as the first program except that it records the 64 Hz rate data, i.e. three body rates and three accelerations. Unlike recording the velocity data, at least 10 minutes of rate data need to be recorded for system alignment before moving the LTN-90-100 from the initial point. Due to the higher data rate, the second program records about 4 Mbytes of data for about one hour of operation.

3.2.3 Data Output

The modified output of the LTN-90-100 relevant to surveying is tabulated in Table 3-1. It shows that the precision of the coordinates of the system is about 17 m which is too low for surveying applications. More precise horizontal coordinates may be recovered by integrating the north and east velocities. These velocities have a precision of 0.008 m/s and have been smoothed by the filter built into the LTN-90-100. They do not change very much when the system is stationary over a short period of time. Thus, if velocity measurements of that period are needed, one observation should be sufficient to represent the entire sample. The low precision of the velocities is due to the truncation error in the output. The data are output as 18-bit integer words plus a sign bit and the range of the velocities is 2117 m/s. Since the largest possible integer of an 18-bit word is 2^{18} then the smallest velocity output possible is

$$\frac{2117 \text{ m/s}}{2^{18}} \approx 0.0081 \text{ m/s} . \tag{3-1}$$

The truncation error is a form of systematic error which can be reduced by adding or subtracting half of the maximum error to the number, i.e. 0.00405 m/s, depending on whether the number is positive or negative.

Parameter	Rate (Hz)	Range	Resolution	Accuracy (2σ)
Latitude	16	$\pm 180°$	19.127m	3.7km/h
Longitude	16	$\pm 180°$	19.127m	3.7km/h
Altitude*	32	±39928m	0.038m	1.524m
H. vel.	16	±2117m/s	0.008m/s	4.0m/s
V. vel.*	32	±162.6m/s	0.152m/s	1.52m/s
Roll & Pitch	64	$\pm 180°$	2.47"	1.0°
Azimuth	32	$\pm 180°$	2.47"	1.0°
Body rates	64	$\pm 128°$/s	1.757"/s	0.1°/s
Body accel.	64	± 39 m/s ^{2}	0.15mm/s^2	0.098m/s^2

* not available at present

Table 3-1 : Output of the LTN-90-100

The rate data on the other hand are a lot noisier. The vibration of the system caused by the dithers in the ring-laser-gyros and the cooling fan introduces high frequency noise to the sensor output. The dithers and fans are manufactured such that their frequency are restricted to the range of 380 to 420 Hz and the separation between the dither frequencies are greater than 5 Hz. Due to the much lower data sampling rate of 64 Hz, the effects of the vibration show up as very low frequency components in the frequency spectrum of the rate data. The apparent reduction in frequency of the output caused by the lower data sampling rate is known as aliasing effect. Detailed description and explanation of the effect can be found in Brigham (1974). As an example, the body accelerations of the SISS along its x-axis and the corresponding frequency plot derived by Fast Fourier Transform techniques are shown in Figure 3-2 and 3-3. Three large components can be seen in the spectrum near the 24-Hz mark. They correspond to the three dither frequencies of the RLG. The fourth component near the 8-Hz mark which is smaller than the three but still larger than the average component may be caused by the cooling fan. Using the least-squares forward-backward technique decribed in Blais and Vassiliou (1987), the relative power spectral densities (PSD) of the data was also derived and shown in Figure 3-4. The PSD plot clearly confirms the locations of these large frequency components. Fortunately, due to their high frequency nature, the effect of the vibration can be treated as random noise with zero mean in the long run. However, it does present a problem when the rate data are used to rapidly and coarsely align the system at the beginning of the system alignment process.

The errors caused by the vibration may be reduced by applying a second-order Butterworth filter to the rate data during coarse alignment. The derivation of a recursive second-order Butterworth for a discrete time-dependent data sample is well known and can, for instance, be found in Kanasewich (1981). Basically, a continuous second-order Butterworth filter satisfies the analogue transfer function

$$\frac{1}{s^2+\sqrt{2}s+1}\,, \tag{3-2}$$

where s is the normalized frequency variable. The recursive filter can be obtained by applying a bilinear transformation of equation (3-2). It consists of two steps. First the Z-transformation of the analog function to a discrete function is performed by substituting

$$s = \frac{\kappa(z - 1)}{(z + 1)}\,, \tag{3-3}$$

where z is the transform operator and κ is a transformation constant. The effect of the bilinear transformation is a warping of the discrete frequency to analog frequency, i.e.

$$\omega_a = \kappa \tan(\pi \omega_d \Delta t) , \tag{3-4}$$

where ω_a is the analogue frequency, ω_d is the discrete frequency and Δt is the sampling interval. In the second step, the transformation constant is chosen such that

$$1 = \kappa \tan (\pi \Delta t f_p) , \tag{3-5}$$

where f_p is the cutoff frequency. The result is a transfer function that links the input X in the frequency domain to the output Y as

$$Y = \frac{z^{-2} + 2z^{-1} + 1}{k_2 z^{-2} + k_1 z^{-1} + k_0} X , \tag{3-6}$$

where

$$k_0 = \kappa^2 + \sqrt{2}\kappa + 1 , \tag{3-7a}$$

$$k_1 = 2(1 - \kappa^2) , \tag{3-7b}$$

$$k_2 = \kappa^2 - \sqrt{2}\kappa + 1 , \tag{3-7c}$$

and

$$\kappa = \frac{1}{\tan(\pi f_p \Delta t)} . \tag{3-7d}$$

Multiplying the left hand side of equation (3-6) with the denominator on the right hand side one gets

$$Y = (z^{-2}X + 2z^{-1}X + X - k_2 z^{-2}Y - k_1 z^{-1}Y)/k_0 . \tag{3-8}$$

Since the effect of the z^{-1} operator on the input X and output Y is a shift in the time domain, the Z inverse transform of equation (3-8) becomes

$$y_k = (x_{k-2} + x_{k-1} + x_k - k_2 y_{k-2} - k_1 y_{k-1})/k_0 . \tag{3-9}$$

Equation (3-8) is the recursive second-order Butterworth filter for input x at epoch k. Note that the subscripts k, k-1, k-2 are used to denote the epoch of the input and output and they should not be confused with the coefficients k_0, k_1 and k_2. The recursive equation (3-9) can be initiated with y_0 and y_1 equal to the expected value of y such as the approximate mean of the sample.

In order to remove most of the noise caused by the system vibration, the cutoff frequency of the second-order Butterworth filter developed for all six rate data was chosen to be 1 Hz and its coefficients are

$$k_0 = 444.13204, \tag{3-10a}$$

$$k_1 = -826.69012, \tag{3-10b}$$

$$k_2 = 386.55808. \tag{3-10c}$$

The initial values of the rate data are computed by the transformations

$$\bar{\omega}_{ib}^{b} = \bar{\mathbf{R}}_{n}^{b}\, \omega_e \begin{pmatrix} 0 \\ \cos\phi \\ \sin\phi \end{pmatrix} \tag{3-11}$$

and

$$\bar{\mathbf{f}}^{b} = \bar{\mathbf{R}}_{n}^{b} \begin{pmatrix} 0 \\ 0 \\ \gamma \end{pmatrix}, \tag{3-12}$$

where γ is normal gravity and $\bar{\mathbf{R}}_{n}^{b}$ is the approximate attitude matrix computed from the approximate Euler angles obtained at initialization.

Results from the application of the filter show that the standard deviation of the sample of the data is reduced by an order of magnitude after filtering. As an example, the RMS of the rate data of a stationary LTN-90-100 before and after filtering are tabulated in Table 3-2 to show the effect of the 1-Hz Butterworth filter. They show that filtering reduces the noise considerably but does not change the mean very much. However, the effect on the mean is large enough to corrupt the precise determination of the Euler angles and velocities of the SISS in fine alignment and navigation. Therefore the filter is not used there.

Data	Before		After	
	Mean	RMS	Mean	RMS
x-body rate ("/s)	1.368	167.148	1.404	3.816
y-body rate ("/s)	-11.520	181.332	-11.448	20.52
z-body rate ("/s)	-12.060	203.580	-12.060	3.492
x-acc. (mgal)	10443	2742	10406	571
y-acc. (mgal)	-41891	3089	-41865	392
z-acc. (mgal)	-1404	3435	-1404	80

Table 3-2 : RMS of the Filtered Rate Data of a Stationary LTN-90-100

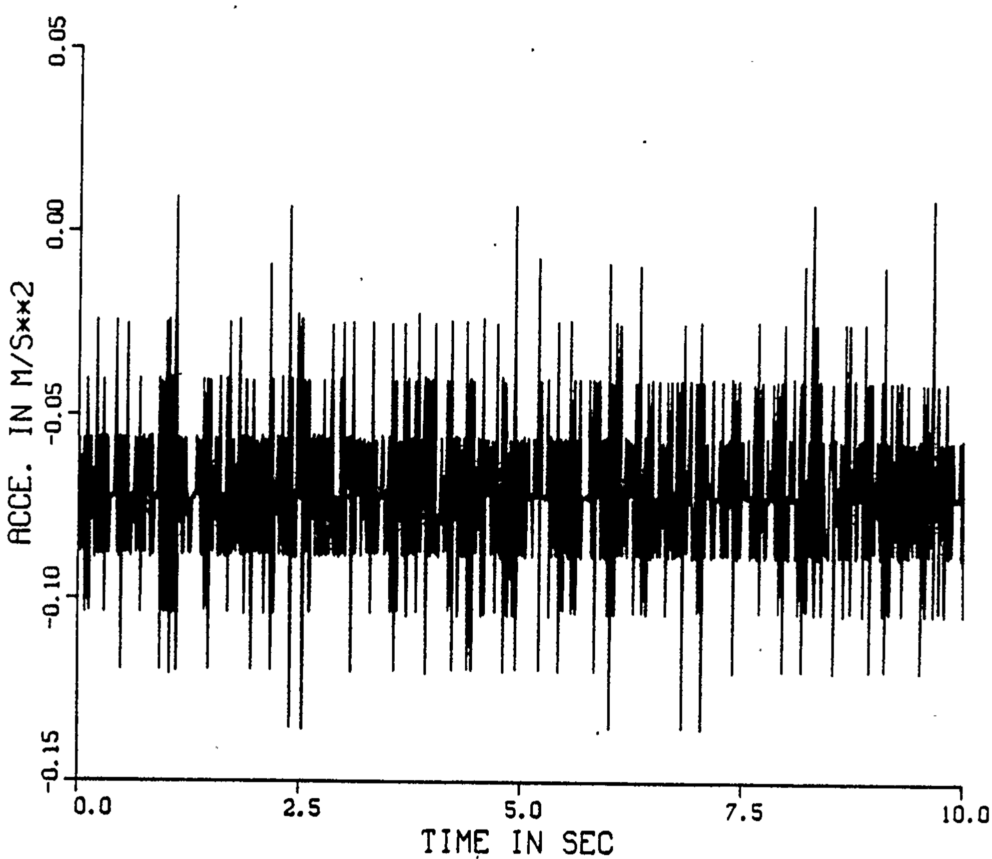

Figure 3-2 : X Body Acceleration of a Stationary LTN-90-100

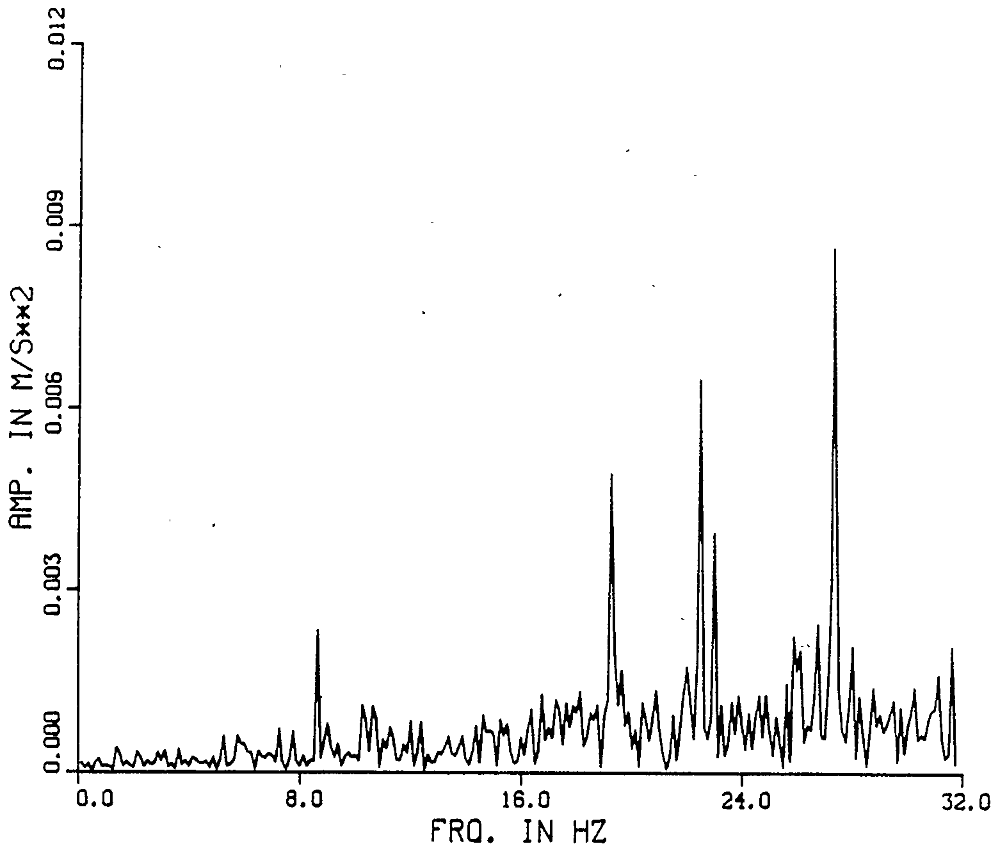

Figure 3-3 : Frequency Plot of the X Body Acceleration

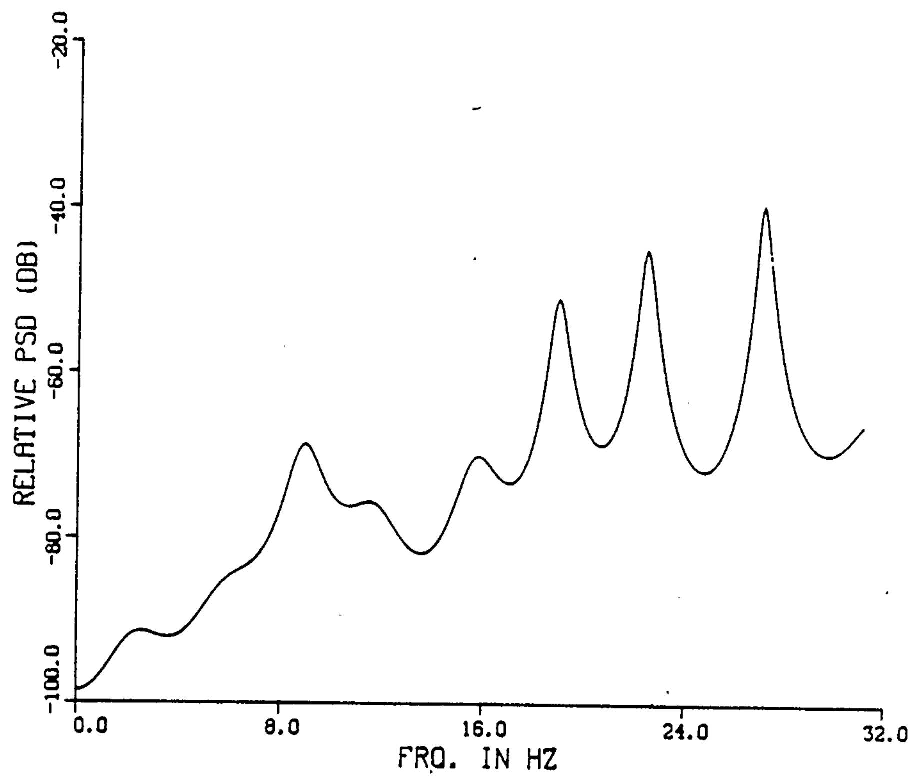

Figure 3-4 : Relative PSD of the X Body Acceleration

CHAPTER 4

NAVIGATION EQUATIONS

The two types of data recorded by the data acquisition software are either velocities and Euler angles or body rates and accelerations. The main task of any navigation software is to integrate these velocities and rates into velocities and coordinates. The integration of the velocity data is straightforward whereas a much more complex set of navigation equations is needed to process the rate data. The navigation equations in general form are well known, see Stieler (1981). However, the application of these equations to practical inertial surveying has never been published. The purpose of this chapter is to list the equations needed to integrate the two types of output of the LTN-90-100 recorded by the data acquisition software into the quantities that surveyors need. The initial Euler angles, 3-D velocities and coordinates are assumed to be approximately known at the beginning.

4.1 Velocity Integration Module

There are six numbers in each velocity data record. For a small time interval Δt, the north and east velocities can be directly integrated into change in the latitude and longitude using the equations

$$\Delta\phi = \frac{\Delta t V_N}{R_M + h} \tag{4-1}$$

and

$$\Delta\lambda = \frac{\Delta t V_E}{R_E + h \sec\phi}\ , \tag{4-2}$$

where

$$R_M = \frac{a(1-e^2)}{(1-e^2 \sin\phi)^{3/2}} \tag{4-3}$$

and

$$R_E = R_P \sec\phi. \quad (4\text{-}4)$$

The quantities R_M and R_E are the radii of curvature along the meridian and parallel respectively, and h is the ellipsoidal height of the strapdown inertial survey system. The current horizontal coordinates of the SISS can be obtained by simply adding these changes to the initial coordinates. The Euler angles in the data set are not used in the integration module for the velocity data. They are only needed later in the estimation process.

Since equations (4-1) and (4-2) require ellipsoidal height and the LTN-90-100 does not output height data without obtaining external height information first, the value of h may only be approximated by the mean height of the area of interest in terrestrial surveying. The accuracy of the integration can be significantly affected if the change in height in the area in drastic and large. The velocities are the result of integrating the rate data by the built-in software. Their accuracy is dependent on the alignment accuracy of the LTN-90-100 which deteriorates with time until a re-alignment is performed. In post-mission processing, the errors in the velocities can only be estimated but not removed. In other words, the situation is the same as processing the data from a gimballed system.

4.2 Rate Integration Module

Unlike the velocity integration, the navigation equations for the rate data are lengthy and more complex. Each record of rate data contains six numbers : the x-y-z body rates and the corresponding body accelerations. The integration of the data requires two recursive steps. First, the change of the Euler angles are computed from the body rates and then, in the second step, the body accelerations are transformed to the wander frame where they are integrated into changes in velocities and coordinates. The computation of the Euler angles can be accomplished by using numerical techniques such as the three-parameter propagation or the quaternion approach, see Giardina et al. (1981). All these methods have their advantages and disadvantages. The quaternion approach was adopted in this research mainly because it is numerically stable and efficient, and the normalization of the attitude matrix, i.e.body to wander frame transformation matrix, is less complex than the other methods. The use of quaternion and other methods for the propagation of the attitude matrix are well documented in the literature, e.g. Grubin (1970) , therefore it is not given here.

The LTN-90-100 is factory calibrated and the sensor biases in the system are compensated with the stored calibration parameters. However, due to errors in the calibration and is the different environments in which the systems are used, the biases cannot be completely removed by the application of calibration parameters alone. Users may have to perform, from time to time, their own in-house calibration to obtain additional calibration parameters which can account for the biases in the sensors and their working environment. The results of such an in-house calibration are usually 3 gyro drift and accelerometer bias correction parameters. The calibration procedure used in this research will be discussed in the next chapter.

The body rates of a SISS can be computed from the sensed body rates by the equation

$$\bar{\omega}_{ib}^{b} = \tilde{\omega}_{ib}^{b} - \bar{\mathbf{d}} \qquad (4\text{-}5)$$

and the specific force by

$$\bar{f}_{ib}^{b} = \tilde{\mathbf{a}} - \bar{\mathbf{b}} + g_o , \qquad (4\text{-}6)$$

where

$$g_o = \begin{pmatrix} 0 \\ 0 \\ 9.7802703 + 0.0517993\sin^2\phi - 19.694059h/a \end{pmatrix}, \qquad (4\text{-}7)$$

$\bar{\mathbf{d}}$ is the correction vector for the body rates, and $\bar{\mathbf{b}}$ is the correction vector for the body accelerations. The third element in g_o is the equation used in the LTN-90-100 for the computation of normal gravity. When external height information is not available the value of h in the formula is set to zero. This formula is not consistent with the normal gravity formula of the reference ellipsoid of interest therefore the value of g_o is added back to the measured accelerations to recover the specific force so that a proper formula may be applied later to compute the body acceleration with respect to the ellipsoid.

The raw angular rotation of the body with respect to the inertial frame, i.e. θ_{ib}^{b}, can be integrated from the compensated body rate, $\bar{\omega}_{ib}^{b}$ by

$$\theta_{ib}^{b} = \bar{\omega}_{ib}^{b}\,\Delta t\,. \tag{4-8}$$

Expanding the sine and cosine of the angular rotation body frame with respect to the inertial frame into Taylor series and truncating them after the fourth term results in

$$s\theta \equiv \frac{2\sin(\theta/2)}{\theta} \cong 1 - \frac{\theta^2}{24}\,, \tag{4-9}$$

$$c\theta \equiv 2(\cos(\theta/2) - 1) \cong 0.25(\,-\theta^2 + \frac{\theta^4}{48})\,, \tag{4-10}$$

where θ is the magnitude of θ_{ib}^{b}. Let

$$\theta_{iw}^{b} = \mathbf{R}_{w}^{b}\,\bar{\omega}_{iw}^{w}\,\Delta t \tag{4-11}$$

and

$$\Delta\theta = s\theta\,\theta_{ib}^{b} - \theta_{iw}^{b}\,, \tag{4-12}$$

then the quaternion components of the body to wander frame transformation can be propagated by the equations

$$q1 = q1 + 0.5(\,c\theta q1 + \Delta\theta_x q2 - \Delta\theta_y q3 + \Delta\theta_z q4\,) \tag{4-13a}$$

$$q2 = q2 + 0.5(\,-\Delta\theta_z q1 + c\theta q2 + \Delta\theta_x q3 + \Delta\theta_y q4\,) \tag{4-13b}$$

$$q3 = q3 + 0.5(\,\Delta\theta_y q1 - \Delta\theta_x q2 + c\theta q3 + \Delta\theta_z q4\,) \tag{4-13c}$$

$$q4 = q4 + 0.5(\,-\Delta\theta_x q1 - \Delta\theta_y q2 - \Delta\theta_z q3 + c\theta q4\,) \tag{4-13d}$$

for $\Delta\theta_x$, $\Delta\theta_y$ and $\Delta\theta_z$ being the x-y-z components of $\Delta\theta$. A detailed explanation of the propagation of the quaternion components is given in Appendix A. These quaternion components can be used to construct the body to wander frame transformation matrix. The relationship between individual element in the transformation matrix and quaternion components is given by the following equation:

$$R_b^w = \begin{pmatrix} q1^2 - q2^2 - q3^2 + q4^2 & 2(q1q2 - q3q4) & 2(q1q3 + q2q4) \\ 2(q1q2 + q3q4) & q2^2 - q1^2 - q3^2 + q4^2 & 2(q2q3 - q1q4) \\ 2(q1q3 - q2q4) & 2(q2q3 + q1q4) & q3^2 - q1^2 - q2^2 + q4^2 \end{pmatrix}. \tag{4-14}$$

In order to apply equation (4-13), one has to know the initial latitude and Euler angles so that the matrix R_w^b and the vector $\bar{\omega}_{iw}^w$ may be constructed for the initialization of the process. This information is obtained during the coarse alignment process. More discussion on the initialization will be given later.

The specific force in the body frame can be transformed to the wander frame via

$$\bar{f}_{ib}^w = R_b^w \bar{f}_{ib}^b . \tag{4-15}$$

The raw specific force contains the vehicle, Coriolis, gravitational and centrifugal accelerations. The non-vehicle accelerations must be removed from f_{ib}^w before it can be integrated into velocity increments.

The Coriolis acceleration is a velocity-dependent quantity and it can be computed as

$$\bar{a}_c^w = -\bar{V}_N(2\bar{\omega}_{ie}^w + \bar{\omega}_{ew}^w), \tag{4-16}$$

where

$$\bar{\omega}_{ie}^w = \begin{pmatrix} \omega_e \sin\bar{\alpha}\cos\bar{\phi} \\ \omega_e \cos\bar{\alpha}\cos\bar{\phi} \\ \omega_e \sin\bar{\phi} \end{pmatrix}, \tag{4-17}$$

$$\bar{\omega}_{ew}^{w} = \begin{pmatrix} -\bar{V}_y^w R_y^{-1} \\ \bar{V}_x^w R_x^{-1} \\ 0 \end{pmatrix}, \tag{4-18}$$

$$R_X = \frac{R_M R_P}{(R_M \cos\alpha - R_P \sin\alpha)}, \tag{4-19}$$

and

$$R_y = \frac{R_M R_P}{(R_M \sin\alpha + R_P \cos\alpha)} \quad . \tag{4-20}$$

The combined effect of the gravitational and the centrifugal acceleration on the specific force may be approximated by the free-air normal gravity formula for the WGS 80 ellipsoid (Moritz, 1984).

$$\hat{\gamma}_z^w = 9.780327(1 + 0.00527094\sin^2\phi + 0.0000232718\sin^4\phi) - 0.3086\cdot10^{-5}\hat{h} \tag{4-21}$$

The estimated height $\hat{h}$ in metre, is used in equation (4-21) to minimize the height-dependent vertical acceleration error, which accounts for the exponential growth behaviour of the error in height.

Once all components of the specific force are calculated, the change in velocity can be computed as

$$\Delta\bar{\mathbf{V}}_k^w = \Delta t\,(\bar{\mathbf{f}}_{ib}^w - \bar{\mathbf{a}}_c^w - \hat{\gamma}^w) \tag{4-22}$$

where the subscript k denotes the present epoch. The velocity of the present epoch can be expressed as

$$\bar{\mathbf{V}}_k^w = \bar{\mathbf{V}}_{k-1}^w + 0.5(\,\Delta\bar{\mathbf{V}}_k^w + \Delta\bar{\mathbf{V}}_{k-1}^w)\,. \tag{4-23}$$

Since the computation of the various components of the specific force are dependent on the velocity of the vehicle, the errors due to the use of time-lagged velocity in the computation may be reduced by repeating equations (4-16) to (4-23). Obviously, the change in velocity must be stored for the computation in the next epoch.

The integration of the change in velocity into change in position can be divided into two parts : the propagation of the wander to earth transformation matrix and the computation of the change in height. The horizontal coordinates of the SISS and the wander azimuth can be computed from the elements of the matrix $\mathbf{R}_w^e$ after the propagation of the matrix. The required equations for the two parts are

$$(\mathbf{R}_w^e)_k = (\mathbf{R}_w^e)_{k-1} + \Delta t\, \Omega_{ew}^w\, (\mathbf{R}_w^e)_{k-1} \,, \tag{4-24}$$

and

$$\bar{h}_k = \bar{h}_{k-1} + \Delta t V_z^w \,. \tag{4-25}$$

After the propagation of the wander to earth transformation matrix, a new $\bar{\omega}_{ew}^w$ can be computed, and thus a more accurate $\mathbf{R}_b^w$ matrix by repeating equations (4-8) to (4-14).

Whenever they are needed, the Euler angles of the SISS can be computed from the elements of the body to wander frame transformation matrix, i.e.

$$\text{pitch} = \sin^{-1}\left(\mathbf{R}_{wd}^w(3,2)\right), \tag{4-26}$$

$$\text{roll} = \tan^{-1}\left(\frac{-\mathbf{R}_{wb}^w(3,1)}{\mathbf{R}_{wb}^w(3,3)}\right), \tag{4-27}$$

and

$$\text{azimuth} = \tan^{-1}\left(\frac{-\mathbf{R}_{wb}^w(1,2)}{\mathbf{R}_{wb}^w(2,2)}\right) - \alpha \tag{4-28}$$

The wander angle α, the latitude, and longitude of the SISS can be obtained from the elements of the wander to earth transformation matrix, i.e.

$$\bar{\phi} = \sin^{-1}\left(\mathbf{R}_w^e(3,3)\right), \tag{4-29}$$

$$\bar{\lambda} = \tan^{-1}\left(\frac{\mathbf{R}_w^e(2,3)}{\mathbf{R}_w^e(1,3)}\right), \tag{4-30}$$

and

$$\bar{\alpha} = \tan^{-1}\left(\frac{\mathbf{R}_w^e(3,1)}{\mathbf{R}_w^e(3,2)}\right). \tag{4-31}$$

The navigation equations given in this section describe an iterative process therefore certain quantities must be made available or initialized before the process can start. These quantities are the Euler angles, the velocities and the coordinates of the SISS at the initial epoch. During the coarse alignment process, approximate values for each of the Euler angles are computed from the raw measurements for the initialization. With these angles, one can compute the body to wander transformation matrix by substituting the yaw in equations (2-14a) to (2-14i) by the wander yaw. If the wander angle is set to zero at the initial epoch, then the wander azimuth is equal to the azimuth of the SISS. The quaternion components corresponding to the transformation matrix are :

$$q4 = 0.5\sqrt{1 + \mathbf{R}_b^w(1,1) + \mathbf{R}_b^w(2,2) + \mathbf{R}_b^w(3,3)} \tag{4-32a}$$

$$q1 = 0.25(\mathbf{R}_b^w(3,2) - \mathbf{R}_b^w(2,3))/q4 \tag{4-32b}$$

$$q2 = 0.25(\mathbf{R}_b^w(1,3) - \mathbf{R}_b^w(3,1))/q4 \tag{4-32c}$$

$$q3 = 0.25(\mathbf{R}_b^w(2,1) - \mathbf{R}_b^w(1,2))/q4 \tag{4-32d}$$

Another quantity that must be initialized at the starting epoch is the wander to earth transformation matrix. Given the initial latitude, longitude and wander angle, the matrix can be computed with the equation (2-12). A general flowchart, that describes the flow of data within the integration module developed for the rate data from the LTN-90-100 with the navigation equations listed in this chapter, is shown in Figure 4-1. The equations in this chapter are written specifically for an inertial strapdown survey system in the land-vehicle mode. However, only minor changes may be necessary to adapt these equations to the aircraft or ship-mode SISS. In the airborne or marine environment, external height information may be available and can be used instead of the estimated height to compute normal gravity. The different dampening effects when using various external heights would cause small changes to the error model used in estimating the height error.

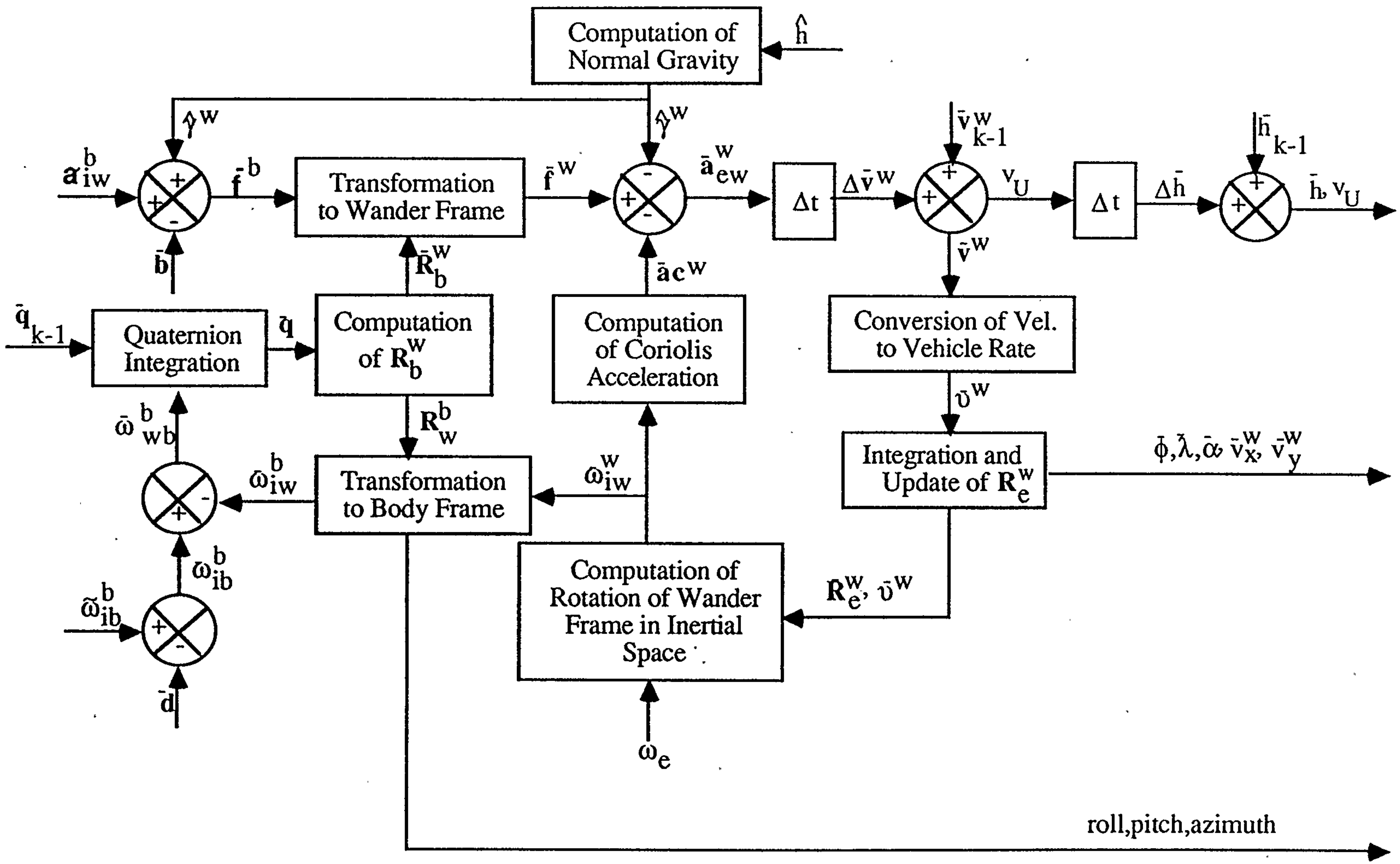

Figure 4-1 : Flow Chart of the Integration Module for the Rate Data

CHAPTER 5

ALIGNMENT

Alignment of a stationary strapdown inertial survey system is a process whereby the initial Euler angles or the attitude matrix of the system are determined from its sensor output, approximate coordinates and the observed velocities. This process is divided into two parts : the coarse and the fine alignment. During the coarse alignment, approximate values for the roll, pitch and azimuth of the system are rapidly obtained from the rate data and approximate coordinates. The approximate Euler angles are refined in the fine alignment process by a Kalman filter using the raw velocity data from the rate integration module as external observations in the measurement update. Alignment is necessary when processing the rate data because the initial orientation of the SISS is unknown. Usually, the surveyor can obtain a rough indication of the yaw of the system with a magnetic compass and, since the SISS is usually set up on a relatively level surface, the roll and pitch of the system may be considered zero. However, the errors in these values are too large to be used as initial values for fine alignment . The Kalman filter used in fine alignment is a first-order error estimation tool therefore the coarse alignment process is needed to estimate a better set of Euler angles. This chapter presents the equations used in the alignment module developed for the LTN-90-100 rate data.

5.1 Coarse Alignment

The approximate value of the yaw of the SISS can be directly computed from the mean value of the x and y body rotation rates through an iterative process if the approximate coordinates of the system are given. When the system is stationary the sensed rate data are the components of earth's rate of rotation and of the gravity vector in the body frame. Assuming that the rate data have been filtered by the second-order Butterworth filter, the mean value of the x and y body rates can be written as

$$[\hat{\omega}_i]^b_{ie} = \frac{1}{J}\sum_{k=0}^{J} {}_k[\bar{\omega}_i]^b_{ie} , \tag{5-1}$$

where J is the size of the data sample used and i denotes the x or y-axis. The body rates in equations (5-1) should be the body rates corrected for gyro biases. The approximate wander yaw of the system, i.e. the angle on the horizontal plane measured from the y-axis of the wander frame, can be computed with equations

$$\bar{\omega}^w_{ie} = \bar{R}^w_b \, \bar{\omega}^b_{ie} , \tag{5-2}$$

$$\bar{y}^w = -\tan^{-1}\left(\frac{[\hat{\omega}_x]^w_{ie}}{[\hat{\omega}_y]^w_{ie}}\right)$$

$$= \bar{y} + \alpha_0 . \tag{5-3}$$

The quantities $[\hat{\omega}_x]^w_{ie}$ and $[\hat{\omega}_y]^w_{ie}$ in equation (5-3) are the x and y components of the vector $\hat{\omega}^w_{ie}$. If the initial wander angle is chosen to be zero, then the yaw is equal to the wander yaw at the initial point. Since equation (5-2) requires the knowledge of the attitude matrix, the computation of the yaw or wander yaw can only be done in an iterative manner. In the coarse alignment module developed for the LTN-90-100 data, the attitude matrix is updated and reset every 4 seconds with the approximate yaw obtained in the coarse alignment. The roll and pitch of the system, needed to complete the update, will be discussed later in this section.

The error in the approximate wander yaw can be derived by applying the law of error propagation to equation (5-3) to get

$$\delta\bar{y}^w = \frac{-\cos(y)\,\delta[\hat{\omega}_x]^w_{ie} + \sin(y)\,\delta[\hat{\omega}_y]^w_{ie}}{\omega_e \cos\phi}\,. \tag{5-4}$$

Equation (5-4) show that, due to the fact that the earth has a rotation rate of ≈ 15 arcsec/s, an error of 0.26 arcsec/s in the body rates can introduce a one degree error in the wander yaw. That is the reason for the application of the second-order Butterworth filter to reduce the size of the random noise caused by the vibration of the system. The effect of the random noise can also be reduced if a large sample of data is used to determine the mean value of the x and y body rates, although that increases the computation time.

The coarse leveling of the SISS involves the use of the raw velocities from the integration module. The approximate roll and pitch of the system can be determined in two steps. First, the 3-D velocities are transformed to the body frame by

$$\bar{v}^b = \bar{\mathbf{R}}^b_n\, v^{\bar{n}} \tag{5-5}$$

and then, in the second step, the error in roll and pitch are computed by the equations

$$\delta\bar{r} = \sin^{-1}\left(\frac{\bar{v}^b_x}{T\gamma}\right) \tag{5-6}$$

and

$$\delta\bar{p} = -\sin^{-1}\left(\frac{\bar{v}^b_y}{T\gamma}\right), \tag{5-7}$$

where T is the time between velocity and attitude resets. During the reset, the velocities are set to zero and the errors in the Euler angles are subtracted from the approximate values.

If the initial latitude of the SISS is known, the drift in the z-gyro may be computed as

$$b_z = [\hat{\omega}_z]^b_{ib} - \omega_e \sin\phi\,. \tag{5-8}$$

The coarse alignment usually takes about 1 minute to converge to an accurate solution. Lab tests show that, during coarse alignment on a stable surface, the yaw or azimuth of the system can be determined to an accuracy of one degree while the roll and pitch are good to about 40 arcsec. Figure 5-1 shows the general flow of data in the coarse alignment module developed for the data from the LTN-90-100.

5.2 Fine Alignment

The fine alignment process that follows the coarse alignment is actually a special case of inertial surveying. During standard inertial surveying, the system stops regularly to update its error states with velocity measurements and, whenever it is necessary, resets its raw navigation quantities with the estimated values. In fine alignment, the system is stationary. The interval between updates is much shorter, for example 10 seconds, and the reset is done after every update. The estimation software required for the fine alignment is the same as the one used in surveying with some minor changes. A Kalman filter was developed to estimate the errors in the navigation quantities, and any residual biases in the sensors that are not removed in the system calibration. The errors are called the error states of the SISS, and the vector that contains these errors are the state vector. In this section, only the use of the estimated error states to align the SISS is discussed. Details on the Kalman filter will be presented later in Chapter 6.

The state vector of the Kalman filter consists of the misalignment errors between the platform frame and the local-level frame, errors in the coordinates and velocities, residual gyro drifts and accelerometer biases. These errors are estimated with velocity measurements during fine alignment. If the alignment errors are denoted as

$$\varepsilon^n = [\ \varepsilon_E, \varepsilon_N, \varepsilon_U\ ]^T , \qquad (5\text{-}9)$$

where

ε_E is the misalignment of the east axis,

ε_N is the misalignment of the north axis, and

ε_U is the misalignment of the vertical axis, i. e. yaw error,

and if it is assumed that the second-order errors are negligible, the relationship between the true and approximate attitude matrix can be expressed as

$$\mathbf{R}_b^n = (\mathbf{I} - \mathbf{E})\, \tilde{\mathbf{R}}_b^n , \tag{5-10}$$

where $\mathbf{E}$ is the skew-symmetric matrix

$$\mathbf{E} = \begin{pmatrix} 0 & -\varepsilon_U & \varepsilon_N \\ \varepsilon_U & 0 & -\varepsilon_E \\ \varepsilon_N & \varepsilon_E & 0 \end{pmatrix} . \tag{5-11}$$

This relationship can be applied to reset the attitude matrix and the Euler angles with the misalignment errors estimated by the Kalman filter. Equation (5-10) is based on the assumption that the misalignment errors of the system are small. Any large misalignment and second-order errors can cause the process to diverge. That is the reason for performing the coarse alignment as accurately as possible before the fine alignment.

Since the yaw is different from the wander yaw by the wander angle, α, equations similar to equations (5-10) can be derived to reset the $\mathbf{R}_b^w$ matrix. The relationship between the error in the yaw and the wander yaw can be written as

$$\varepsilon_{\text{wander yaw}} = \varepsilon_U - \delta\alpha . \tag{5-12}$$

Since

$$\dot{\alpha} = -\dot{\lambda} \sin\phi , \tag{5-13}$$

the error $\delta\alpha$ can be expressed as

$$\delta\alpha = -\int_0^t \delta\dot{\lambda} \sin\phi \, d\tau$$

$$\cong -\sum_{i=1}^{n} \Delta t \; \delta\dot{\lambda}_i \sin\phi_i , \tag{5-14}$$

where $\delta\dot{\lambda}$ is the error of the rate of longitude, for $n = t/\Delta t$. Thus, the roll, pitch and wander yaw can be updated with equations (5-10) and (5-11) by substituting ε_U by $\varepsilon_{\text{wander yaw}}$ and $\mathbf{R}_b^n$ by $\mathbf{R}_b^w$.

During fine alignment, the coordinates of the initial point, if known, can be used as update measurements to improve the estimates of the Kalman filter. However, due to the accurate velocity updates, the coordinate update usually does not bring substantial improvement to the estimated misalignment errors. It is recommended that these be performed only at the beginning and end of the fine alignment period.

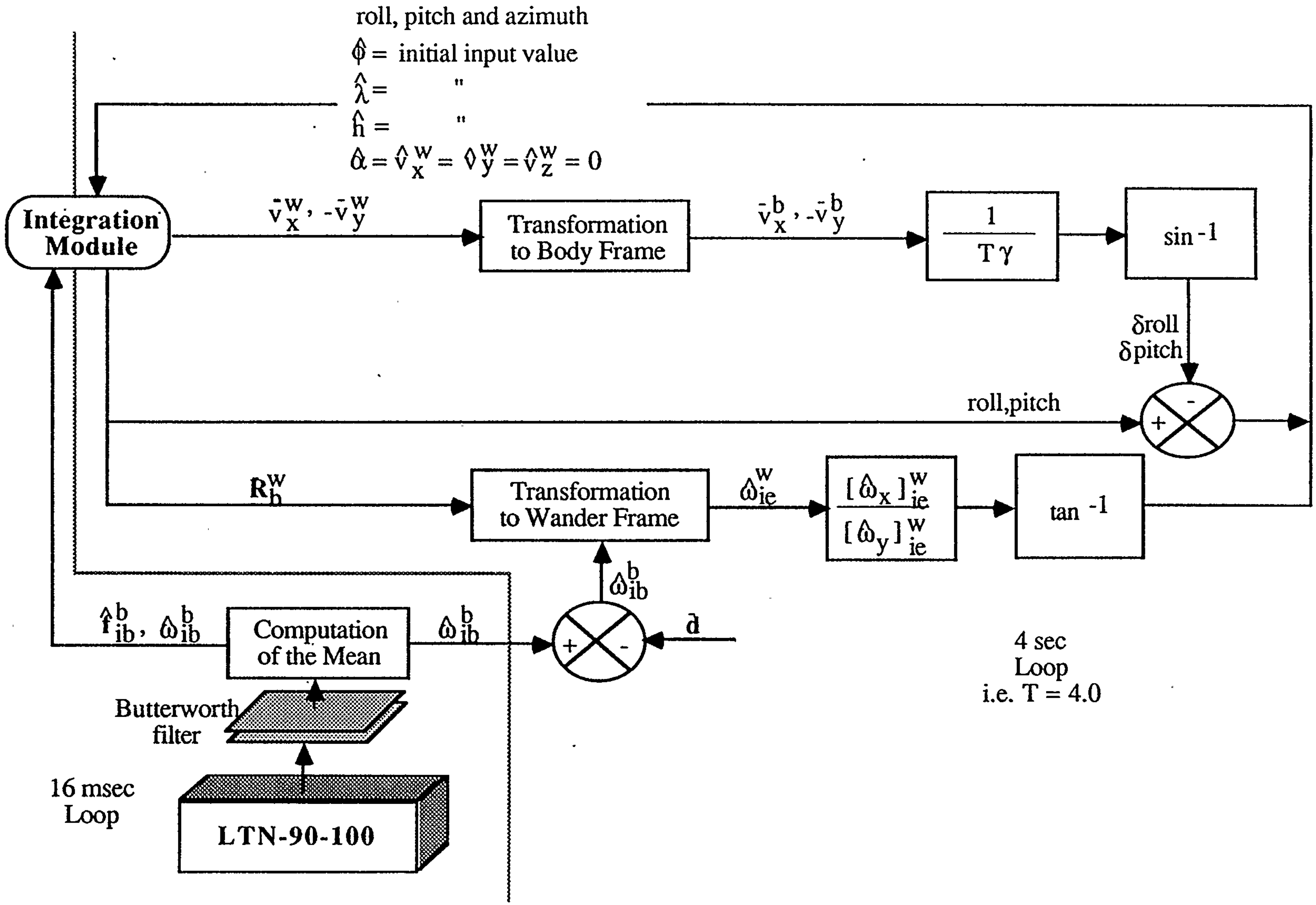

Figure 5-1 : The General Flow of Data in the Coarse Alignment Module

CHAPTER 6

ERROR ESTIMATION

Systematic errors in the sensors of a strapdown inertial survey system are usually invariant with respect to time. Unfortunately, due to the interdependent relationship between the navigation quantities, the effect of the sensor errors on the error states of the SISS is cumulative and time-dependent. Analytical formulae for the behaviour of the effect given in Wong (1979) show that the errors in the alignment, horizontal velocities and coordinates are bounded and sinusoidal while errors in the vertical velocity and height grow exponentially. The unbounded growth of the errors in the vertical velocity and height are mainly caused by the error in computing the normal gravity with the raw height. They can be dampened if an external height is used instead.

There are many ways to estimate the time-dependent errors of the raw navigation quantities generated by the integration module. Some of the techniques are stochastic, such as Kalman filtering and smoothing (Wong, 1982), and others are combinations of stochastic and deterministic methods, for example the spectral decomposition method (Vassiliou, 1983) and least-squares quadratic curve fitting (Schwarz, 1985). Results from the application of these techniques show that they all yield sub-metre (1σ) accuracy on an L-shaped traverse. The spectral decomposition method, which can only be applied in post mission, and least-squares curve fitting have been tested with data from a Ferranti Inertial Land Surveyor on land. However, these two methods are either incapable or not refined enough to utilize a wide variety of external measurements to estimate the error states of the inertial survey system. On the other hand, the Kalman filtering and smoothing approach allows the user to include data from external sensors, such as GPS satellite receivers, radio-navigation systems and baro-altimeters, to update its state vector. For that reason, a

Kalman filter-smoother was developed to estimate the error states of the strapdown inertial survey system.

6.1 Kalman Filtering

The derivation of the Kalman filtering equations is well documented in literature on linear optimal estimation, e.g. Gelb (1974) and Schwarz (1980) therefore it is not given here. The filter is a linear optimal estimator for a set of time-dependent error states $\mathbf{x}$ which obeys the condition that

$$\dot{\mathbf{x}} = \mathbf{F}\mathbf{x} + \mathbf{w} , \tag{6-1}$$

where

$\mathbf{x}$ is the state vector,

$\mathbf{F}$ is the dynamics matrix of the system and

$\mathbf{w}$ is the system noise.

In this case, the error states are the first-order error of the navigation quantities generated by the integration module and the residual sensor errors, i.e.

$$\mathbf{x} = [\ \varepsilon_N, \varepsilon_E, \varepsilon_U, \delta\phi, \delta\lambda, \delta\dot{\phi}, \delta\dot{\lambda}, \delta h, \delta\dot{h}, d_x, d_y, d_z, b_x, b_y, b_z\ ]^T , \tag{6-2}$$

where

$\varepsilon_N, \varepsilon_E, \varepsilon_U$ are the three misalignments of the platform frame,

$\delta\phi, \delta\lambda, \delta h$ are the error states in latitude, longitude and height,

$\delta\dot{\phi}, \delta\dot{\lambda}, \delta\dot{h}$ are the error states in latitude, longitude and height rates,

d_x, d_y, d_z are the x-y-z residual gyro drifts in the body frame in arcsec/sec and

b_x, b_y, b_z are the x-y-z residual accelerometer biases in m/s^2.

The variance-covariance matrix of the state vector at epoch k

$$\mathbf{C}_{x,\,k} = E\{[x_k-\hat{x}_k][x_k-\hat{x}_k]^T\} = \mathbf{C}_{X,\,k} , \tag{6-3}$$

becomes the variance-covariance matrix of the estimated navigation quantities

$$\hat{X}_k = \bar{X}_k - \hat{x}_k . \tag{6-4}$$

The vector $\bar{\mathbf{X}}$ in equation (6-4) contains raw integrated data from the integration modules and the corrections $\bar{\mathbf{d}}$ and $\bar{\mathbf{b}}$ obtained from system calibration. The estimated navigation quantities are obtained by subtracting the corresponding error states from these integrated data.

Assuming a zero mean for the system noise $\mathbf{w}$ in between epoch o and k, the solution to the first-order homogeneous differential equation (6-1) is

$$x_k = \Phi_{k,o}\, x_o \,, \tag{6-5}$$

where Φ is the transition matrix which can be expressed as

$$\Phi = e^{\Delta t \mathbf{F}} \,, \tag{6-6}$$

for a dynamics matrix with constant coefficients. Equation (6-4) can be expanded into a Taylor series

$$\Phi = \mathbf{I} + \Delta t\mathbf{F} + 0.5\Delta t\mathbf{F}^2 + \ldots\ldots\ldots\ldots\ldots \tag{6-7}$$

if $\mathbf{F}$ is constant in the interval Δt (see Wong, 1979). For small Δt, equation (6-7) can be approximated by

$$\Phi = \mathbf{I} + \Delta t\mathbf{F} \,. \tag{6-8}$$

The total transition matrix between epoch o and k becomes the product

$$\Phi_{o,k} = \prod_{i=1}^{k} \Phi_{i,i-1} \,. \tag{6-9}$$

The error propagation of the state vector is obtained from equation (6-5), i.e.

$$x_i = \Phi_{i,i-1}\, x_{i-1} \,, \tag{6-10}$$

and its variance-covariance matrix from the application of the covariance law

$$\mathbf{C}_{x,i} = \Phi_{i,i-1}\, \mathbf{C}_{x,i-1}\, \Phi^T_{i,i-1} + \mathbf{C}_w \,, \tag{6-11}$$

where

$$\mathbf{C}_w = \int_0^{\Delta t} \Phi_{i,i-1}\, \mathbf{Q}\, \Phi^T_{i,i-1}\, dt \tag{6-12}$$

$$\cong \int_0^{\Delta t} (\mathbf{I} + \Delta t\mathbf{F})\mathbf{Q}(\mathbf{I} + \Delta t\mathbf{F})^T$$

$$\cong [\,\Delta t\mathbf{Q} + 0.5\Delta t^2\mathbf{FQ} + 0.5\Delta t^2\mathbf{QF}^T + \ldots\ldots]_0^{\Delta t}$$

$$\cong \Delta t\mathbf{Q}\ ,$$

and $\mathbf{Q}$ is the spectral density matrix of the system noise $\mathbf{w}$. The matrix $\mathbf{C_w}$ is the variance-covariance matrix that accounts for the noise in the sensors.

Whenever an external measurement is available in the form of

$$\mathbf{y} = \mathbf{Hx} + \mathbf{e}\ , \tag{6-13}$$

where $\mathbf{y}$ is the vector of measurements, $\mathbf{H}$ is the design matrix and $\mathbf{e}$ is the measurement noise, the propagated state vector can be estimated or updated by the Kalman update equations

$$\mathbf{K} = \mathbf{C_x}(-)\mathbf{H}^T(\mathbf{HC_x}(-)\mathbf{H}^T + \mathbf{C_y})^{-1}\ , \tag{6-14}$$

$$\mathbf{x}(+) = \mathbf{x}(-) - \mathbf{K}(\mathbf{Hx}(-) - \mathbf{y}) \tag{6-15}$$

and

$$\mathbf{C_x}(+) = (\mathbf{I} - \mathbf{KH})\mathbf{C_x}(-)\ . \tag{6-16}$$

Here

$\mathbf{K}$ is the gain matrix and

$\mathbf{C_y}$ is the variance matrix of the measurements.

The symbols (-) and (+) in equations (6-14) to (6-16) denote quantities before and after measurement update.

During alignment or navigation, velocity information can be obtained either by stopping the vehicle or by external velocity sensors. If the vehicle is not moving the non-zero raw velocity output is equal to the velocity error states. The observation equations for the 3 velocities become

$$\tilde{v}_E = \overline{v_E} - R_E\,\delta\dot{\lambda}\ , \tag{6-17}$$

$$\tilde{v}_N = \overline{v_N} - R_M\,\delta\dot{\phi}\ , \tag{6-18}$$

and

$$\tilde{v}_U = \bar{v_U} - \delta\dot{h} \,. \tag{6-19}$$

Similar equations can also be derived for the control coordinates of the known stations on the traverse, i.e.

$$\tilde{\lambda} = \bar{\lambda} - R_E \, \delta\dot{\lambda} \,; \tag{6-20}$$

$$\tilde{\phi} = \bar{\phi} - R_M \, \delta\dot{\phi} \,, \tag{6-21}$$

$$\tilde{h} = \bar{h} - \delta\dot{h} \,. \tag{6-22}$$

There are two quantities in the Kalman filtering equations that distinguish them from sequential adjustment formulae : the dynamics matrix **F** and the spectral density matrix **Q**. Sequential adjustment is basically a special case of Kalman filtering when

$$\mathbf{F} = \mathbf{Q} = 0. \tag{6-23}$$

The most difficult part of implementing a Kalman filter is finding the most efficient way to propagate the variance-covariance matrix of the state vector. More than 70% of the computation time of the filtering process may be spent on repeating the execution of equation (6-11). In the Kalman filter developed for the LTN-90-100, a simple algorithm that takes advantage of the sparsely populated characteristic of the dynamics matrix is used to propagate the variance-covariance matrix of the state vector of the SISS. The flow chart of the Kalman filter and its error propagation routine are shown in Figures 6-1a, 6-1b and 6-2.

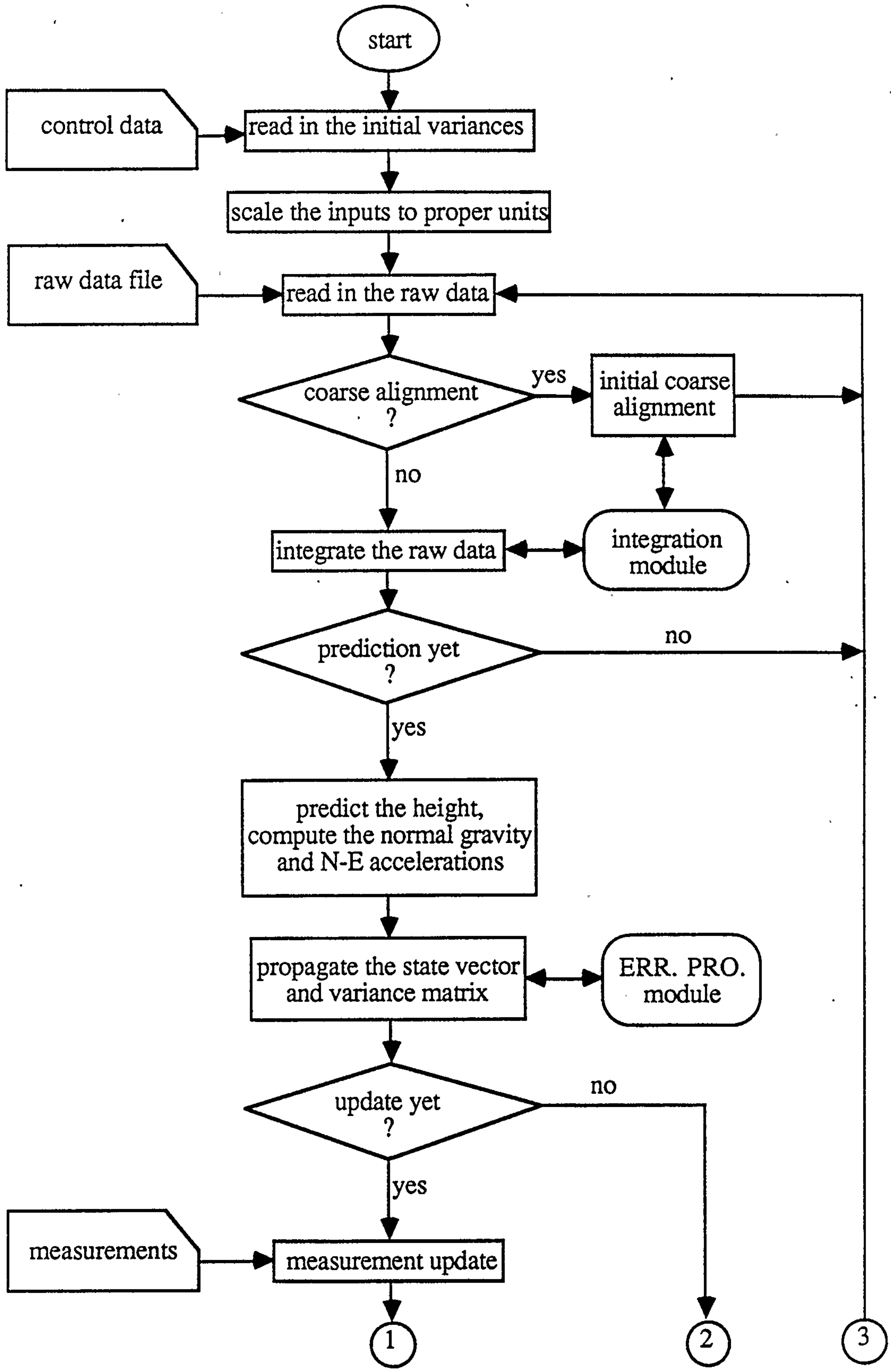

Figure 6-1a : Part 1 of the Flow Chart of the Kalman Filter

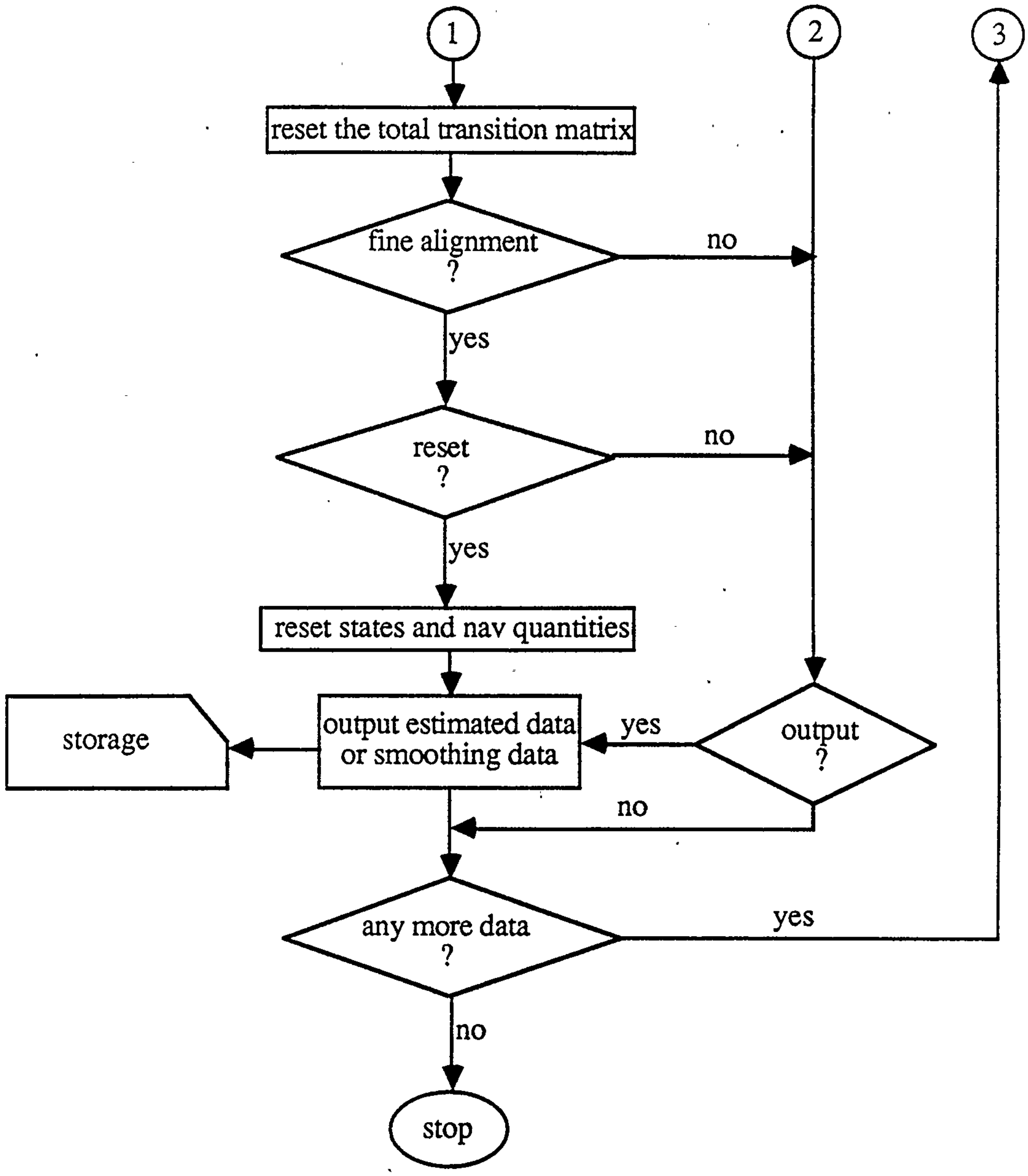

Figure 6-1b : Part 2 of the Flow Chart of the Kalman Filter

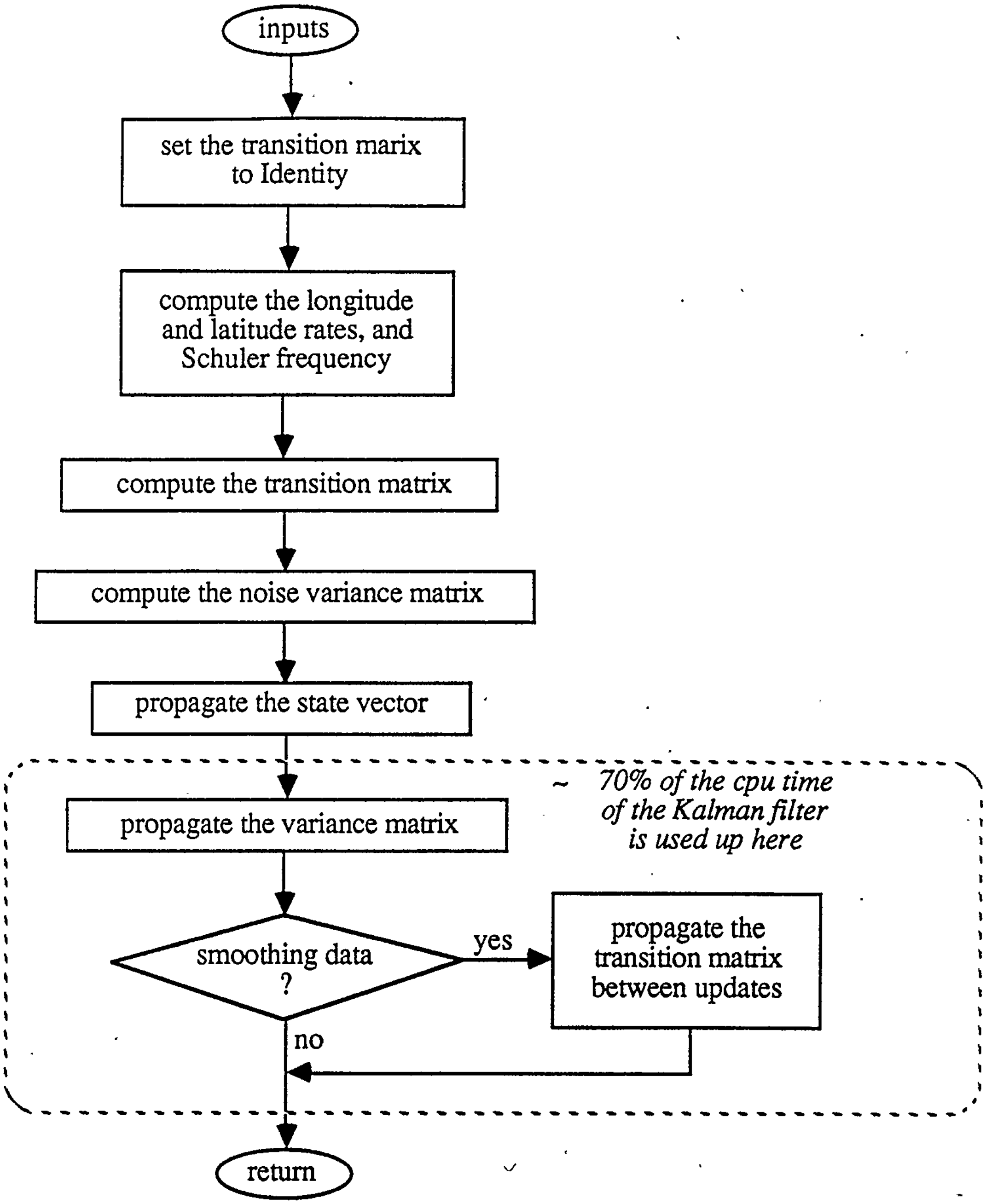

Figure 6-2 : Flow Chart of the Error Propagation Routine

6.2 Error Equations

In order to apply the Kalman filtering equations in the estimation of the error states of a strapdown inertial survey system, one must develop a dynamics matrix that can describe their rates of change. This section contains the derivation of the error equations used in the development of the dynamics matrix of a SISS. The error equations are equations that satisfy the condition given by equation (6-1). These equations can be derived by the perturbation approach which examines the error states as perturbation of the navigation quantities under the influence of various error sources (Benson, 1975). In this approach, the first-order differential equation for the error states is obtained by applying the law of error propagation to the expression for the rate of change of the navigation quantities.

The raw angular rate of the body frame with respect to the local-level frame can be derived by subtracting the angular rate of the local-level frame with respect to inertial space from the measured body rates of the SISS

$$\bar{\omega}^{b}_{nb} = \tilde{\omega}^{b}_{ib} - \bar{\mathbf{R}}^{b}_{n}\bar{\omega}^{n}_{in} , \tag{6-24}$$

where

$$\bar{\mathbf{R}}^{b}_{n} = \mathbf{R}^{b}_{n}(\mathbf{I} - \mathbf{E}) . \tag{6-25}$$

Since ω^{b}_{nb} is the relative angular rate between the body and the local-level frame, its errors are also the rates of the three misalignments of the sensor block coordinatized in the body frame. These errors $\delta\bar{\omega}^{b}_{nb}$ can be expressed as

$$\delta\bar{\omega}^{b}_{nb} = \mathbf{R}^{b}_{n}\, \mathbf{E}\, \bar{\omega}^{n}_{in} - \mathbf{R}^{b}_{n}\, \delta\bar{\omega}^{n}_{in} + \delta\tilde{\mathbf{d}} , \tag{6-26}$$

where $\delta\mathbf{d}$ is the residual gyro drift vector. By rearranging the elements in the first term of equation (6-26) and multiplying both sides of the equation by $\mathbf{R}^{n}_{b}$, one can obtained the final vector expression of the error equations of the misalignments

$$\delta\bar{\omega}_{nb}^{n} = \dot{\varepsilon}$$

$$= -\Omega_{in}^{n}\varepsilon - \delta\bar{\omega}_{in}^{n} + \mathbf{R}_{b}^{n}\,\delta\mathbf{d} \qquad (6\text{-}27)$$

for

$$-\Omega_{in}^{n} = \begin{pmatrix} 0 & \omega_e\sin\phi & -\omega_e\cos\phi \\ -\omega_e\sin\phi & 0 & -\dot{\phi} \\ \omega_e\cos\phi & \dot{\phi} & 0 \end{pmatrix} \qquad (6\text{-}28)$$

and

$$\delta\bar{\omega}_{in}^{n} = \begin{pmatrix} -\delta\dot{\phi} \\ -(\omega_e+\dot{\lambda})\sin\phi\delta\phi + \cos\phi\delta\dot{\lambda} \\ (\omega_e+\dot{\lambda})\cos\phi\delta\phi + \sin\phi\delta\dot{\lambda} \end{pmatrix}, \qquad (6\text{-}29)$$

where ω_e is the rate of rotation of the earth. For a detailed discussion of the system errors, see Britting (1971). The transformation matrix $\mathbf{R}_b^n$ has been given in Chapter 2 therefore it is not listed here.

The first three rows of the dynamics matrix can be constructed by substituting equations (6-28), (6-29) and (2-14a) to (2-14i) into (6-27). If the misalignments are expressed in radian and the drift rates are in arcsec/s then the elements in equations (2-14a) to (2-14i) must be divided by 206264.8 before they can be put into the dynamics matrix.

Since the rates of change of the coordinate states are part of **x**, their error equations are simply

$$\delta\dot{\phi} = \delta\dot{\phi} \;, \qquad (6\text{-}30a)$$

$$\delta\dot{\lambda} = \delta\dot{\lambda} \;, \qquad (6\text{-}30b)$$

$$\delta\dot{h} = \delta\dot{h} \;. \qquad (6\text{-}30c)$$

They form the 4th, 5th and 8th rows of the dynamics matrix.

The derivation of the equation for the acceleration errors of the SISS is more involved than that of the other states. From the specific force equation given in Britting (1971), i.e.

$$f^n = a^n + (\Omega^n_{en} + 2\Omega^n_{ie})\, v^n - \gamma^n, \tag{6-31}$$

the equation for the raw acceleration can be written as

$$\bar{a}^n = \bar{R}^n_b \tilde{f}^b - (\bar{\Omega}^n_{en} + 2\bar{\Omega}^n_{ie})\, \bar{v}^n + \bar{\gamma}^n$$

$$= (\mathbf{I} + \mathbf{E})\, \mathbf{R}^n_b (f^b + \delta\mathbf{b}) - (\bar{\Omega}^n_{en} + 2\bar{\Omega}^n_{ie})\, \bar{v}^n + \bar{\gamma}^n \;, \tag{6-32}$$

where $\delta\mathbf{b}$ is the vector of residual accelerometer biases. The errors in acceleration can be obtained by applying perturbation theory to $\bar{a}^n$. Subtracting the true acceleration from equation (6-32) and multiplying the errors in velocity and coordinates into the partial derivatives of the Coriolis acceleration, the error in acceleration can be written as

$$\delta\bar{a}^n = \mathbf{E}f^n - (\bar{\Omega}^n_{en} + 2\bar{\Omega}^n_{ie})\, \delta\bar{v}^n + \mathbf{V}^n (\delta\omega^n_{en} + 2\delta\omega^n_{ie}) + \mathbf{R}^n_b\, \delta\mathbf{b} - \frac{\partial\gamma}{\partial h}\delta h \,. \tag{6-33}$$

The first term of equation (6-33) can be rearranged in terms of the misalignments i.e.

$$\mathbf{E}f^n = \begin{pmatrix} 0 & f_U & -f_N \\ -f_U & 0 & f_E \\ f_N & -f_E & 0 \end{pmatrix} \begin{pmatrix} \varepsilon_E \\ \varepsilon_N \\ \varepsilon_U \end{pmatrix}. \tag{6-34}$$

With the vectors

$$\omega^n_{en} = [\, -\dot{\phi},\ \dot{\lambda}\cos\phi,\ \dot{\lambda}\sin\phi \,]^T \tag{6-35a}$$

and

$$\omega^n_{ie} = [\, 0,\ \omega_e \cos\phi,\ \omega_e \sin\phi \,]^T, \tag{6-35b}$$

one can construct their skew-symmetric matrices and write the second term of equation (6-33) as

$$-(\bar{\Omega}^n_{en} + 2\bar{\Omega}^n_{ie})\,\delta\bar{v}^n$$

$$= \begin{pmatrix} 0 & -R(2\omega_e+\dot{\lambda})\sin\phi & (2\omega_e+\dot{\lambda})\cos\phi \\ R(2\omega_e+\dot{\lambda})\sin\phi\cos\phi & 0 & \dot{\phi} \\ -R(2\omega_e+\dot{\lambda})\cos^2\phi & -R\dot{\phi} & 0 \end{pmatrix} \begin{pmatrix} \delta\dot{\lambda} \\ \delta\dot{\phi} \\ \delta\dot{h} \end{pmatrix}, \qquad (6\text{-}36)$$

where R is the mean radius of the earth. The third term in equation (6-33) can be obtained by cross-multiplying

$$V^n = \begin{pmatrix} 0 & -v_U & v_N \\ v_U & 0 & -v_E \\ -v_N & v_E & 0 \end{pmatrix}, \qquad (6\text{-}37)$$

with

$$\delta\omega^n_{en} + 2\delta\omega^n_{ie} = \begin{pmatrix} -\delta\dot{\phi} \\ -(2\omega_e+\dot{\lambda})\sin\phi\delta\phi + \cos\phi\delta\dot{\lambda} \\ (2\omega_e+\dot{\lambda})\cos\phi\delta\phi + \sin\phi\delta\dot{\lambda} \end{pmatrix} \qquad (6\text{-}38)$$

The result is

$$V^n\,(\delta\omega^n_{en} + 2\delta\omega^n_{ie})$$

$$= \begin{pmatrix} 2v_U\omega\sin\phi+2v_N\omega\cos\phi & -v_U\cos\phi+v_N\sin\phi & 0 \\ -2v_E\omega\cos\phi & -v_E\sin\phi & -v_U \\ -2v_E\omega\sin\phi & v_E\cos\phi & v_N \end{pmatrix} \begin{pmatrix} \delta\phi \\ \delta\dot{\lambda} \\ \delta\dot{\phi} \end{pmatrix}, \qquad (6\text{-}39)$$

where ω is used to denote $(\omega_e+\dot{\lambda})$. Assuming that the products of velocities are relatively small, and

$$\omega_e >> \dot{\phi},\ \dot{\lambda} \text{ and } \dot{\phi},\ \dot{\lambda} >> \dot{h}/R,$$

the third term can be written as

$$V^n(\delta\omega^n_{en} + 2\delta\omega^n_{ie}) = \begin{pmatrix} 0 & 0 & 0 \\ -R\dot{\lambda}\cos\phi\sin\phi & 0 & 0 \\ R\dot{\lambda}\cos^2\phi & R\dot{\phi} & 0 \end{pmatrix} \begin{pmatrix} \delta\dot{\lambda} \\ \delta\dot{\phi} \\ \delta\dot{h} \end{pmatrix} \qquad (6\text{-}40)$$

and the sum of the second and third terms becomes

$$- (\bar{\Omega}^n_{en} + 2\bar{\Omega}^n_{ie})\, \delta\bar{v}^n + V^n (\delta\omega^n_{en} + 2\delta\omega^n_{ie})$$

$$= \begin{pmatrix} 0 & 2R\omega\sin\phi & -2\omega\cos\phi \\ -2R\omega\sin\phi\cos\phi & 0 & -\dot{\phi} \\ 2R\omega\cos^2\phi & 2R\dot{\phi} & 0 \end{pmatrix} \begin{pmatrix} \delta\dot{\lambda} \\ \delta\dot{\phi} \\ \delta\dot{h} \end{pmatrix}. \tag{6-41}$$

The second last term in equation (6-33) transforms the accelerometer biases from the body frame to the local-level frame. The last term in equation (6-33) is the error in normal gravity due to the uncertainty in the raw height. It can be dampened by using other more accurate height information to compute normal gravity. The normal gravity gradient can be approximated by

$$\frac{\partial\gamma}{\partial h} = -2\gamma/R\,. \tag{6-42}$$

A damping factor k can be added to equation (6-42) if external and more accurate height (e.g. estimated, weighted or measured height) is used to compute normal gravity. In this research, the estimated height is used to compute normal gravity. As shown later in Chapter 8, the accuracy of the estimated height is well below 10 m, therefore the error in the computed normal gravity may be considered as negligible. Thus, the factor k is set to $2\gamma/R$.

The acceleration errors in equation (6-33) are in m/s^2. They can be reduced to angular acceleration errors in $\dot{x}$ by the relation

$$\begin{pmatrix} \delta\ddot{\lambda} \\ \delta\ddot{\phi} \\ \delta\ddot{h} \end{pmatrix} = \begin{pmatrix} \delta a_E/(R_P\cos\phi) \\ \delta a_N/R_M \\ \delta a_U \end{pmatrix}. \tag{6-43}$$

For a first-order error analysis, R_P and R_M can be replaced by the mean radius of the earth because the influence of the approximation on the error states is smaller than 0.35%. It leads to a major simplification and thus requires less computer time. The scaled form of equation (6-33) fills the 6^{th}, 7^{th} and 9^{th} rows of the dynamics matrix.

The variation of the residual gyro drifts and accelerometer biases contained in x from one alignment to the next is random but bounded. Therefore, they can be modeled by a first-order Gauss-Markov process

$$\dot{x} = -\zeta x + w , \tag{6-44}$$

where ζ is 1/(correlation time) of the process. The assumption behind equation (6-44) is that the auto-correlation function of the error can be described by

$$\psi_{xx} = C_o \, e^{-\xi t} , \tag{6-45}$$

where C_o is the initial variance (see Gelb, 1974). The initial variances of the biases are determined by the range of the error and the correlation time of the process is dependent on its stability. Thus, the error equations for the drifts and biases are

$$\dot{\mathbf{d}} = -\zeta \mathbf{d} + \mathbf{w} \tag{6-46}$$

and

$$\dot{\mathbf{b}} = -\beta \mathbf{b} + \mathbf{w} . \tag{6-47}$$

Together, they form the 10^{th} to 15^{th} rows of the dynamics matrix. The correlation length of the drifts and biases is either obtained from factory calibration, or can be determined from the error behaviour of the sensors observed over a long period of time in the laboratory or from the results of field tests.

The dynamics matrix developed from the error equations derived in this chapter is given in the Figure 6-3. A similar matrix can also be found in Schmidt (1978).

$$
\begin{bmatrix}
0 & -\omega\sin\phi & -\dot{\phi} & \omega\sin\phi & 0 & 0 & -\cos\phi & 0 & 0 & R_{21} & R_{22} & R_{23} & 0 & 0 & 0 \\
\omega\sin\phi & 0 & -\omega\cos\phi & 0 & 0 & 1 & 0 & 0 & 0 & R_{11} & R_{12} & R_{13} & 0 & 0 & 0 \\
\dot{\phi} & \omega\cos\phi & 0 & -\omega\cos\phi & 0 & 0 & -\sin\phi & 0 & 0 & R_{31} & R_{32} & R_{33} & 0 & 0 & 0 \\
0 & 0 & 0 & 0 & 0 & 1 & 0 & 0 & 0 & 0 & 0 & 0 & 0 & 0 & 0 \\
0 & 0 & 0 & 0 & 0 & 0 & 1 & 0 & 0 & 0 & 0 & 0 & 0 & 0 & 0 \\
0 & -f_U/R_M & f_E/R_M & 0 & 0 & 0 & -\omega\sin2\phi & 0 & -\dot{\phi}/R_M & 0 & 0 & 0 & D_{21} & D_{22} & D_{23} \\
f_U/R_E & 0 & -f_N/R_E & 0 & 0 & 2\omega\tan\phi & 0 & 0 & -2\omega/R_P & 0 & 0 & 0 & E_{11} & E_{12} & E_{13} \\
0 & 0 & 0 & 0 & 0 & 0 & 0 & 0 & 1 & 0 & 0 & 0 & 0 & 0 & 0 \\
-f_E & f_N & 0 & 0 & 0 & 2R_M\dot{\phi} & 2R_E\omega\cos\phi & c & 0 & 0 & 0 & 0 & F_{31} & F_{32} & F_{33} \\
0 & 0 & 0 & 0 & 0 & 0 & 0 & 0 & 0 & -\zeta & 0 & 0 & 0 & 0 & 0 \\
0 & 0 & 0 & 0 & 0 & 0 & 0 & 0 & 0 & 0 & -\zeta & 0 & 0 & 0 & 0 \\
0 & 0 & 0 & 0 & 0 & 0 & 0 & 0 & 0 & 0 & 0 & -\zeta & 0 & 0 & 0 \\
0 & 0 & 0 & 0 & 0 & 0 & 0 & 0 & 0 & 0 & 0 & 0 & -\beta & 0 & 0 \\
0 & 0 & 0 & 0 & 0 & 0 & 0 & 0 & 0 & 0 & 0 & 0 & 0 & -\beta & 0 \\
0 & 0 & 0 & 0 & 0 & 0 & 0 & 0 & 0 & 0 & 0 & 0 & 0 & 0 & -\beta
\end{bmatrix}
$$

$c = -2\gamma/R + k$,

F_{ij} is the element in the i^{th} row and j^{th} column of the matrix $\mathbf{R}_b^n$,

R_{ij} is F_{ij} divided by 206264.8,

D_{ij} is F_{ij} divided by R_M and

E_{ij} is F_{ij} divided by R_E.

Figure 6-3 : Dynamics Matrix of a 15-state Kalman Filter for an SISS for $f \neq 90°$

6.3 Initial Variances and Spectral Densities

At the starting epoch of the Kalman filtering process, the values of the error states are unknown. They are usually assumed to be zero because, for a well calibrated system, the errors of the navigation quantities at the end of the coarse alignment are random from one alignment to the next. Thus, the Kalman filtering process can be initiated by setting

$$x_0 = 0 \qquad (6\text{-}48)$$

and the diagonal initial variance-covariance matrix

$$C_{x0} = E\{x_0 x_0^T\}. \qquad (6\text{-}49)$$

The initial variance of the misalignments of the platform frame should be dependent on the accuracy of the coarse alignment. In this case, at the starting epoch,

$$\sigma\varepsilon_E = \sigma\varepsilon_N = 40 \text{ arcsec}, \qquad (6\text{-}50)$$

and

$$\sigma\varepsilon_U = 1 \text{ degree}. \qquad (6\text{-}51)$$

If velocity data were used in the analysis, the value of $\sigma\varepsilon_U$ is reduced to 100 arcsec which is the estimated alignment accuracy of the LTN-90-100.

The initial variance of the coordinates is given by the accuracy of the input coordinates of the starting point. When processing the velocity data and the initial coordinates are not accurately known, the approximate coordinates may be entered into the LTN-90-100 during alignment in the field and a coordinate update can be performed with the known coordinates at the beginning of filtering in post mission processing. In that case, a larger value should be used as the initial variance of the coordinates. The Kalman filter developed for the SISS is designed to start with standard deviations

$$\sigma\phi = \sigma\lambda = \sigma h = 20 \text{ m}, \qquad (6\text{-}52)$$

even when the initial coordinates are known and perform a coordinate update with the known coordinates at the end of fine alignment.

If the SISS is stationary during alignment and the velocities are reset to zero at the end of of alignment, the initial variance of the velocities should be set to a very small value. The initial standard deviations for velocities in the Kalman filter developed for the SISS are

$$\sigma v_E = \sigma v_N = \sigma v_U = 0.0001 \text{ m/s} . \tag{6-53}$$

The initial variance of the residual gyro drifts and accelerometer biases are dependent on the accuracy of the system calibration. The system calibration of the LTN-90-100 conducted at The University of Calgary for the determination of the drifts and biases in the rate data will be given in the next chapter. The standard deviation of the residual gyro drifts and accelerometer biases from their zero mean are estimated to be

$$\sigma d_x = \sigma d_z = \sigma d_z = 0.01 \text{ deg/h}, \tag{6-54}$$

$$\sigma b_x = \sigma b_y = \sigma b_z = 10 \text{ mgal} . \tag{6-55}$$

These values should be increased as time elapses until the next system calibration.The amount increased depends on the change of the drift rates and biases in between calibrations.

Another set of variances that must be determined for the Kalman filter is the diagonal of the spectral density matrix. The non-zero elements in **Q** are determined from sensor accuracies and system calibration. They account for the noise in the rate of change of the error states due to noise in the sensors and vibration from the vehicle. The elements pertaining to the non-sensor errors can be determined by examinating the RMS of the basic sensor noise and by field calibration. In field calibration, the errors of the estimated navigation quantities are compared with their estimated standard deviation and the elements in the spectral density matrix are adjusted until an acceptable agreement between the size of the errors and their standard deviations is reached. Usually many calibration runs performed in a typical surveying environment are needed before an optimal set of spectral densities can be obtained for a particular system. Since the vibration of the vehicle is dependent on the dynamics of the environment in which the system is used, the spectral density matrix changes for different applications.

The spectral densities for the error states modelled as a first-order Gauss-Markov process can be computed from the equation

$$\dot{\sigma}^2 = 2\zeta\sigma_0^2 , \tag{6-56}$$

where σ_0^2 is the initial variance of the error (Gelb, 1974). Results from field tests show that the spectral densities tabulated in Table 6-1 are the most appropriate for the LTN-90-100 at the University of Calgary. In order to account for the time-stationary behaviour of the residual drifts and biases, the correlation length for the system is chosen to be 40 hours for all sensor errors.

state	spectral density
$\varepsilon_E, \varepsilon_N, \varepsilon_U$	0.1 $arcsec^2/s$
$\delta\phi, \delta\lambda, \delta h$	0
$\delta\dot{\phi}, \delta\dot{\lambda}, \delta\dot{h}$	$1.0 \cdot 10^{-6} m^2/s^3$
d_x, d_z, d_y	$1.4 \cdot 10^{-9} deg^2/h^3$
b_x, b_y, b_z	$1.4 \cdot 10^{-3} mgal^2/s$

Table 6-1 : Spectral Densities

6.4 Optimal Smoothing

During Kalman filtering, the error states of a SISS at a particular epoch are estimated with the external information gathered up to that epoch. In optimal smoothing, the process utilizes all the information obtained after the epoch to improve the estimates of the Kalman filter. Obviously such a process can only be applied after the fact or in post-mission analysis. The derivation of the discrete optimal smoothing equations can be found in Bierman (1973), and therefore it is not given here. The basic equations are :

$$\chi_k(+) = \Phi^T_{k,k+1}\ \chi_{k+1}(-), \tag{6-57}$$

$$Z_k(+) = \Phi^T_{k,k+1}\ Z_{k+1}(-)\ \Phi_{k,k+1}\ , \tag{6-58}$$

$$\mathbf{D}_k = \mathbf{H}\mathbf{C}_{x,k}(-)\mathbf{H}^T + \mathbf{C}_{y,k}$$

$$\chi_k(-) = \chi_k(+) - \{\ \mathbf{H}^T\mathbf{D}^{-1}\,(\mathbf{y} - \mathbf{H}\mathbf{x} + \mathbf{D}\mathbf{K}^T\chi(+))\ \}_k\ , \tag{6-59}$$

$$Z_k(-) = (\mathbf{I} - \mathbf{K}_k\mathbf{H}_k)\ Z_k(-)\ (\mathbf{I} - \mathbf{K}_k\mathbf{H}_k)^T + \mathbf{H}^T_k\mathbf{D}^{-1}_k\mathbf{H}_k\ , \tag{6-60}$$

$$\mathbf{x}^s_k = \mathbf{x}_k(-) - \mathbf{C}_{x,k}(-)\chi_k(-) \tag{6-61}$$

and

$$\mathbf{C}^s_k = \mathbf{C}_{x,k}(-) - \mathbf{C}_{x,k}(-)\ Z_k(-)\ \mathbf{C}_{x,k}(-). \tag{6-62}$$

In equations (6-57) to (6-62), the first subscript of a variance-covariance matrix $\mathbf{C}$ denotes the vector to which the matrix is associated. The subscript after the comma is the epoch of interest. The superscript "s" is used to denote smoothed quantities. The matrix $\mathbf{D}_k$ is called the innovation matrix. The optimal smoothing of the state vector can be initiated at any epoch n under the assumption that there is no observation after n, i.e.

$$\mathbf{H}_k = \chi_k(+) = 0 \tag{6-63}$$

for k > n, thus

$$\chi_k(-) = -\mathbf{H}^T_n\mathbf{D}^{-1}_n\ (\mathbf{y} - \mathbf{H}\mathbf{x})_n \tag{6-64}$$

and

$$Z_k(-) = \mathbf{H}^T_n\mathbf{D}_n\mathbf{H}_n. \tag{6-65}$$

The smoother described by equations (6-57) to (6-61) is called the optimal modified Bryson-Fraser smoother (Bierman, 1973). This smoother is based on the algorithm presented in Bryson and Ho (1969). It was chosen for refinement of the estimates from the Kalman filter because the smoother avoids the implementation problems in other optimal methods. An optimal backward smoothing method such as the Rauch-Tung-Streibel smoother is elegant but, as shown by Bierman (1977, pp 222-223), it is too complex to implement in practice. Other approaches like square-root filtering and smoothing can only provide estimates at the observation epochs. The duality of equations (6-57) to (6-61) with the Kalman filtering equations makes implementation of this smoother very simple. If the measurements are uncorrelated, the efficiency of Kalman filtering equations is maximized by processing the measurements one at a time. Thus, the innovation matrix becomes a scalar quantity, and the inversion of the matrix is reduced to a division. The modified Bryson-Fraser smoother retains this efficiency by utilizing the duals of the Kalman filtering mechanization. Such an approach is essentially a form of recursive backward filtering of the filtered estimates (Blais, 1988). The duals in the modified Bryson-Fraser smoother are the χ vector (dual of the state vector) and the $\mathbf{Z}$ matrix (dual of the variance-covariance matrix). By propagating and estimating these quantities backward in time, the smoother can work on the estimates from the Kalman filter in the same way as the forward filtering on the predicted states. This method is not only computationally less costly but also numerically more stable. Unlike square-root filtering, the smoother can provide estimates as well as their variance-covariance matrices at epochs where there is no measurement update.

The quantities required from the Kalman filter for optimal smoothing at every update epoch k are the measurements, design matrix, variance-covariance matrix of the measurements, total transition matrix since last update, state vector and its variance-covariance matrix. Raw navigation quantities and other surveying information should also be stored so that smoothed Euler angles, velocities and coordinates of the SISS can be computed from the smoothed state vector. In general, optimal smoothing is less time-consuming than filtering but it requires a lot computer disk space for data storage. A general flow chart of the smoother developed for the SISS is shown in Figure 6-4.

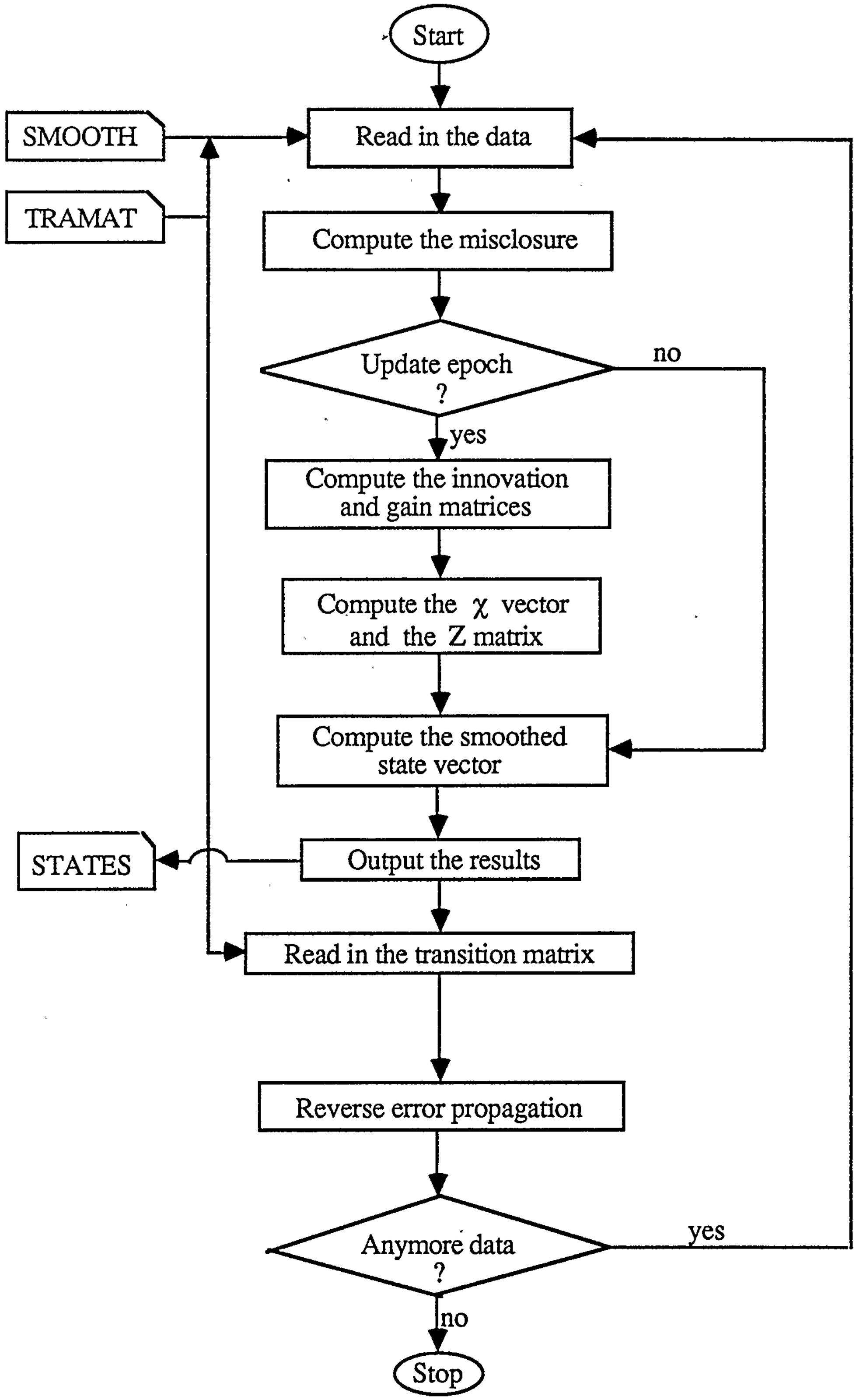

Figure 6-4 : Flow Chart of the Optimal Smoother

CHAPTER 7

FIELD TESTING

In the spring and summer of 1988, tests of the hardware and software of the LTN-90-100 based strapdown inertial survey system were conducted over two L-shaped baselines near Calgary. The objectives of the tests were :

(1) to gain more experience with the operation of the LTN-90-100 and the data acquisition system;

(2) to conduct field calibration of the SISS;

(3) to determine the spectral densities for an SISS operating in the land surveying environment;

(4) to test various modules; and

(5) to test the design of the Kalman filter-smoother.

The tests were conducted on L-shaped traverses because some of the less well-known errors in the SISS are azimuth-dependent. On a straight traverse, these errors are usually buried in the larger time-dependent but better modeled errors and are removed along with them. Deficiencies in the error model of the azimuth-dependent errors would only show up if data from an L-shaped traverse were used in the field tests.

There were two separate groups of tests in the over-all testing program. In the first test, velocity data were recorded to check the survey procedures, data acquisition hardware and software, and the Kalman filter-smoother. After correcting the shortcomings discovered in the tests, the four tests were conducted on a longer baseline to check the accuracy of the rate integration and alignment modules. In this chapter, the description of the baselines, procedures used in the tests and lab calibration are presented and discussed.

7.1 Baselines

The baseline used in the velocity-data test is located 10 km north of Calgary. The total length of the baseline is about 10 km. There are 11 stations on the baseline which are approximately 800 m apart. It requires 3 minutes to travel from one station to the next, position the vehicle at the station and perform the velocity update. A two-way survey which consists of a forward and backward run takes about 1 hour. The speed limit for the north-south section of the baseline is 80 km/h and for the east-west section 100 km/h. The baseline is situated on a paved road but the north-south section had not been properly maintained and was therefore very bumpy. The maximum height difference between any two adjacent stations is less than 20 m. The gentle terrain is the main reason for chosing the baseline as testing ground for the velocity-data test. Since the LTN-90-100 does not estimate its vertical velocity and height, the gentle terrain may help to minimize any height-dependent errors in the horizontal velocities. The coordinates of the baseline were determined by conventional means to 0.5 m (1σ). Due to the lack of geodetic control information in that area, only the first point of the traverse was tied to an Alberta geodetic control point. Figure 7-1 is a general diagram of the L-shaped Calgary baseline.

The second and longer baseline used in the field test is located north west of Calgary, near the town of Cochrane. The length of the baseline is about 24 km and there are 11 stations on the traverse. It is a baseline established by Nortech Survey (Canada) Ltd. for testing their inertial survey systems and GPS satellite receivers. The coordinates of the stations were determined from differential GPS phase measurements to 10 cm (1σ). The road condition of the baseline is generally good except for part of the north-south section which is a gravel road. There are potholes on the gravel part of the baseline where the vehicle must be slowed down to 40 km/h in order to minimize the vibration due to road conditions. As on the first baseline, the speed limit of the north-south section of the baseline is 80 km/h and the east-west section 100 km/h. The distance between two stations is about 2.5 km and the time required to complete one leg of

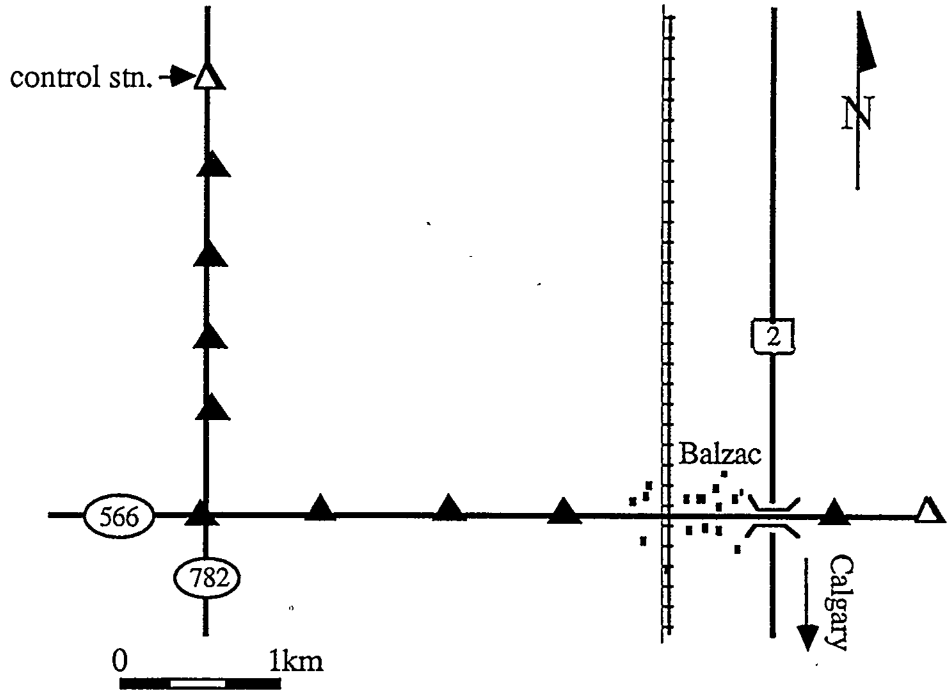

Figure 7-1 Calgary Baseline

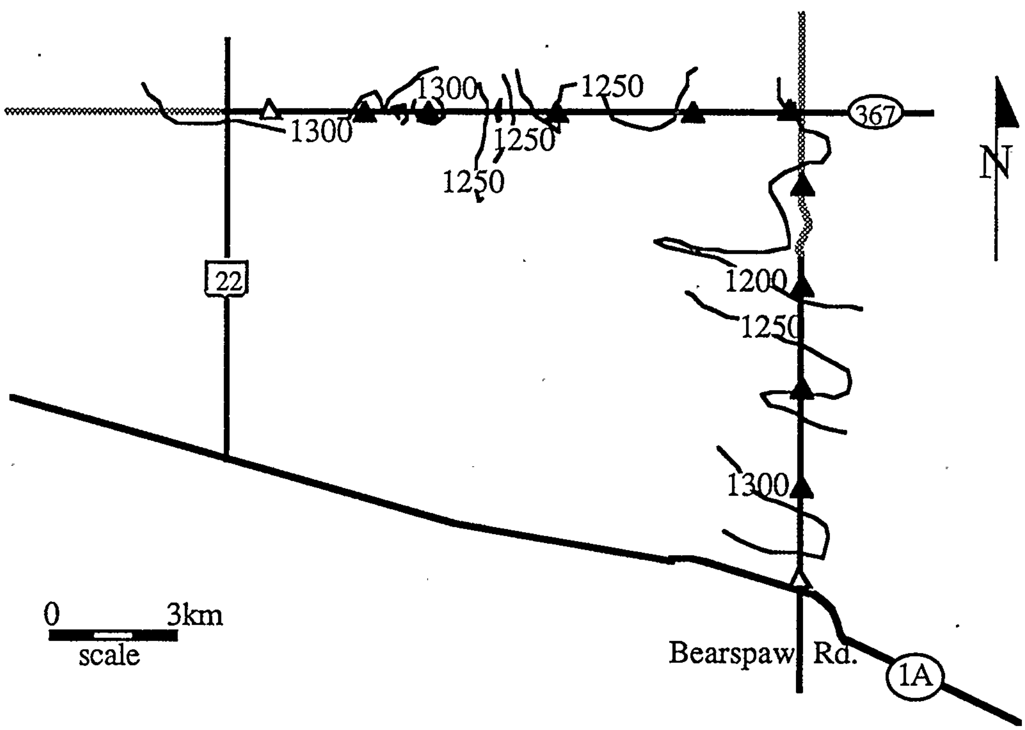

Figure 7-2 : Cochrane Baseline

the survey is about 4.5 minutes. A two-way survey takes slightly more than one and half hour. The terrain in the area is more undulating than in the first case. Maximum change in height between two adjacent stations is more than 100 m. The large change in height makes it a baseline better suited for testing the rate data processing software which estimates and outputs the vertical velocity and height.

7.2 Velocity-Data Test

The velocity-data test was conducted on the Calgary baseline in the spring of 1988. North and east velocities along with the Euler angles were recorded in the test. The vehicle used was a 9-passenger suburban without the backseat. At that time, the case for the LTN-90-100 was not developed yet therefore two pieces of wood were used to support the system in the vehicle. The survey was performed by a three-man crew although a two-man crew should have been sufficient to complete the job. The SISS was placed at the back of the vehicle approximately 2 m away from the back door. The trailer hitch of the vehicle was selected to be the reference point. The plan was to have the driver position the vehicle such that the reference point was located directly above the station marker. The x-y-z offsets of the hitch from the SISS were measured so that they could be transformed to N-E-U offsets between the SISS and the station marker via the body to local-level frame transformation matrix constructed from the Euler angles given by SISS during velocity update. Figure 7-3 shows the relationship between the SISS and the reference point on the vehicle.

A ten-minute alignment was performed at the beginning of the survey. At the end of the alignment, the data acquisition software was activated and station information was entered into the data acquisition system. The surveying procedure was simple. Upon arrival at each point, one of the members of the crew would leave the vehicle and direct the driver to the station marker. Once the reference point had been placed above the marker, the engine of the vehicle would be turned off and the other member of the crew could press the 'c' key of the keyboard of the data acquisition system to signal the beginning of the update period. The update period of the test was about 20 second. The procedure was repeated on every station until the vehicle returned to the starting point. The crew discovered that a great deal of time was spent directing the driver to position the reference point above

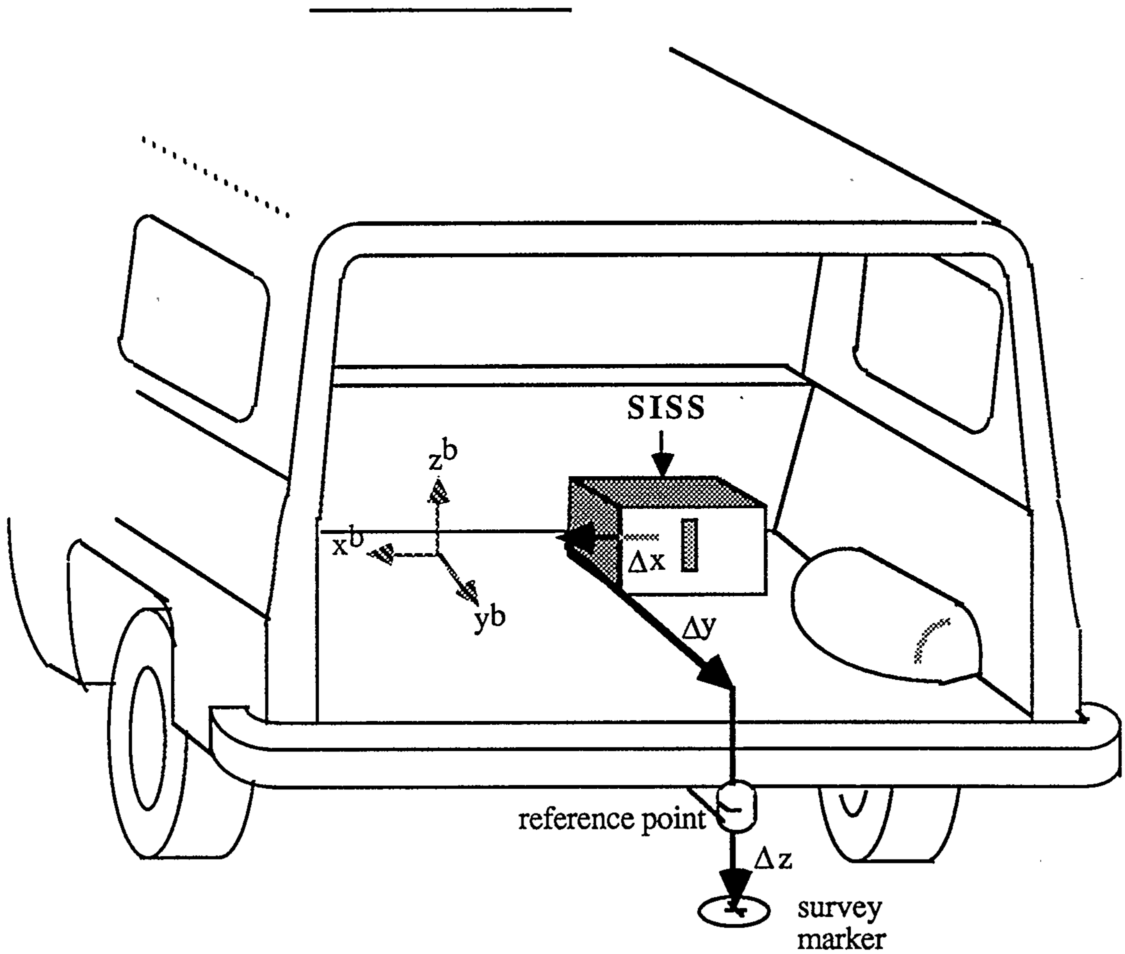

Figure 7-3 : Offsets between the SISS and the Reference Point

the station marker. The total surveying time could be shortened if the reference point was moved to within 1 m of the station marker and the offsets of the reference point to the marker were measured. The offsets required would be the horizontal angle from the y body axis to the plumbline through the station marker measured at the reference point and the horizontal distance between the reference point and the marker. Since the area around the markers was generally flat, no vertical offset was needed. This procedure was later adopted in the second group of tests conducted in the summer.

7.3 Lab Calibration

Four tests were conducted in the summer on the 24 km baseline to gather data for the system calibration and the testing of the rate integration and alignment module. The system calibration consists of a lab calibration and field refinement test. In the lab calibration, 1-minute samples of rate data of a stationary LTN-90-100 in four different azimuths are collected on a stable and level surface and the mean of the body rates and accelerations in each sample were calculated. The azimuths are : 0°, 90°, 180°, 270°. Since the system is sitting on a level surface, the roll and pitch of the system may be assumed as zero in the calibration and the biases in means can be computed from the equations

$$\bar{\mathbf{d}} = \frac{1}{4}\sum_{i=1}^{4} [\hat{\omega}_{ie}^{b} - \bar{\mathbf{R}}_{n}^{b}\omega_{ie}^{n}]_i \tag{7-1}$$

and

$$\bar{\mathbf{b}} = \frac{1}{4}\sum_{i=1}^{4} [\hat{\mathbf{f}}^{b} - \bar{\mathbf{R}}_{n}^{b}\mathbf{g}]_i$$

where

$$\bar{\mathbf{R}}_{n}^{b} = \begin{pmatrix} \cos(az) & -\sin(az) & 0 \\ \sin(az) & \cos(az) & 0 \\ 0 & 0 & 1 \end{pmatrix}, \tag{7-2}$$

$$\omega_{ie}^{n} = \omega_e \begin{pmatrix} 0 \\ \cos\phi \\ \sin\phi \end{pmatrix}, \tag{7-3}$$

$$g = \begin{pmatrix} \gamma\xi \\ \gamma\eta \\ \gamma + \Delta g \end{pmatrix}, \tag{7-4}$$

where i is the sample number, and az is the azimuth of the sample. The symbol "^" is used to denote the mean value of the sample. The latitude and height required in equation (7-3) and the computation of normal gravity can be approximated by the known coordinates of the lab. The local-level to body transformation given in equation (7-2) is an approximate quantities. A more accurate matrix can also be constructed from the Euler angles given by the LTN-90-100 or other instruments available in the lab.

In this case, due to the absence of any turntable, the lab calibration was performed on a trolley and the orientation of the system was determined by the azimuth displayed on the LTN-90-100. Results from the lab calibration show that the drift and biases in this particular LTN-90-100 are

$$\bar{d} = \begin{pmatrix} -0.864 \\ -0.828 \\ -0.900 \end{pmatrix} \text{arcsec/s} \tag{7-5}$$

and

$$\bar{b} = \begin{pmatrix} -50 \\ 20 \\ -110 \end{pmatrix} \text{mgal.} \tag{7-6}$$

The magnitude of the accelerometer biases is within the specification of the sensors but drift rates appeared to be large and systematic. At present, an explanation for these large values is not yet available.

7.4 Field Tests

The correction parameters for the body rates and accelerations obtained from lab calibration are still too crude to be used as an approximation to the gyro drifts and biases in high-accuracy inertial surveying. However, they can be improved by information from the field calibration of the system. Field calibration is the refinement of the correction parameters by estimating the residual drifts and biases in the corrected sensor output via the Kalman filter-smoother with the rate data collected on a baseline. During the field calibration, all coordinates on the baseline are used as control measurements to update the state vector. The coordinate updates at the two ends of the baseline help the Kalman filter-smoother to accurately separate the azimuth-dependent effect of the residual drift rates and biases from the initial azimuth misalignment.

The 24-km Cochrane baseline was used to calibrate the strapdown inertial survey system. The survey procedure was slightly changed from the velocity-data test. A point at the front of the vehicle was used as the reference point which was moved within a metre of the marker at each station before the velocity update. The horizontal angle and distance between the reference point and the marker were measured with a protractor, ruler and plumbob. Ten minutes of rate data were recorded at the initial point for system alignment and the Euler angles estimated by the LTN-90-100 were also recorded for comparison of the system output and that of the fine alignment module. The two-way survey took approximately one hour and forty minutes.

After the field calibration of the system, the estimated residual drift rates and biases were added to those obtained in lab calibration. Three more surveys were conducted on the Cochrane baseline to test the Kalman filter-smoother. Unfortunately, due to the presence of other users at the two ends of the baseline, only a one-way run was possible in the last survey. Since the second and the last survey did not reach the ends of the baseline, the second and 10th point were used as the end points of the traverse. Due to the improper mounting of the SISS in the vehicle, the SISS was also bouncing up and down in the last survey. These three sets of data along with the first set of rate data were processed with the Kalman filter-smoother using the stations at the two ends of the traverse as control stations.

Experience from the field tests shows that two deep-cycle batteries can power the SISS for about 4 hours. A simple protractor, ruler and plumball can be used to measure the offsets between the reference point and the marker with adequate speed. The accuracy of the offset determined in this manner is dependent how carefully the measurements are made and the accuracy of the estimated Euler angles. Higher accuracy may be obtained by using precise optical survey instruments to measure the horizontal offsets. However, such an approach is more expensive because it is time-consuming and dependent on the experience of the operator of the instruments.

In order to minimize the effect of system vibrations during alignment and navigation, the system should be properly mounted and the engine should not be running. Shock absorption material may be used to reduced the vibration but care should be taken to ensure that the material and the system do not shake with respect to the vehicle.

CHAPTER 8

RESULTS AND ANALYSIS

There are two parts to the error analysis of the field tests and calibration. In the first part, the software and error model developed for the SISS is checked for proper functioning. They comprise the Kalman filter-smoother, integration module, alignment modules and error model for the field calibration. The second part of the analysis concentrates on the refinement of the weighting scheme and the accuracy of the estimates. The results and analysis of the field tests of the strapdown inertial survey system are presented and discussed in this chapter.

8.1 Velocity Data

The post-mission analysis of the velocity data was performed on the VAX main frame computer of the Department of Surveying Engineering at the University of Calgary. The binary data from the LTN-90-100 were converted into ASCII characters in the data acquisition system and sent to the VAX computer via a inter-computer communication program called Kermit provided by the university. The size of an ASCII file is more than twice that of a binary file. A 45-minute survey would produce a ASCII file of approximately 2 Mbytes. At 9600 baud, the program Kermit needs almost half an hour to transfer the whole file to the VAX computer. The analysis of the field data can also be done in the data acquisition system, but due to some ventilation problem in the system, it requires 4 to 5 times the CPU time the VAX computer needs to complete the job.

The velocity data were put through the velocity integration routine and Kalman filter to produce the filtered coordinates of the stations on the Calgary baseline. Since the LTN-90-100 did not output any vertical velocity due the absence of external height information, the height of the system was assumed to be equal to the height of the initial point and the error states of the vertical channel, i.e. height error, vertical velocity error and z accelerometer biases, were not used during filtering. The CPU time needed was about 80 to 90% of the surveying time. The long processing time is mainly due to the numerical approach used to propagate the variance-covariance matrix of the state vector. These filtered coordinates were compared to the known coordinates of the stations and the difference between them were calculated for the error analysis. During the test, the velocity error of the LTN-90-100 grew to a maximum of about 0.9 m/s in about 1 hour which is within the specification of the system. Comparison between the displayed coordinates and the known coordinates shows that the position error of the LTN-90-100 was less than 500 m at the end of the two-way survey which took about one hour. The errors and standard deviations of the filtered coordinates, i.e. the coordinate difference between the filtered and known coordinates, are plotted in Figure 8-1. They grow steadily to about 3.5 m in half an hour. The behaviour of the errors is clearly azimuth-dependent. Since it is not possible to reset the azimuth of the SISS when processing velocity data, the trend continues at a slower rate even after the coordinate update at the end of the forward run. The estimated standard deviation of the filtered coordinates exhibit the same behaviour as the errors but in a larger magnitude. They indicate that the weighting scheme of the Kalman filter is slightly pessimistic. The azimuth error ε_U of the system at the end of the survey was estimated to be 72 arcsec. The residual gyro drifts and accelerometer biases were estimated to be about :

$$\delta\hat{\mathrm{d}} = \begin{pmatrix} -0.0014 \\ -0.0051 \\ 0.0004 \end{pmatrix} \text{arcsec/s} \tag{8-1a}$$

and

$$\delta\hat{\mathrm{b}} = \begin{pmatrix} 26 \\ 17 \end{pmatrix} \text{mgal.} \tag{8-1b}$$

Due to the lack of vertical velocity data, only the biases in the x and y acceleration could be estimated from the velocity data.

The output from the Kalman filter was processed again by the optimal smoother which requires approximately 5 minutes of CPU time to finish the job. The results of the smoothing are plotted in Figure 8-2. They show that the smoother has improved the accuracy of the coordinates to the 1-metre level and the errors appear to be random. These results indicate that the error states were accurately modelled by the dynamics matrix of the Kalman filter. Since there is a coordinate update at the end of the forward run, the smoothed coordinates of the forward and backward run may be considered as independent (see Wong, 1982). The weighted mean of the coordinates of the stations on the baseline can be computed by assigning the reciprocal of the variance of smoothed coordinates as weights. The error of the weighted means of the smoothed coordinates are shown in Figure 8-3. The RMS computed from the error of the weighted mean of the latitudes and longitudes are 0.64 m and 0.26 m respectively. However, due to the pessimistic weights used in the Kalman filter, the estimated standard deviation of the weighted means are twice as big as the errors. These results show that sub-metre horizontal positioning accuracy is achievable on a 10-km L-shaped traverse using the velocity data from the SISS but more experiments are needed to confirm the accuracy and to determine a more optimal weighting scheme for the Kalman filter.

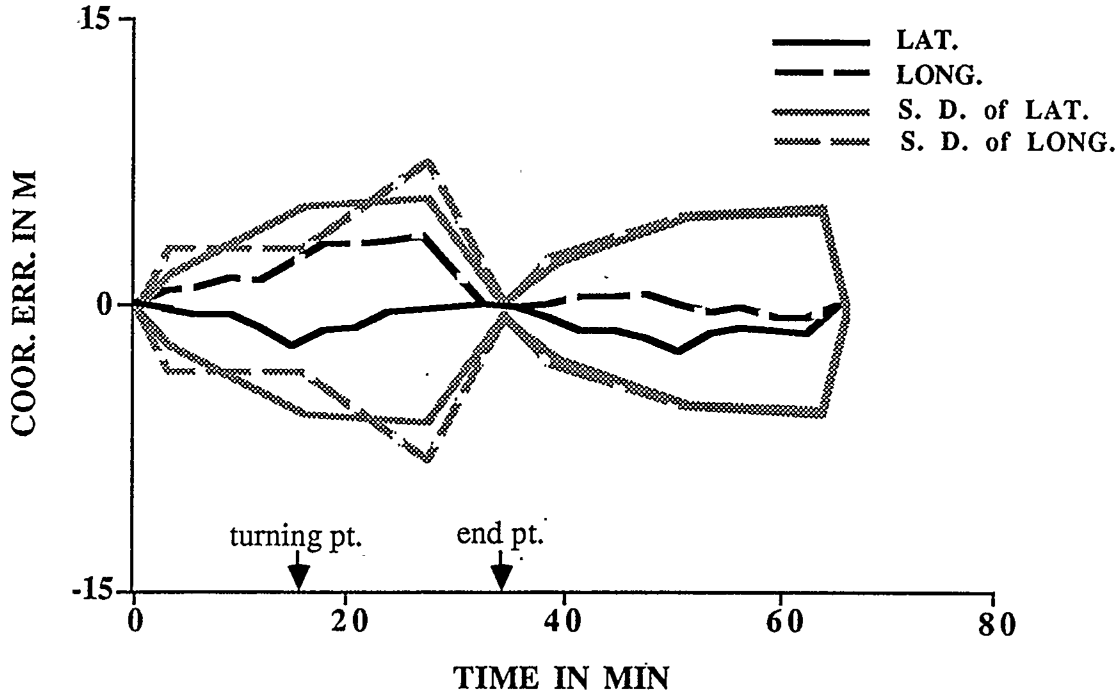

Figure 8-1 : Errors of Filtered Coordinates Using Velocity Data

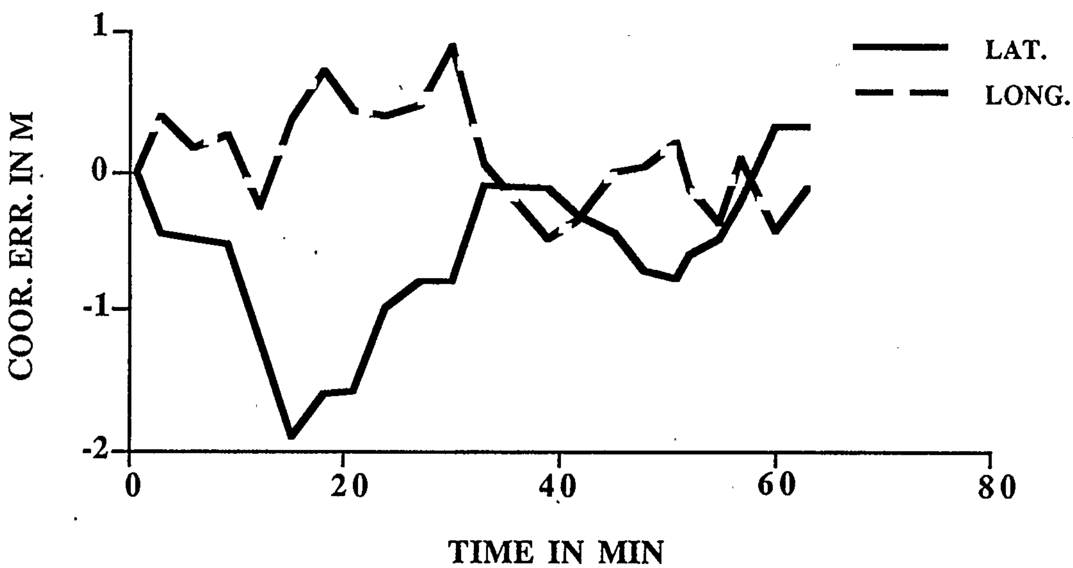

Figure 8-2 : Errors of Smoothed Coordinates Using Velocity Data

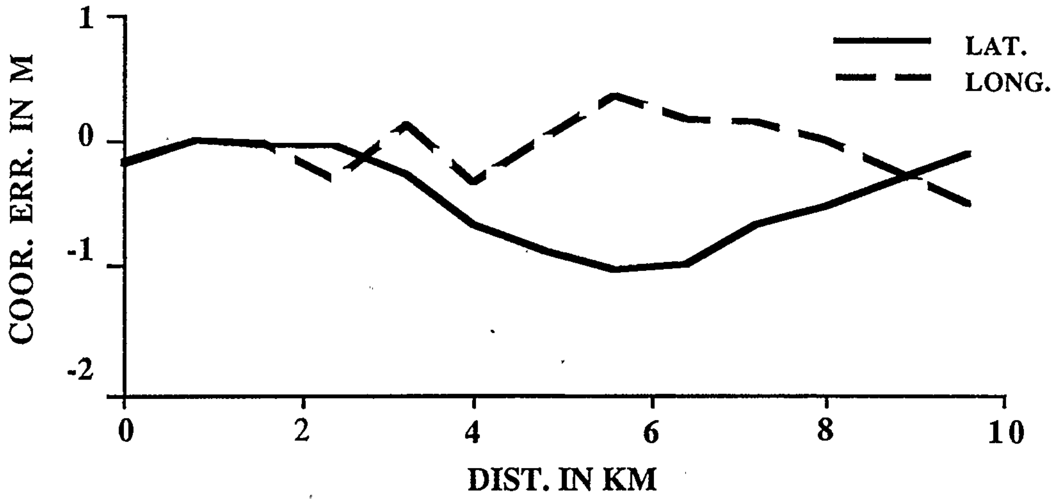

Figure 8-3 : Errors of Weighted Means Using Velocity Data

8.2 Rate Data

In the first rate-data test, data were collected for the field calibration of the SISS and the refinement of the Kalman filter-smoother. Using the initial weighting scheme given in Chapter 7, the data were put through integration and alignment modules to produce the navigation quantities which were then processed by the Kalman filter-smoother. A coordinate update was performed on every station to determine the residual drifts and biases in the corrected body rates and accelerations. These residual drifts and biases were added to the correction parameters obtained from lab calibration to form the refined correction parameters for all subsequent tests of the Kalman filter-smoother. The combination of the lab and field calibration is called the system calibration of the SISS. The refined correction for the body rates form the LTN-90-100 were found to be

$$\bar{d} = \begin{pmatrix} -0.864 \\ -0.864 \\ -0.900 \end{pmatrix} \text{arcsec/s} . \qquad (8\text{-}2)$$

No significant changes of the acceleration biases were estimated therefore the parameters from the lab calibration were kept.

After the field calibration, all four data sets were processed with the Kalman filter-smoother. This time, only the stations at the two ends of the traverse were treated as known point and the data were processed as if they had been collected in a standard field survey. The rate data were corrected with the parameters given in equations (7-6) and (8-2) before they were integrated into angular and velocity increments. The alignment process took about 10 minutes. The estimated roll and pitch converged to a stable solution immediately after the first velocity update in fine alignment whereas the azimuth, as shown in Figure 8-4, required approximately 5 to 7 minutes. Results from the alignments show that the roll and pitch estimated by the Kalman filter were within 20 arcsec of the ones given by the LTN-90-100 and that the differences between the azimuths were below 300 arcsec. These differences were within the 95% confidence region of the estimated Euler angles. They show that the alignment software in the LTN-90-100 and estimation package developed at The University of Calgary are compatible.

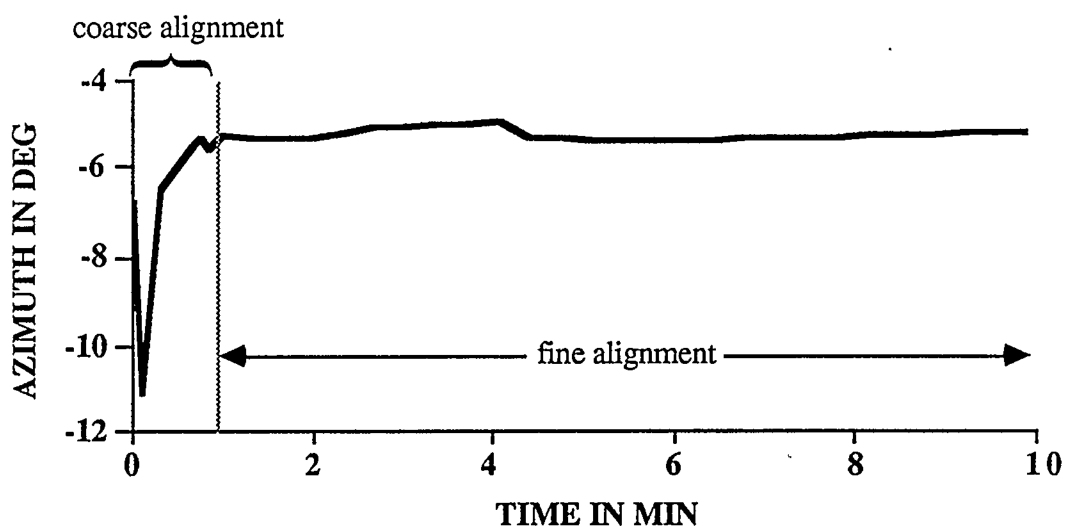

Figure 8-4 : Azimuth During Alignment

During filtering, the estimation package resets the navigation quantities after every coordinate update, which only happened at the two ends of each run. By resetting the navigation quantities, the filter minimized the effect of any second-order errors in the process and reduced the errors in the filtered results. As an example, the filtered coordinate errors, i.e. differences between the filtered and known coordinates, and the standard deviation of the filtered latitudes are plotted in Figure 8-5. The azimuth-dependent trend of the horizontal coordinates is obvious in the forward run which ended about 40 minutes after the start of the survey. The size of the error drops to less than 2 m after the coordinate update at the end of the forward run. It indicates that the reset after the coordinate update, which significantly improved the accuracy of the estimated azimuth, helps to reduce the error in the filtered coordinates. Results from the processing of the other sets of data also indicate that the reset also improved the over-all accuracy of the smoothed coordinates. As shown by the plot of the standard deviation of the filtered latitudes in Figure 8-5, the estimated variances, although slightly pessimistic in this particular survey, follow closely the error behaviour of the coordinates. The height error shows a different and more favourable behaviour than the latitude and longitude errors. In this survey all errors were below one metre. Results from the other surveys show that one metre (1σ) height accuracy is achievable after filtering. The plots of the filtered errors of the other three runs are shown in Appendix B. The estimated residual drift rates $\delta\mathbf{d}$ and accelerometer biases $\delta\mathbf{b}$ were found to be compatible with the initial standard deviation of the residual sensor errors except for the z residual drift of the second run. The z residual drift was estimated to about 0.05 arcsec/s which indicates that its initial standard deviation was slightly optimistic.

Like the velocity-data test, the accuracy of the estimated coordinates was improved after smoothing. The errors in the smoothed coordinates of the same run shown in Figure 8-5 are plotted in Figure 8-6 for comparison. In this survey, the first and eleventh station of baseline were occupied by other users during the backward run, and a less accurate station was established near the first station as the end point of the traverse. Thus, the second and tenth station were used as control points in the iterating process. The azimuth-dependent trend is still there but it has been reduced to the one-metre range and it is harder to distinguish from other time-dependent and random errors. The errors of the weighted means of the survey, plotted in Figure 8-7, show that sub-metre (1σ) accuracy for the horizontal coordinates and 0.5 m (1σ) for height determination are achievable with the SISS on a L-shaped traverse up to 24 km in length. The errors of the smoothed coordinates of the the other three runs and their weighted means are shown in Appendix B. The RMS computed with errors of the weighted means from the 4 surveys are tabulated in Table 8-1. The larger height errors of the 4th survey may be caused by the bouncing of the system during the survey. It shows the importance of proper mounting of the SISS while surveying on rugged terrain.

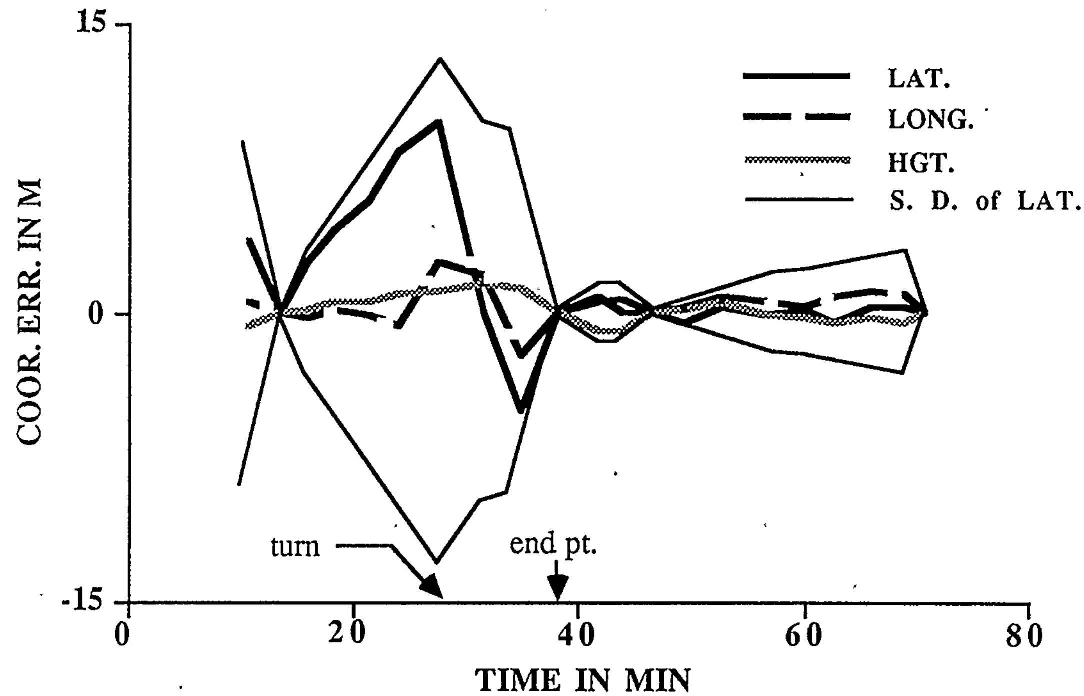

Figure 8-5 : Errors of Filtered Coordinates Using Rate Data

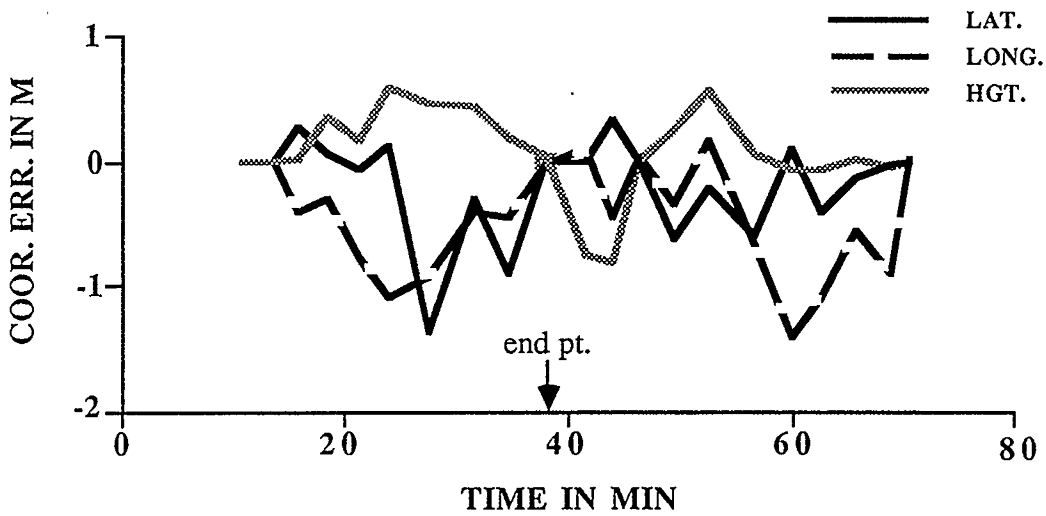

Figure 8-6 : Errors of Smoothed Coordinates Using Rate Data

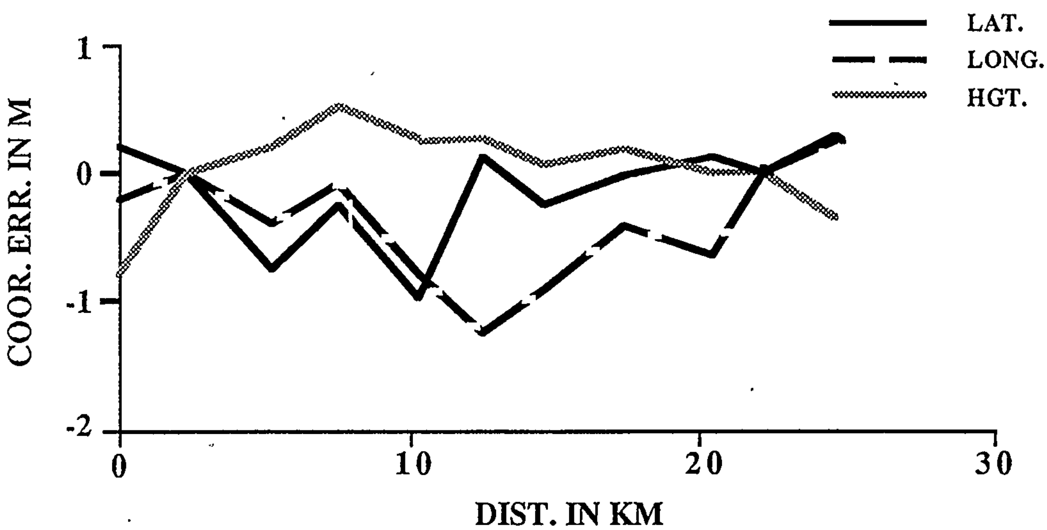

Figure 8-7 : Errors of Weighted Means Using Rate Data

Survey	RMS (m)		
	Lat.	Long.	Hgt.
1	0.48	0.66	0.35
2	0.60	0.58	0.48
3	0.49	0.77	0.29
4*	0.74	0.59	0.67

* one-way run

Table 8-1 : Accuracy of the Weighted Means from Rate Data

8.3 Applications in Airborne and Shipborne Environment

In the land-vehicle mode, the error states of the SISS can be accurately determined by zero-velocity updates. The application of the SISS may be extended to other environments, where the carrier of the system cannot be stopped regularly for measurement update. However, the error states of the strapdown inertial survey system can be estimated by using other form of surveying measurements which satisfy the condition given by equation (6-13).

In airborne or underground applications, velocities from other sources such as the Doppler radar in the aircraft, can be used to provide the external velocities needed to update the error states. The positioning accuracy of the SISS would not be as high as in the land-vehicle mode due to the larger measurement errors in the observed velocities. If continuous homogeneous velocity measurements are available for updates then the use of the optimal smoother will not improve the accuracy of the system.

As a crude attempt to show the effect of the higher velocity measurement noise on the positioning accuracy of the SISS, the observed velocities of the third survey, i.e the example shown in the last section, were corrupted with random noise and re-processed with the Kalman filter-smoother. The noise levels were set at 0.01 and 0.1 m/s, which are one and two orders of magnitude, respectively, higher than the standard zero-velocity measurements. The errors of the weighted means of the simulation are tabulated in Table 8-2. As expected, The results show the same general error pattern after filtering, and an overall poorer accuracy after smoothing due to larger uncertainty in the update measurements.

Noise level (m/s)	RMS (m)		
	Lat.	Long.	Hgt.
0.01	2.10	0.80	1.13
0.1	3.75	4.24	3.60

Table 8-2 : RMS of Weighted Means from Noisy Velocity Update Measurements

The SISS can also be integrated with other positioning systems such as GPS satellite receivers or radio navigation systems used at sea. The range measurements or the coordinates provided by these positioning systems can be treated as external measurements for updating the error states. In these cases, there is no velocity update but positioning accuracies are maintained by continuous position or range updates (Wong et al., 1987), and the level of accuracy achievable is dependent on the external positioning system used. Since the accuracy of the external positioning system is usually affected by the geometry of the ranges, the accuracy of the integrated system can change from one period to another. The optimal smoother can be used to improve the accuracy of the integrated system in periods of poor geometry with information gathered afterward, when the geometry has improved.

CHAPTER 9

CONCLUSIONS AND RECOMMENDATIONS

A Litton LTN-90-100 inertial reference unit has been successfully converted into a ring-laser-gyro strapdown inertial survey system (SISS). The system consists of the inertial reference unit and a IBM PC-compatible data acquisition system. The data processing software package includes a velocity integration routine, rate data integration module, alignment module and Kalman filter-smoother. The data acquisition software was designed to record either the velocity or rate data from the LTN-90-100. In case of velocity data, the integration routine can be used to integrate the data into raw coordinates. The error states of the LTN-90-100 are estimated by a Kalman filter and then refined by an optimal smoother. If the rate data are recorded, the rate integration module is used to integrate the data into changes in navigation quantities, i.e. Euler angles, 3-D velocities and coordinates. At the beginning of the survey, the alignment module is activated to determine the initial Euler angles of the system from the rate and velocity measurements. Navigation quantities at any epoch are calculated by adding increments to the value at the previous epoch. The errors of these navigation quantities are estimated by the same Kalman filter-smoother used in processing the velocity data.

Results from the testing of the LTN-90-100 in the laboratory show that there are gyro drifts of the order of 0.8 arcsec/s, in the body rates which were apparently not removed by factory calibration. These gyro drifts, as well as the small but significant biases left in the body accelerations, may be estimated by a combination of lab and baseline calibration of the system. The accuracy of the gyro drifts and acceleration biases calculated from the calibrations are estimated to be 0.01 to 0.02 arcsec/s and 10 mgal respectively.

The hardware and software were tested with data from surveys on two L-shaped baselines near Calgary. Results of the error analysis indicate that sub-metre (1σ) horizontal positioning accuracy is achievable on a 10-km L-shaped traverse if the raw data are the north and east velocities, and controls are available at both ends of the traverse. The results also show that the same accuracy for the horizontal coordinates and 0.5 m (1σ) for height can be obtained over a 24-km L-shaped baseline if rate data are used as raw data.

High frequency system noise caused by the dithers in the RLG and the cooling fans is the major source of errors during coarse alignment. The noise can be reduced by an order of magnitude using a 1-Hz second-order Butterworth filter which, however, may introduce a small bias to the data. Since the noise has a very high frequency, i.e. approximately 400 Hz, and zero mean in the long run, the use of the filter during fine alignment and navigation is not recommended.

The major error sources detected in the field tests are the initial azimuth misalignment and residual gyro drifts in the system. These errors and their effect may be minimized by frequent system calibration and reset of the error states after each coordinate update. Vibration caused by the dithers in the gyros and the cooling fans is the main limiting factor for the accuracy of the initial alignment.

At present offsets between the reference point on the vehicle and the station are measured with a protractor, ruler and plumbob. The accuracy of the offsets can be improved by measuring horizontal angles with precise optical instruments but it is operator-dependent and more time-consuming. Such an approach is recommended for very precise and short-distance surveying only.

The level of positioning accuracy achievable with the present LTN-90-100 based SISS may be reduced to < 0.5 m (1σ) if the residual drifts and biases can be removed by better system calibration. However, due to large system noise in the data, it is unlikely that the positioning accuracy can be improved to < 0.3 m (1σ) without any modification to the sensors.

The use of velocity data for positioning requires less computation time and storage space than rate data but it does not permit the user to reset any navigation quantities in the

SISS. The accuracy of the survey is dependent on the alignment accuracy of the real-time software in the system.

The residual drifts and biases left in the corrected rate data are large and random from one alignment to the next but they remain stable through the survey. Thus, with accurate coordinate and deflection controls on both ends of the traverse, it may be possible to use the SISS for the recovery of the anomalous gravity field.

Stochastic and empirical methods such as spectral decomposition, least-squares adjustment and Kalman filtering/empirical smoothing can be applied to estimate the errors of a strapdown inertial survey system in the same way as for the local-level system, with minor changes to the transition matrix or design matrix to account for the azimuth-dependent effect of the sensor biases.

At present, the LTN-90-100 does not output any vertical velocity or height to the user because it cannot obtain the external height data from the data acquisition system. The system interface device in the data acquisition system should be upgraded so that it can supply such height information to the LTN-90-100. The data acquisition system should also be modified so that it can be used for prolonged numerical computation at the 10-MHz clock rate.

A special mounting rack should be designed to hold the SISS firmly to the floor of the vehicle to prevent it from sliding or bouncing when the vehicle is travelling on rough terrain. A turntable may be built to facilitate the lab calibration of the SISS which requires the body rates and accelerations to be measured on a very level surface in different azimuths.

In the land surveying mode, the Kalman filter-smoother uses the velocity measurements obtained at each stop and the known coordinates on the traverse to update its error states. It can also be modified to accept other data, such as ranges and phase measurements from the a GPS satellite receiver or other radio navigation system, for the update. Integration of the SISS with these sensors would permit inertial surveys to be conducted in the airborne or marine environment where the carrier cannot be stopped regularly for velocity update.

REFERENCES

Babbage G. (1981) : "Inertial surveying - A study in accuracy and versatility". Proceedings of the Second International Symposium on Inertial Technology for Surveying & Geodesy. pp 351-357, Banff, Canada, June 1-5, 1981.

Benson, J. (1975) : "A comparison of two approaches of pure-inertial and doppler-inertial error analysis". IEEE Transc. on Aerospace and Electronic Systems, Vol. AES-11, No. 4, pp 447-454.

Bierman, G. J. (1973) : "Fixed interval smoothing with discrete measurements". International Journal of Control, Vol. 18, No. 1, pp 65-75.

Bierman, G. J. (1977) : Factorization Methods for Discrete Sequential Estimates. Academic Press, New York, U. S. A.

Blais, J. A. R. and A. A. Vassiliou (1987) : "Spectral analysis of one-dimensional data sequences". Technical report, Publication # 30010, Department of Surveying Engineering, University of Calgary, Calgary, Canada.

Blais, J. A. R. (1988) : Estimation and Spectral Analysis. The University of Calgary Press, Calgary, Alberta, Canada.

Brigham, E. O. (1974) : The Fast Fourier Transform. Prentice-Hall, Englewood, Cliffs, New Jersey, U. S. A.

Britting, K. R. (1971) : Inertial Navigation System Analysis. Wiley-Interscience, New York, U. S. A.

Bryson, A. E. and Y. C. Ho (1969) : Applied Optimal Control. Blaisdell Publishing Company, Waltham, Massachusett, U. S. A.

Catford, J. R. (1978) : "Application of strapdown inertial system with particular reference to underwater vehicle". AGARD Lecture Series No. 95.

Farrell, J. L. (1976) : Integrated Aircraft Navigation. Academic Press, New York, NY, U. S. A.

Forsberg, R. and R. V. C. Wong (1987) : "Methods to extract gravity information from inertial Data", The Proceedings of the IAG Symposia, Vol. 1 of the XIX General Assembly of IUGG/IAG, Vancouver, Canada, Aug 10-22, 1987.

Gelb, A. (1974) : Applied Optimal Estimation. The M. I. T. Press, Cambridge, Mass., U. S. A. Fourth Print.

Giardina, C. R., J. Heckathorn and D. Krasnjanski (1981) : "A comparative study of strapdown algorithms", Navigation, Journal of the Institute of Navigation. Vol. 28, No. 2, pp 101-106.

Grubin, C. (1970) : "Derivation of the quaternion scheme via the Euler axis and angle". Engineering Notes, Journal of Spacecraft, Vol. 7, No. 10, pp 1261-1263.

Hadfield, M. (1985) : "High precision positioning and gravity measurements with GEOSPIN - An update". Proceedings of the Third International Symposium on Inertial Technology for Surveying and Geodesy, pp 383-389, Banff, Canada, Sept. 16-20, 1985.

Hagglund, J. E. (1987) : "The Ferranti Inertial Land Surveying systems (FILS) as part of an integrated navigation and positioning system". Master Thesis, Publication # 20020, Department of Surveying Engineering, University of Calgary, Calgary, Canada.

Harris, H. C. (1981) : "Status of DMA testing of the Honeywell GEO-SPIN system". Proceedings of the Second international Symposium on Inertial Technology for Surveying and Geodesy, pp 359-371, Banff, Canada, June 1-5, 1981.

Kanasewich, E. R. (1981) : Time Sequence Analysis in Geophysics. University of Alberta Press, Edmonton, Canada.

Krakiwsky, E. J. and D. E. Wells (1971) : "Coordinate systems in geodesy". Lecture Notes #16, Department of Surveying Engineering, University of New Brunswick, Fredericton, Canada.

Litton (1984) : "Technical description of LTN-90-100 inertial reference system". Document # 500406, published by Aero Product Division, Litton Systems California, Canoga Park, California, U. S. A.

Moritz, H. (1984) : "Geodetic Reference System 1980", Bull. Geod., Vol. 58, No. 3, pp 388-398, 1984.

Mueller, I. I. (1977) : Spherical and Practical Astronomy as Applied to Geodesy. Frederick Ungar Publisher Co., New York, U.S.A.

Pfeifer L. and R. Tyszka (1985) : "Results of operational testing of LASS-II systems". Proceedings of the Third International Symposium on Inertial Technology for Surveying and Geodesy, pp 547-560, Banff, Canada, 1985.

Savage, P. G. (1978) : "Strapdown sensors", Strapdown Inertial Systems, AGARD Lecture Series No. 95.

Schmidt, G. T. (1978) : "Strapdown inertial system - Theory and applications - Introduction and review". AGARD Lecture Series, No. 95.

Schwarz, K-P. (1980) : "Error propagation in inertial positioning". The Canadian Surveyor, Vol. 34, No. 3, pp 265-276.

Schwarz, K-P. (1985) : "A unified approach to post-mission processing of inertial data". Bull. Geod. No. 59, pp 35-54.

Stieler, B. and H. Winter (1981) : "Gyroscopic instruments and their application to flight testing", AGARDograph, Vol. 15, No. 160.

Todd, M. S. (1981) : "Rapid Geodetic Survey System (RGSS) White Sand tests for position, height, and anomalous gravity vector components". Proceedings of the Second International Symposium on Inertial Technology for Surveying and Geodesy, pp 373-385, Banff, Canada, June 1-5, 1981.

Vassiliou, A. A. (1983) : "Processing of unfiltered inertial data", Master Thesis, Publication # 20006, Department of Surveying Engineering, University of Calgary, Calgary, Canada.

Wong, R. V. C. and K-P Schwarz (1979) : "Investigation on the analytical form of the transition matrix in inertial geodesy", Technical Report No. 58, University of New Brunswick. Fredericton, Canada.

Wong, R. V. C. (1982) : "A Kalman filter-smoother for an inertial survey system of local level type". Master Thesis, Publication # 20001, Department of Surveying Engineering, University of Calgary, Calgary, Canada.

Wong, R. V. C., K-P Schwarz and M. E. Cannon (1987) : "High-accuracy kinematic positioning by GPS-INS". Navigation : Journal of the Institute of Navigation, Vol. 35, No. 2, summer 1988. pp 275-287.

APPENDIX A

This appendix contains the derivation of the equation for the propagation of the quaternion components for the body to wander frame transformation matrix of a strapdown inertial survey system.

A theorem given by Euler in the 18th century states that a sequence of rotations of a rigid body, represented by the body frame, with respect to a reference frame, represented by the inertial frame, can be expressed as a single rotation θ about a fixed axis. The quaternion components are the four parameters required to describe the rotation without singularity. These components are also functions of the elements in the transformation matrix between the reference frame and the rigid body. The rate of change of the four components satisfy the differential equation :

$$\dot{q} = \frac{1}{2} q \times \dot{\theta} \tag{A-1}$$

where **q**, the quaternion vector, is given in Grubin (1970) and Catford (1978) as

$$\mathbf{q} = \begin{pmatrix} q1 \\ q2 \\ q3 \\ q4 \end{pmatrix} = \frac{1}{\theta} \begin{pmatrix} \theta_x \sin\theta/2 \\ \theta_y \sin\theta/2 \\ \theta_z \sin\theta/2 \\ \theta \cos\theta/2 \end{pmatrix} . \tag{A-2}$$

In equations (A-1) and (A-2), $\dot{\theta}$ is the rotation rate vector of the rigid frame with respect to the reference frame and θ_x, θ_y, and θ_z are the x-y-z components of the rotation vector θ with respect to the reference frame, i.e.

$$\dot{\theta} = \Delta t \, \theta . \tag{A-3}$$

The vector cross-product in equation (A-1) can be re-written into

$$\dot{q} = \frac{1}{2} \dot{\Theta} \times \mathbf{q}$$

$$
= \frac{1}{2}\begin{pmatrix} 0 & \dot\theta_z & -\dot\theta_y & \dot\theta_x \\ -\dot\theta_z & 0 & \dot\theta_x & \dot\theta_y \\ \dot\theta_y & -\dot\theta_x & 0 & \dot\theta_z \\ -\dot\theta_x & -\dot\theta_y & -\dot\theta_z & 0 \end{pmatrix}\begin{pmatrix} q1 \\ q2 \\ q3 \\ q4 \end{pmatrix} \tag{A-3}
$$

where $\dot\theta_x, \dot\theta_y$ and $\dot\theta_z$ are the x-y-z components of the vector $\dot\theta$. the Assuming that $\dot\theta$ is constant over a small interval Δt, the solution of equation (A-3) can be written as

$$
\begin{aligned}
q_{k+1} &= e^{0.5\dot\Theta\Delta t}\, q_k \\
&= \{\mathbf{I} + \frac{1}{2}\dot\Theta\Delta t + \frac{1}{4\cdot 2!}\dot\Theta^2\Delta t^2 + \frac{1}{8\cdot 3!}\dot\Theta^3\Delta t^3 + \frac{1}{16\cdot 4!}\dot\Theta^4\Delta t^4 + \dots\dots\dots\}\, q_k
\end{aligned} \tag{A-4}
$$

Since

$$
\dot\Theta^2 = -\dot\theta^2\, \mathbf{I}\,, \tag{A-5}
$$

equation (A-5) can be expressed as the sum of two Taylor's series, i.e.

$$
\begin{aligned}
q_{k+1} &= \{\mathbf{I} + \frac{1}{2}\dot\Theta\Delta t - \frac{1}{4\cdot 2!}\dot\theta^2\,\mathbf{I}\Delta t^2 - \frac{1}{8\cdot 3!}\dot\theta^2\,\mathbf{I}\,\dot\Theta\Delta t^3 + \frac{1}{16\cdot 4!}\dot\theta^4\,\mathbf{I}\Delta t^4 + \dots\dots\dots\}\, q_k \\
&= \{[\,\mathbf{I} - \frac{1}{4\cdot 2!}\dot\theta^2\,\mathbf{I}\Delta t^2 + \frac{1}{16\cdot 4!}\dot\theta^4\,\mathbf{I}\Delta t^4 + \dots\dots\dots] \\
&\quad + [\,\frac{\Delta t}{2} - \frac{1}{8\cdot 3!}\dot\theta^2\,\Delta t^3 + \frac{1}{32\cdot 5!}\dot\theta^4\,\Delta t^5 + \dots\dots]\,\dot\Theta\,\}\, q_k
\end{aligned} \tag{A-6}
$$

Obviously, the two series are the Taylor expansions of the sine and cosine functions, therefore equation (A-6) can be expressed as

$$
q_{k+1} = q_k + [\,(\cos\frac{\theta}{2} - 1)\mathbf{I} + \frac{1}{\theta}\sin\frac{\theta}{2}\,\Theta\,]\, q_k\,, \tag{A-7}
$$

where

$$\Theta = \Delta t \begin{pmatrix} 0 & \dot{\theta}_z & -\dot{\theta}_y & \dot{\theta}_x \\ -\dot{\theta}_z & 0 & \dot{\theta}_x & \dot{\theta}_y \\ \dot{\theta}_y & -\dot{\theta}_x & 0 & \dot{\theta}_z \\ -\dot{\theta}_x & -\dot{\theta}_y & -\dot{\theta}_z & 0 \end{pmatrix}. \tag{A-8}$$

If there is another rigid body, represented by the wander frame, which is also rotating with respect to the reference frame at a known rate ω, then the rate of change of the quaternion components of the relative rotation between the two rotating frame is

$$\dot{\mathbf{q}} = \frac{1}{2}\mathbf{q} \times \dot{\theta} - \frac{1}{2}\omega \times \mathbf{q}\,. \tag{A-9}$$

The solution to the second term of equation (A-8) can be approximated by

$$\frac{\Delta t}{2}\omega \times \mathbf{q} = \frac{\Delta t}{2} \begin{pmatrix} 0 & \omega_z & -\omega_y & \omega_x \\ -\omega_z & 0 & \omega_x & \omega_y \\ \omega_y & -\omega_x & 0 & \omega_z \\ -\omega_x & -\omega_y & \omega_z & 0 \end{pmatrix} \mathbf{q}\,, \tag{A-10}$$

provided ω is very small. In the case of strapdown inertial surveying, the rotation of the wander frame with respect to the inertial frame is so small ($\cong$ 15 arcsec/s) that equations (A-7) and (A-9) can be applied for the propagation of the quaternion components for the relative rotation between the body and wander frame, i.e.

$$\mathbf{q}_{k+1} = \mathbf{q}_k + [\ (\cos\frac{\theta}{2} - 1)\mathbf{I} + \frac{1}{\theta}\sin\frac{\theta}{2}\Theta - \frac{1}{2}\Delta t\ \omega\ ]\ \mathbf{q}_k\,, \tag{A-11}$$

where

$$\theta = \Delta t\ |\omega_{ib}^{b}| \tag{A-12}$$

and

$$\omega = \omega_{iw}^{b}\,. \tag{A-13}$$

Equation (A-11) is the expression used in Chapter 4 for the propagation of the quaternion components of the body to wander frame transformation matrix of the SISS.

APPENDIX B

This appendix contains the plots of the errors of the filtered and smoothed coordinates, and the weighted means of the coordinates of three of the four surveys performed on the 25-km L-shaped traverse. The results of the third survey are shown in Chapter 8.

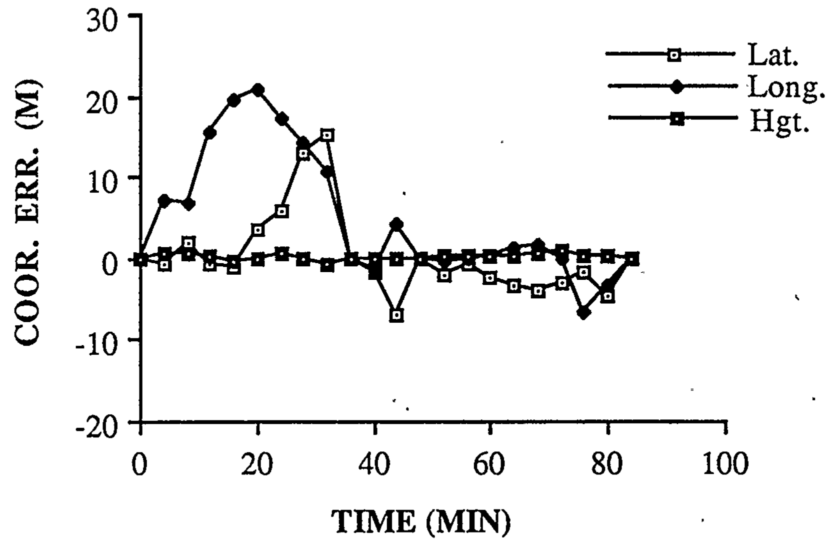

Figure B-1 : Errors After Filtering (1st Survey)

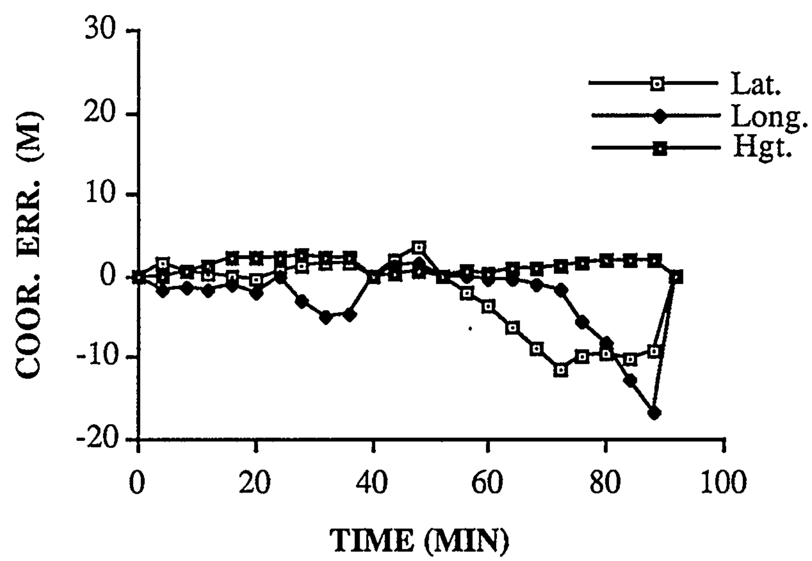

Figure B-2 : Errors After Filtering (2nd Survey)

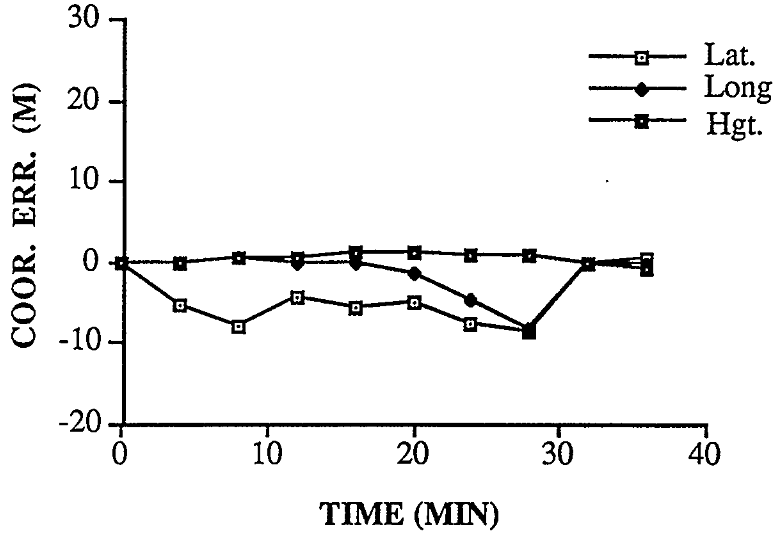

Figure B-3 : Errors After Filtering (4th Survey)

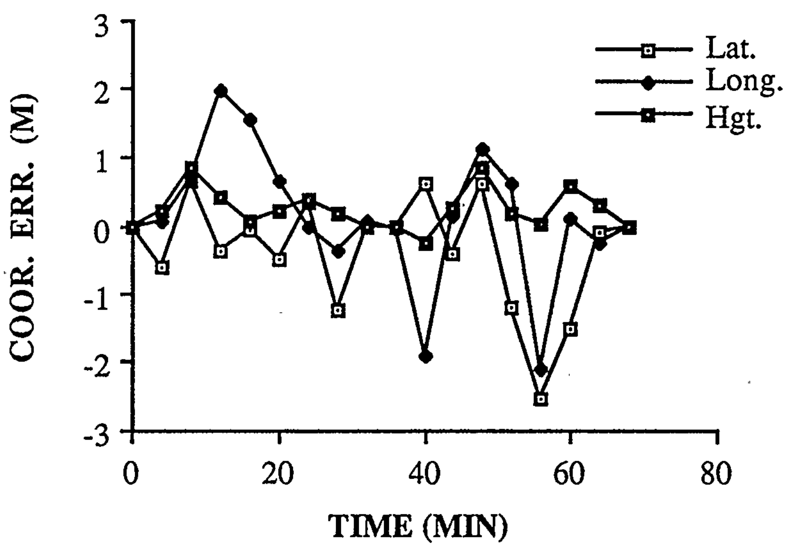

Figure B-4 : Errors After Smoothing (1st Survey)

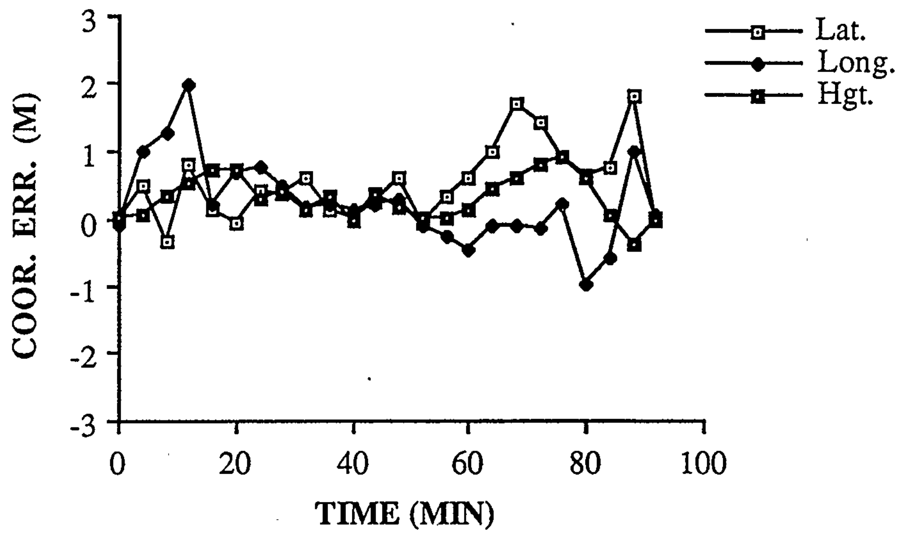

Figure B-5 : Errors After Smoothing (2nd Survey)

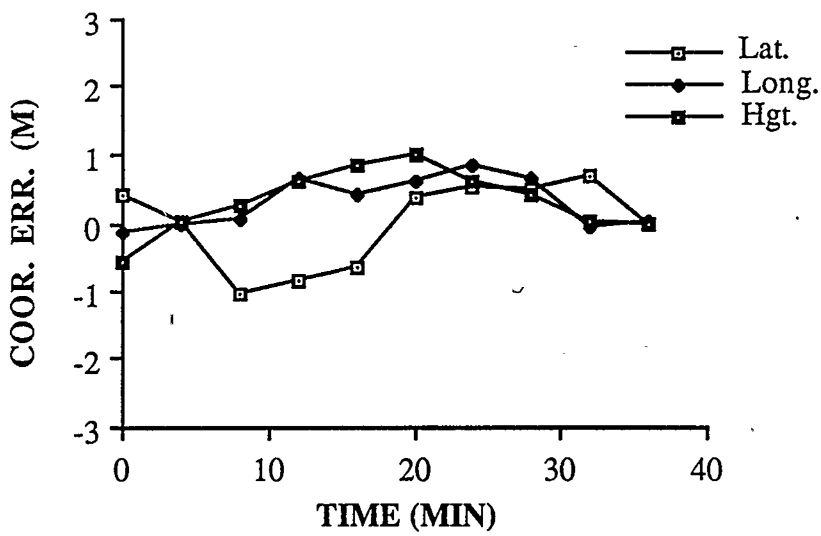

Figure B-6 : Errors After Smoothing (4th Survey)

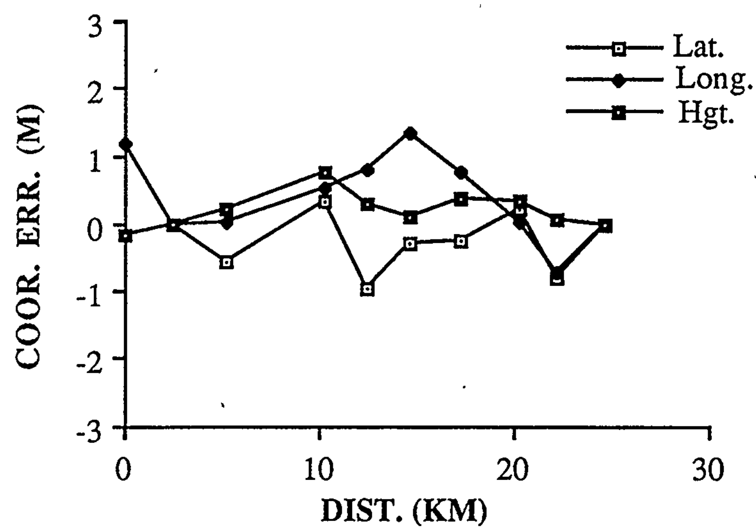

Figure B-7 : Errors of the Weighted Means (1st Survey)

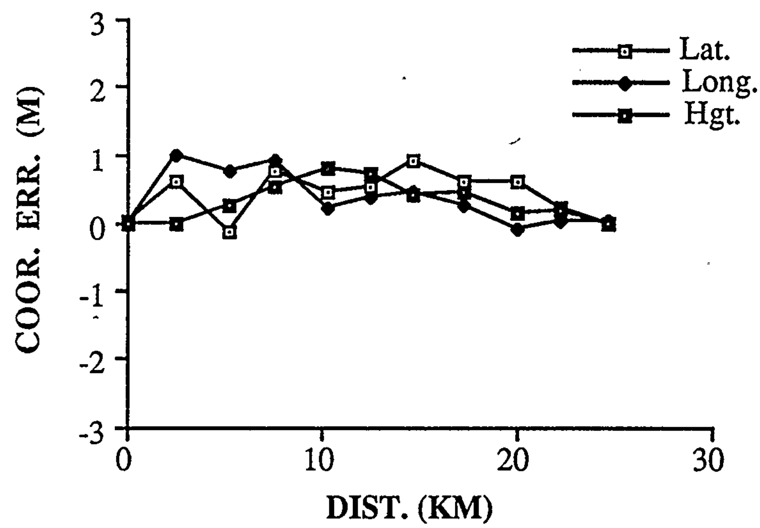

Figure B-8 : Errors of the Weighted Means (2nd Survey)